

THE DEVELOPMENT OF GRAPHITE SENSING ELEMENTS FOR SLUG  
CALORIMETERS AND A HIGH TEMPERATURE BLACKBODY SOURCE

Final Report

to

National Aeronautics and Space Administration  
George C. Marshall Space Flight Center  
Huntsville, Alabama

Contract No. NAS8-5196  
Task Order 6

Southern Research Institute  
Birmingham, Alabama  
7384-1481-6-XLI  
July 26, 1965

## TABLE OF CONTENTS

	Page
SCOPE AND SUMMARY . . . . .	1

### PART I

INTRODUCTION . . . . .	3
DEVELOPMENT OF THE SENSING ELEMENT . . . . .	4
Material Review . . . . .	4
Emittance Stability of Graphite . . . . .	5
Effect of Carbon Contamination on Thermocouple Output . . . . .	7
Development of a Carbon Diffusion Barrier . . . . .	9
Attachment and Protection of the Thermocouple . . . . .	14
CALIBRATION AND EVALUATION OF THE SENSING DISC . . . . .	18
THE PROTOTYPE CALORIMETER . . . . .	19
Design and Fabrication . . . . .	20
Calibration . . . . .	21
RECOMMENDATIONS FOR FUTURE WORK . . . . .	22
REFERENCES . . . . .	23

### PART II

INTRODUCTION . . . . .	93
DEVELOPMENT OF THE BLACKBODY . . . . .	93
CALIBRATION OF THE BLACKBODY . . . . .	94
ACKNOWLEDGMENTS . . . . .	95
APPENDIX FOR PARTS I AND II . . . . .	116

## LIST OF ILLUSTRATIONS

### PART I

<u>Figure Number</u>		<u>Page</u>
1	Change in the Emittance of ATJ Graphite Finished with "4/0" Grit Paper Run in Argon (Specimen No. 1) . . . . .	24
2	Comparison of the Emittances of Two ATJ Graphite Specimens Finished with "4/0" Grit Paper During the First Run for Each in Argon .	25
3	Stability of the Emittance of ATJ Graphite Finished with "4/0" Grit Paper, Heat Soaked at 1500°F in Air and Run in Argon (Specimen No. 3) . . . . .	26
4	Stability of the Emittance of ATJ Graphite Finished with "4/0" Grit Paper Run in Argon; Specimen Heat Soaked in Air after the First Run (Specimen No. 4) . . . . .	27
5	Comparison of the Emittances of Two "4/0" ATJ Graphite Specimens Finished with "4/0" Grit Paper; First Run for Argon with Prior Heat Soak in Air . . . . .	28
6	Comparison of the Emittances of Two ATJ Graphite Specimens Finished with "4/0" Grit Paper During the Second Run for Each in Argon with Prior Heat Soak in Air . . . . .	29
7	Emittance of ATJ Graphite During the First and Fifth Runs in Argon with Prior Heat Soak in Air (Specimen 5) . . . . .	30
8	Emittance of ATJ Graphite During the First and Sixth Runs in Argon with Prior Heat Soak in Air (Specimen No. 2) . . . . .	31

## LIST OF ILLUSTRATIONS (continued)

<u>Figure Number</u>		<u>Page</u>
8	Emittance of ATJ Graphite During the First and Sixth Runs in Argon with Prior Heat Soak in Air (Specimen No. 2) . . . . .	31
9	Emittance of ATJ Graphite During the First and Sixth Runs in Argon with Prior Heat Soak in Air (Specimen No. 3) . . . . .	32
10	Emittance of Two ATJ Graphite Specimens During the First Run for Each in Argon with Prior Heat Soak in Air (Specimens No. 2 and 3)	33
11	Comparison of the Emittances of Two ATJ Graphite Specimens During the Sixth Run for Each in Argon; Specimens Were Heat Soaked in Air Prior to the First Run in Argon . . . . .	34
12	Drawing Showing the Location of the Thermocouple Well in the $\frac{1}{2}$ " Diameter Graphite Specimen . . . . .	35
13	Effect of Slow and Rapid Thermal Cycling on an Unprotected Pt/Pt-10 Rh Thermocouple in a Graphite Specimen (Specimen No. 1) . . . . .	36
14	Effect of Slow and Rapid Thermal Cycling on an Unprotected Pt/Pt-10 Rh Thermocouple in a Graphite Specimen (Specimen No. 2) . . . . .	37
15	Effect of Slow and Rapid Thermal Cycling on an Unprotected Pt/Pt-10 Rh Thermocouple in a Graphite Specimen (Specimen No. 3) . . . . .	38
16	Configuration of Assembled Sensing Element and Components Used in Evaluating Effect of Protection Tube on Thermocouple Output . . . . .	39
17	The Effect of Thermal Cycling on a Pt/Pt-10 Rh Thermocouple in a Molybdenum Protection Tube (Specimen No. 1) . . . . .	40



## LIST OF ILLUSTRATIONS (continued)

<u>Figure Number</u>		<u>Page</u>
18	The Effect of Thermal Cycling on a Pt/Pt-10 Rh Thermocouple in a Molybdenum Protection Tube (Specimen No. 2) . . . . .	41
19	The Effect of Thermal Cycling on a Pt/Pt-10 Rh Thermocouple in a Tantalum Protection Tube (Specimen No. 2) . . . . .	42
20	The Effect of Thermal Cycling on a Pt/Pt-10 Rh Thermocouple in a Tungsten Protection Tube (Specimen No. 2) . . . . .	43
21	Comparison of the Thermoelectric Output from Four Pt/Pt-10 Rh Thermocouples During the First Cycle for Each in Protection Tubes . . .	44
22	Photomicrograph of Molybdenum Vapor Deposited onto ATJ Graphite Specimen No. 1, 150X . . . . .	45
23	Photomicrograph of Tungsten Vapor Deposited onto ATJ Graphite Specimen No. 15, 150X . . .	46
24	Photomicrograph of Tungsten Vapor Deposited onto ATJ Graphite Specimen No. 15 After Thermal Cycling to 3000°F (1649°C), 150X . . .	46
25	The Configuration of Three Types of Sensing Element Assemblies Evaluated . . . . .	47
26	The Effect of Thermal Cycling on a Pt/Pt-10 Rh Thermocouple Flash-Welded to the Tungsten Diffusion Barrier on a Graphite Substrate. See Figure 25a (Specimen No. 22)(Graphite Surface was Pre-oxidized) . . . . .	48

## LIST OF ILLUSTRATIONS (continued)

<u>Figure Number</u>		<u>Page</u>
27	The Effect of Thermal Cycling on Pt/Pt-10 Rh Thermocouple Flash-Welded to the Tungsten Diffusion Barrier on a Graphite Substrate. See Figure 26a (Specimen No. 23)(Graphite Surface was Pre-oxidized) . . . . .	49
28	The Effect of Thermal Cycling on a Pt/Pt-10 Rh Thermocouple Flash-Welded to the Tungsten Diffusion Barrier on a Graphite Substrate. See Figure 25a (Specimen No. 25)(Graphite Surface Finished with Medium Grit Paper) . . . . .	50
29	The Effect of Thermal Cycling on a Pt/Pt-10 Rh Thermocouple Flash-Welded to the Tungsten Diffusion Barrier on a Graphite Substrate. See Figure 25a (Specimen No. 26)(Graphite Surface Finished with Medium Grit Paper) . . . . .	51
30	Comparison of the Thermoelectric Output from Four Sensor Assemblies of the Type in Figure 25a During the First Cycle for Each . . . . .	52
31	The Effect of Thermal Cycling on a Pt/Pt-10 Rh Thermocouple Flash-Welded to the Tungsten Diffusion Barrier on a Graphite Substrate. See Figure 25b (Specimen No. 27) . . . . .	53
32	The Effect of Thermal Cycling on a Pt/Pt-10 Rh Thermocouple Flash-Welded to the Tungsten Diffusion Barrier on a Graphite Substrate. See Figure 25b (Specimen No. 28) . . . . .	54
33	The Effect of Thermal Cycling on a Pt/Pt-10 Rh Thermocouple Flash-Welded to a Tungsten Diffusion Barrier on a Graphite Substrate. See Figure 25c (Specimen No. 29) . . . . .	55
34	Comparison of the Thermoelectric Output from Three Sensor Assemblies of the Type Shown in Figure 25b and c During the First Cycle for Each . . . . .	56

## LIST OF ILLUSTRATIONS (continued)

<u>Figure Number</u>		<u>Page</u>
35	The Effect of Thermal Cycling on a Sensing Element with a Second Tungsten Vapor Deposition Applied over the Thermocouple Junction Protected with Alumina Cement (Specimen No. 32) . . . . .	57
36	The Effect of Thermal Cycling on a Sensing Element Assembly with a Second Tungsten Vapor Deposition Applied over the Thermocouple Junction Protected with Alumina Cement (Specimen No. 36) . . . . .	58
37	Diagram of Graphite Sensing Disc Prepared for a Second Tungsten Vapor Deposition . . . . .	59
38	The Effect of Thermal Cycling on a Sensing Element Assembly of the Type Shown in Figure 37 (Specimen No. 40) . . . . .	60
39	Comparison of the Thermoelectric Output from Three Sensing Element Assemblies with a Second Tungsten Vapor Deposition During the First Cycle for Each . . . . .	61
40	Photomicrograph of Assembly No. 36 with Two Tungsten Vapor Depositions and the Thermocouple Bead Covered with Alundum Cement, 75X . . . . .	62
41	Photomicrograph of Assembly No. 40 with Tungsten Vapor Deposited onto Graphite, Tungsten Powder and a Tungsten Retainer Ring Bonded to the Assembly with a Second Vapor Deposition, 75X . . . . .	62
42	The Laboratory Calorimeter for Calibration of the Graphite Sensing Element . . . . .	63
43	Millivolt Output (temperature) versus Time on Laboratory Calorimeter No. 38 with a Graphite Sensing Element, for Different Heat Flux Densities from the 1 inch Diameter Blackbody Radiation Source . . . . .	64

## LIST OF ILLUSTRATIONS (continued)

<u>Figure Number</u>		<u>Page</u>
44	Calibration of Laboratory Calorimeter No. 38 with a Graphite Sensing Element for Different Heat Flux Densities and Sensing Element Temperatures . . . . .	65
45	Calibration of Laboratory Calorimeter No. 106 with a Graphite Sensing Element for Different Heat Flux Densities and Sensing Element Tempera- tures . . . . .	66
46	Prototype Total Calorimeter with Graphite Sensing Element . . . . .	67
47	Millivolt Output (temperature) versus Time Curves for the Prototype Calorimeter Subject to Three Heat Flux Densities from the 1 inch Diameter Radiation Source . . . . .	68
48	Calibration of the Prototype Calorimeter for Different Heat Flux Densities and Sensing Element Temperatures . . . . .	69

## PART II

1	Cross Section of Blackbody Assembly Showing Induction Coil and Aperture Plate . . . . .	98
2	Final Configuration of Graphite Cavity Used in the Blackbody . . . . .	99
3	$\frac{1}{4}$ " Diameter Copper Induction Coil for Black- body Cavity . . . . .	100
4	Water Cooled Aperture Plate . . . . .	101
5	Water Cooled Optical Stop . . . . .	102
6	Housing for Blackbody Cavity . . . . .	103

## LIST OF ILLUSTRATIONS (continued)

<u>Figure Number</u>		<u>Page</u>
7	Sketch Showing Insulation Between Cavity and Aperture . . . . .	104
8	Initial Configuration of Graphite Blackbody Cavity for High Temperature Radiation Source . . . . .	105
9	Photograph from the Vertical of the Blackbody Housing Showing the $\frac{1}{8}$ " Diameter Copper Cooling Coil Surrounded by Fiberfrax . . . . .	106
10	Cross-Sectional View and Sensing Surface of the Assembled Copper Calorimeter for Calibrating the Blackbody Cavity. . . . .	107
11	Grooved Copper Slug for Radiation Calorimeter Assembly Used in Calibrating the Blackbody Cavity . . . . .	108
12	The Emittance During Repeated Cycles in Argon of a Grooved Copper Disc Painted with "Japalac" Flat Black Paint. Calorimeter No. 1 Used in Calibrating the Blackbody Cavity . . . . .	109
13	Theoretical and Measured Irradiances During Calibration Runs on the High Temperature Blackbody Radiation Source Using Four Copper Disc Calorimeters . . . . .	110

## LIST OF TABLES

### PART I

<u>Table Number</u>		<u>Page</u>
1	Potential Calorimeter Heat Sink Materials . . . . .	70
2	Change in Emittance of ATJ Graphite Finished with "4/0" Grit Paper, Run in Argon (Specimen No. 1) . .	71
3	Stability of the Emittance of ATJ Graphite Finished with "4/0" Grit Paper, Heat Soaked in Air and Run in Argon (Specimen No. 3) . . . . .	72
4	Stability of the Emittance of ATJ Graphite Finished with "4/0" Grit Paper, Run in Argon; Specimen Heat Soaked in Air After the First Run (Specimen No. 4) . .	73
5	The Emittance of ATJ Graphite During the First and Fifth Runs in Argon with a Prior Heat Soak in Air (Specimen No. 5) . . . . .	74
6	Effect of Slow and Rapid Thermal Cycling on an Unprotected Pt/Pt-10 Rh Thermocouple in a Graphite Specimen (Specimen No. 2) . . . . .	75
7	Effect of Slow and Rapid Thermal Cycling on an Unprotected Pt/Pt-10 Rh Thermocouple in a Graphite Specimen (Specimen No. 3) . . . . .	76
8	Effect of Slow and Rapid Thermal Cycling on an Unprotected Pt/Pt-10 Rh Thermocouple in a Graphite Specimen (Specimen No. 1) . . . . .	77
9	Effect of Thermal Cycling on a Pt/Pt-10 Rh Thermo- couple in a Molybdenum Protection Tube (Specimen No. 1) . . . . .	78
10	Effect of Thermal Cycling on a Pt/Pt-10 Rh Thermo- couple in a Molybdenum Protection Tube (Specimen No. 2) . . . . .	79
11	Effect of Thermal Cycling on a Pt/Pt-10 Rh Thermo- couple in a Tantalum Protection Tube (Specimen No. 2) .	80

# LIST OF TABLES (continued)

<u>Table Numbers</u>		<u>Page</u>
12	Effect of Thermal Cycling on a Pt/Pt-10 Rh Thermo- couple in a Tungsten Protection Tube (Specimen No. 2) . . . . .	81
13	Thickness of Tungsten Diffusion Barrier on Sectioned Graphite Discs . . . . .	82
14	Effect of Thermal Cycling on a Pt/Pt-10 Rh Thermo- couple Flash-Welded to the Tungsten Diffusion Barrier on a Graphite Substrate. (See Figure 25a)(Graphite Surface was Preoxidized)(Specimen No. 22) . . . . .	82
15	Effect of Thermal Cycling on a Pt/Pt-10 Rh Thermo- couple Flash-Welded to the Tungsten Diffusion Barrier on a Graphite Substrate. ( See Figure 25a)(Graphite Surface was Preoxidized)(Specimen No. 23) . . . . .	84
16	Effect of Thermal Cycling on a Pt/Pt-10 Rh Thermo- couple Flash-Welded to the Tungsten Diffusion Barrier on a Graphite Substrate. (See Figure 25a)(Graphite Surface Finished with Medium Grit Paper)(Specimen No. 25) . . . . .	85
17	Effect of Thermal Cycling on a Pt/Pt-10 Rh Thermo- couple Flash-Welded to the Tungsten Diffusion Barrier on a Graphite Substrate. (See Figure 25a)(Graphite Surface Finished with Medium Grit Paper)(Specimen No. 26) . . . . .	86
18	Effect of Thermal Cycling on a Pt/Pt-10 Rh Thermo- couple Flash-Welded to the Tungsten Diffusion Barrier on a Graphite Substrate (See Figure 25b)(Specimen No. 27) . . . . .	87
19	Effect of Thermal Cycling on a Pt/Pt-10 Rh Thermo- couple Flash-Welded to the Tungsten Diffusion Barrier on a Graphite Substrate (See Figure 25b)(Specimen No. 28) . . . . .	88

## LIST OF TABLES (continued)

<u>Table Number</u>		<u>Page</u>
20	Effect of Thermal Cycling on a Pt/Pt-10 Rh Thermocouple Flash-Welded to the Tungsten Diffusion Barrier on a Graphite Substrate. (See Figure 25c)(Specimen No. 29) . . . . .	89
21	Effect of Thermal Cycling on a Sensing Element with a Second Tungsten Vapor Deposition Applied over the Thermocouple Junction Protected with Alumina Cement (Specimen No. 32) . . . . .	90
22	Effect of Thermal Cycling on a Sensing Element with a Second Tungsten Vapor Deposition Applied over the Thermocouple Junction Protected with Alumina Cement (Specimen No. 36) . . . . .	91
23	Effect of Thermal Cycling on a Sensing Element Assembly of the Type Shown in Figure 37 (Specimen No. 40) . . .	92

## PART II

1	The Emittance of Grooved Copper Disc Painted with "Japalac" Flat Black Paint During Repeated Runs in Argon (Calorimeter No. 1) . . . . .	111
2	Results of Calibration Runs on the High Temperature Blackbody Radiation Source . . . . .	112
3	Results of Calibration Runs on the High Temperature Blackbody Radiation Source . . . . .	113
4	Results of Calibration Runs on the High Temperature Blackbody Radiation Source with Copper Sensing Discs and Exposing Three Prototype Graphite Calorimeters to the Radiation Source . . . . .	114
5	Results of Calibration Runs on the High Temperature Blackbody Radiation Source Using Copper Disc Calorimeters . . . . .	115



# THE DEVELOPMENT OF GRAPHITE SENSING ELEMENTS FOR SLUG CALORIMETERS AND A HIGH TEMPERATURE BLACKBODY SOURCE

## SCOPE AND SUMMARY

This is the final report on Task Order 6 of Contract NAS8-5196 to NASA, Astrionics Division in Huntsville, Alabama. This task order was for the development of (1) a graphite sensing disc for use in slug type calorimeters, and (2) a blackbody radiation source with a 1 inch diameter aperture and an output irradiance of 100 Btu/ft<sup>2</sup>/sec. This report is divided into two parts discussing both development programs.

The development of a graphite sensing disc for slug calorimeters was initiated due to the apparent advantages, such as good high temperature stability, of a graphite sensing element in comparison to the materials presently employed in commercially available units. Since this was a new concept in the state-of-the-art, a considerable amount of research and development was necessary. Under the program, therefore, developments that were accomplished are summarized in the following paragraphs.

Initially a thorough literature search was performed to confirm that graphite would be the best material for this application. The literature revealed that graphite would be the optimum choice due to its high emittance, high diffusivity, and good stability in addition to its availability and machinability. Other good candidates were hafnium diboride (HfB<sub>2</sub>) and beryllium oxide (BeO).

To demonstrate the emittance stability of graphite and also provide values that may be required for future analytical study, the emittance of ATJ graphite was determined from 1800°F to 3000°F. The measurements indicated that a very constant and repeatable emittance between 0.8 and 0.9 was obtained for graphite after preoxidizing in air at 1500°F.

The major problem associated with using a graphite sensing element was the attachment and contamination of the thermocouple. The effect of contamination resulted in an unpredictable decrease in thermocouple output with thermal cycling up to approximately 2650°F. Therefore, a carbon diffusion barrier to protect and attach the thermocouple was required. After a thorough literature search into possible diffusion barrier materials and considerable experimental evaluation, the solution was found. A tungsten coating was applied to the back

face of the graphite disc by vapor deposition, and the platinum/platinum-10 rhodium thermocouple was flash welded to the tungsten. This was found to be effective up to 2500°F.

After these developments, the graphite sensing elements were mounted in laboratory calorimeters, and standard calibrations were preformed. The calibrations demonstrated consistent performance and high temperature capability.

One prototype calorimeter (total type) was designed, fabricated, calibrated and forwarded to NASA ready for use. Under the scope of this task order, the calorimeter was not certified under all flight specifications. However, the unit closely approximates anticipated flight units in design and performance. During calibration, the sensing element temperature was taken to a maximum 2300°F over a range of heat flux densities from 40 to 90 Btu/ft<sup>2</sup>/sec. Results of this calibration indicated excellent repeatability and consistency.

Therefore, the use of a graphite sensing element is feasible and exhibits many advances in the state-of-the-art. Some future work is recommended to develop this technique further and provide prototype flight units which meet all flight specifications.

Part II of this report describes the development of a high temperature blackbody radiation source used in calibration of heat flux sensors. This blackbody was constructed of graphite and was inductively heated. The blackbody was calibrated over a range of temperatures from 2000°F to 4100°F. The range (distance from the aperture to receiver) was varied from  $\frac{1}{4}$  inch to 12 inches. The blackbody performed well at heat flux densities up to 100 Btu/ft<sup>2</sup>/sec. Considerable effort was given to the design of the cavity and induction coil, so that thermal gradients within the cavity were reduced to a minimum.

## PART I

### DEVELOPMENT OF A GRAPHITE SENSING ELEMENT FOR SLUG CALORIMETERS

#### INTRODUCTION

The development of a graphite sensing element for the "slug" type calorimeters appeared to have several advantages over the present state-of-the-art due to the better high temperature performance of graphite when compared to copper or nickel that are presently being used in commercial calorimeters. The emittance of graphite is relatively high providing an element that would absorb most of the incident radiation. The variation of its emittance is little affected by changing temperatures, and the maximum temperature to which graphite can be exposed without serious alteration of its physical properties is normally much higher than for previously designed units. Therefore, the sensing element would be capable of repeated use under more extreme temperature conditions.

The primary disadvantage associated with the development of a graphite sensing element was in joining a thermocouple to the graphite, such that repeated temperature exposures did not change the thermocouple output. Most thermocouple metals carburize readily in the presence of graphite, especially at higher temperatures. Several possible solutions were (1) staking a thermocouple to a metal slug that would act as a diffusion barrier for the carbon and press fitting the slug into the base of the graphite element; (2) pre-coating or spray-welding one surface of the graphite element with a metal to act as a diffusion barrier and joining the thermocouple to this coating; and (3) treating the thermocouple with a diffusion barrier and wedging the couple into the base of the graphite element with a graphite wedge. In all these techniques, the difference in expansion of the graphite and the applied material would require careful consideration.

The object of this program was to determine feasibility of this new concept, and the subsequent development and design of the graphite sensing element. The sensing element design would include the best methods for a maximum temperature exposure, maximum thermocouple sensitivity, maximum response rate, and minimum effect of temperature cycling. The results of this research and development would be the construction and calibration of a prototype calorimeter incorporating these design features.

To accomplish the above objectives, systematic efforts were expended in (1) the review and selection of materials, (2) the attachment and protection of the thermocouple, and (3) design, evaluation and calibration of a complete calorimeter assembly with a continuous awareness of the flight application for which this type of unit will eventually be employed.

## DEVELOPMENT OF THE SENSING ELEMENT

### Material Review

A literature survey of several materials was made with particular emphasis on the properties of emittance, thermal conductivity, diffusivity, property stability and physical-chemical stability. The initial maximum exposure temperature was assumed to be 3000°F (1649°C) and later extended to 4500°F (2482°C). Table 1 shows the potential materials considered and a comparison of their physical properties. The primary controlling requisite for selecting the sensing element material was high uniform emittance. Materials meeting this requirement were then evaluated, based on thermal diffusivity and physical stability.

Graphite was the prime candidate, having high emittance, highest diffusivity, and good stability in addition to its availability and machineability. Other materials which would perform up to 4500°F included HfC, ZrC, HfO<sub>2</sub>, and HfB<sub>2</sub>. Each of these materials had one or more weak points, making a compromise necessary. HfB<sub>2</sub> and ZrC have high diffusivity and both show some stability in emittance versus temperature. Emittance for HfB<sub>2</sub> increases with temperature and becomes fairly stable between 2500°F (1371°C) and 4800°F (2649°C). The reverse is true for ZrC, which has a high stable emittance at lower temperatures and drops off above 4000°F (2204°C). Emittance for HfC is erratic above 3000°F (1648°C), possibly due to volatilization or the effect of the test atmosphere. HfC and HfO<sub>2</sub> have lower diffusivity values than graphite, and HfO<sub>2</sub> exhibits physical instability above 3000°F. The characteristics of these materials may be affected greatly by impurities and stoichiometry. Material reliability and reproducibility may also be questionable as currently available.

If the temperature limit of 3000°F were employed, SiC and BeO would become possible materials for use as the heat sink. Both have relatively high emittance and diffusivity.

The oxidation resistance of the candidate materials was not reviewed extensively; however, this is only an advantage in the calorimeter application for some special cases. Oxidation is not a problem in the radiation calorimeter since the element is enclosed. The life time of many flight calorimeters, in which the sensing element would be exposed to an oxidizing atmosphere, is short enough that the effects of oxidation on the front surface of the element would not be sufficient to alter the output of the sensor. In cases where oxidation is a critical problem, more review would be necessary into the protective systems available for this high temperature. This will be discussed further under the section on future efforts.

From this review of properties, the selection of graphite was confirmed as the best overall material for the sensing element with  $\text{HfB}_2$  for a possible alternate for operation to  $4500^\circ\text{F}$ .  $\text{SiC}$  was considered a good candidate after graphite if the temperature was limited to  $3000^\circ\text{F}$  and  $\text{BeO}$  if other circumstances require an oxide.

#### Emittance Stability of Graphite

Emittance evaluations were made from  $1800^\circ\text{F}$  to  $3000^\circ\text{F}$  ( $982^\circ\text{C}$  -  $1649^\circ\text{C}$ ) on several ATJ graphite specimens to determine the emittance stability of graphite and also provide values that may be required in future analytical studies of the sensor. The apparatus and procedure utilized for these evaluations are described in the Appendix. The specimens employed were  $\frac{1}{2}$  inch diameter by  $\frac{1}{8}$  inch thick, and the evaluation involved the measurement of emittance after thermal cycling on specimens of different surface finishes.

One specimen was evaluated in an argon atmosphere to show the change in emittance caused by temperature cycling. Prior to exposure, the specimen surface was finished with "4/0" grit paper. The apparatus was evacuated twice and filled with high purity argon. A constant argon purge was maintained during the evaluations. The results of the evaluations made during two cycles are shown in Figure 1 and Table 2. During the first cycle, the emittance rose almost constantly from 0.65 at  $2000^\circ\text{F}$  ( $1093^\circ\text{C}$ ) to 0.75 at  $3000^\circ\text{F}$  ( $1649^\circ\text{C}$ ). The first exposure caused the emittance of the specimen to change to a constant 0.74 over the entire temperature range of the second cycle. The appearance of the specimen surface changed from a polished condition to a surface appearing to have a black velvet finish. This change was probably caused by the residual air and moisture remaining in the apparatus and specimen after evacuation.

A second specimen (specimen No. 4) finished with "4/0" grit paper was evaluated during the first exposure in argon. A comparison of the emittance of specimens No. 1 and No. 4 during the first run for each in argon is shown in Figure 2. The emittance of specimen No. 4 was somewhat

greater than the emittance of specimen No. 1 over the temperature range. Evidently a poorer environment of the second run permitted more surface alteration and higher emittance.

Evaluations were then made to determine the stability of the emittance of ATJ graphite after heat soaking the specimens in air. Specimen No. 3 was heat soaked in air for five minutes at approximately 1500°F (760°C), and then evaluated during three cycles in an argon atmosphere. The results of these evaluations are shown in Figure 3 and Table 3. The emittance of this specimen varied only 5% with increasing temperature and temperature cycling; the emittance was almost constant at 0.84 through the three exposures. Specimen No. 4, previously mentioned, was heat soaked in air after evaluations were made during the first run in argon; see Figure 4 and Table 4. The emittance of this specimen was also nearly constant at 0.84.

A comparison is shown in Figure 5 of the emittances of the two specimens during the first run in argon for each after heat soaking in air. The emittance of specimen No. 3 rose from 0.80 at 1800°F to 0.85 at 3000°F and was slightly higher than the emittance of specimen No. 4 through the temperature range. Figure 6 is a comparison of the emittances of the same specimens during the second run for each in argon after heat soaking in air. The emittance of specimen No. 3 was approximately 0.01 greater than the emittance of specimen No. 4 and rose only slightly from 0.84 to 0.86 from 1800°F to 3000°F.

Emittance evaluations were made during the first and fifth runs in argon on an ATJ graphite specimen (specimen No. 5) with a prior heat soak in air to determine any variations caused by additional cycling; see Figure 7 and Table 5. During the first run the emittance rose only slightly from 0.80 at 1800°F (982°C) to 0.82 at 2500°F (1371°C), and then decreased to 0.80 at 3000°F (1649°C). During the fifth cycle in argon, the emittance appeared to be almost constant at 0.80 over the temperature range.

Emittance determinations also were made on two specimens (specimens No. 2 and No. 3) during the first and sixth cycles in argon. The results of these evaluations are shown in Figures 8 and 9, and in Tables 6 and 7. As can be seen from the tables, these runs were done concurrently with the evaluations, discussed later, concerning the effect of the carbon atmosphere on unprotected thermocouples within the graphite specimen. The emittance of specimen 2 rose from 0.86 at 1800°F to 0.90 at 2300°F (1260°C) and decreased to 0.85 at 2900°F (1594°C). The emittance of this same specimen was slightly higher during the sixth run by 0.01 at 2500°F and by 0.03 at 2900°F.

The emittance of specimen 3 was the same as that of specimen 2 during the first run for each and is shown in Figure 10. Figure 11 is a comparison of the emittances of specimens 2 and 3 during the sixth run for each in argon. The emittance of specimen 2 decreased slightly from 0.91 at 1900°F (1038°C) to 0.88 at 3000°F; the emittance of specimen 3 was approximately 0.02 less than that of specimen 2 over the same temperature range.

The combined results of all emittance evaluations on ATJ graphite indicated that the emittance of the graphite was stabilized and made consistent from specimen to specimen by heat soaking in air prior to evaluation. The emittance of each specimen heat soaked in air varied with temperature by approximately 0.05 from 1800°F to 3000°F and usually reached a maximum at about 2400°F (1316°C). The emittances of all heat soaked specimens were within the range of absolute uncertainty ( $\pm .05$ ) for the equipment by exhibiting values of 0.80 to 0.90 over the temperature range and were not affected by cycling in argon. The minor variations in the emittances of individual specimens were probably caused by variations in texture and purity. Therefore, in using graphite for the sensing element, prior heat soaking to 1500°F is required for suitable operation.

#### Effect of Carbon Contamination on Thermocouple Output

As mentioned previously, the main problem associated with a graphite sensing element is the attachment of the thermocouple to the graphite such that repeated temperature exposures do not change the thermocouple output. Most thermocouple materials, especially platinum/platinum-10 rhodium, which was chosen for this application, are carburized readily in the presence of graphite.

To measure this deleterious effect quantitatively, three ATJ graphite specimens were heated several times in the emittance apparatus to determine the effect of thermal cycling to 3000°F (1649°C) on unprotected platinum/platinum-10 rhodium thermocouples located inside the specimens. Figure 12 shows the location of the thermocouple well in the  $\frac{1}{2}$  inch diameter specimen. The thermocouple wires, 0.005 inch in diameter, were threaded through 0.007 inch diameter holes in a 0.035 inch diameter, double-bore alumina tube which was inserted in the thermocouple well. The millivolt output of the thermocouple was monitored with a null balance potentiometer and corresponding surface temperatures were measured with an optical pyrometer.

During the first and sixth cycles, the temperature was increased stepwise and corresponding temperature measurements were recorded before and after equilibrium was reached. Emittance evaluations also were made on two of

the specimens as discussed in the previous section. During the second through the fifth cycles, the specimens were heated rapidly by selecting a predetermined power setting before starting the heating cycle. Approximately 15 seconds were required to heat the specimen to 2500°F (1371°C), and another 30 seconds for the temperature to stabilize near 2900°F (1594°C). Corresponding temperature measurements were made during the rapid heating and after equilibrium was reached. The rapid heating cycles were performed to determine the amount of time lag inherent in the sensing element.

The results of cycling the first specimen are shown in Figure 13 and Table 8. In Figure 13, the thermocouple output is plotted versus the surface temperature observed with the optical pyrometer. Also shown as a dotted line is the thermocouple output corresponding to the true surface temperature (observed temperature corrected for specimen emittance). Note that the temperature indicated by the thermocouple was less than the true surface temperature with the difference decreasing at higher temperatures. During the second through the fifth cycles, the specimen was heated rapidly and allowed to stabilize at about 2900°F (1594°C) for the remainder of the five-minute heating cycle. During the third cycle, the thermocouple output began to decrease at temperatures corresponding to previously observed values of 2500°F. During the last cycle, the specimen was heated slowly and the thermocouple output had decreased by an almost constant amount (0.42 mv) through the exposure range.

The second specimen evaluated showed very little total change in thermocouple output as a result of thermal cycling; see Figure 14 and Table 6. During the sixth cycle, the thermocouple output dropped slightly below the output of previous cycles, but was not as significant as the change noticed in the thermocouple of the first specimen.

The results of cycling the third specimen appeared very similar to those obtained from the first specimen; see Figure 15 and Table 7. During the second through the fifth heating cycles, the output decreased between runs and near the upper temperature limit of each cycle. The thermocouple failed at the end of the fifth cycle while indicating a true temperature of about 2960°F (1627°C).

The results from the data taken during the rapid cycles indicated a possible time-lag in sensitivity during rapid heating, but this was not clearly distinguishable due to the eventual decrease in thermoelectric output resulting from exposure.



In reviewing the results of the above three evaluations, the effects of carbon contamination were not consistent but caused the millivolt output to decrease as much as 0.45 mv. Obviously this is not acceptable for proper performance of a calorimeter. Therefore, a study into methods for protecting the thermocouples was required. This study was undertaken both experimentally and analytically, as discussed in the following section.

#### Development of a Carbon Diffusion Barrier

To experimentally determine the protection provided by several possible carbon diffusion barriers, an evaluation was conducted on several closed-end protection tubes to determine their effectiveness in protecting the couples from the graphite atmosphere. The protection tubes were machined from unalloyed tantalum, molybdenum, and tungsten and assembled as shown in Figure 16. The graphite discs were preoxidized to prevent any change in the emittance during thermal cycling, and the assemblies were evaluated in the inductively heated emittance apparatus in an argon atmosphere. The millivolt output from the thermocouple located inside the protection tube was monitored with an L and N potentiometer; corresponding temperature readings were made on the graphite surface with an optical pyrometer as done previously with the unprotected thermocouples.

During the first cycle, each assembly was heated slowly to about 2800°F (1538°C) and corresponding temperature measurements were recorded. During the next four cycles, an attempt was made to determine any effect that the protection tube had on the time-lag of the thermocouple. The power selection was preset and two sets of temperature readings were made during the remainder of these five-minute cycles. The sixth cycle was similar to the first in that the specimen was heated slowly over the temperature range to determine any variations from the first cycle. This general procedure was followed for all the evaluations.

The results of cycling the assemblies with the molybdenum protection tubes are shown in Figures 17 and 18 and Tables 9 and 10. The thermocouple in the first assembly failed before the completion of the fifth cycle. For this assembly there was no noticeable effect on the thermocouple as a result of thermal cycling. There was a slight time-lag caused by the protection tube which indicated an output from the thermocouple 0.20 mv less than that obtained during slow heating in the 2100°F to 2300°F observed temperature range (1149°C - 1260°C). The results from the second specimen with the molybdenum protection tube, shown in Figure 18, were very similar to those of the first, except that there was an apparent greater influence on

time-lag in the 2100°F to 2300°F observed temperature range. This amounted to approximately 0.30 mv, or 48°F. Observe that the thermocouple indicated temperatures higher than the true surface temperature.

The results of cycling one specimen with a tantalum protection tube are shown in Figure 19 and Table 11. This assembly was cycled a total of seven times to about 2800°F and did not appear to be affected by the cycling. The thermocouple in this specimen also indicated an output of about 0.30 mv less during the rapid heating. The second specimen with the tantalum protection tube was overexposed during the first cycle and the thermocouple failed while indicating a temperature of approximately 3030°F (1666°C). The indicated thermocouple temperature was lower than the true surface temperature over most of the range, with the two values coinciding at observed surface temperatures above 2500°F.

The thermocouple in the first specimen with a tungsten protection tube failed for no apparent reason during the first cycle at about 2700°F (1482°C). The second assembly, however, was cycled six times to 2700°F and showed no adverse effects from the cycling and almost no deviation during the rapid heating from the initial calibration cycle; see Figure 20 and Table 12. This thermocouple indicated temperatures higher than the true surface temperature over most of the range, the difference being about 40°F at an observed temperature of 2600°F.

A comparison is shown in Figure 21 of the thermoelectric output from each of the four thermocouples during the first cycle for each. The highest output was obtained from the thermocouple in the molybdenum protection tube, for specimen No. 1. For an observed temperature of 1900°F (1038°C), there was a maximum of 40°F (22°C) difference in the temperature indicated by the various thermocouple assemblies. At 2540°F (1393°C), this difference had increased to 60°F (33.4°C). This variation was due to the physical difference in the "hand-fabricated" thermocouples and assemblies. The premature failure of the thermocouple in the first assembly with a tungsten protection tube was probably due to faulty construction of the thermocouple.

In order to clarify the results of the above evaluation, a literature survey was conducted to determine the carbon diffusion rates through potential barrier materials with melting points above 3000°F (1649°C). This survey was designed to assist in the proper selection of a barrier material which would protect a thermocouple attached to graphite for a period up to thirty minutes at 3000°F.

Sixteen metals had high enough melting points to be considered for this application. The diffusion coefficients of carbon for only 4 of the 16 candidate barrier metals were found. They are listed in order of increasing rates at 3000°F.

<u>Metal</u>	<u>Diffusion Coefficient</u>
Tungsten <sup>1</sup>	0.52 - 2.55 x 10 <sup>-12</sup>
Tantalum <sup>2</sup>	4.2 x 10 <sup>-7</sup>
Niobium <sup>2</sup>	11 x 10 <sup>-7</sup>
Vanadium <sup>2</sup>	5.3 x 10 <sup>-6</sup>

A method of determining the maximum value of the diffusion coefficient allowable for a given maximum degree of saturation with carbon is described by Jost<sup>1</sup> in which the relations

$$C/C_0 = 1 - \operatorname{erf} \left( \frac{x}{2\sqrt{Dt}} \right) \text{ and } y = \frac{x}{2\sqrt{Dt}}$$

apply.  $C_0$  is the surface concentration and  $C$  is the concentration at  $x$  distance (in cm) from the surface of the metal in contact with the carbon.  $D$  is the diffusion coefficient and  $t$  is the time in seconds. The  $y$  value can then be determined from a table of  $y$  vs  $\operatorname{erf} y$  (error function) values. The maximum value of  $D$  is determined from the relation

$$y = \frac{x}{2\sqrt{Dt}}$$

A table of maximum  $D$  values is shown below for a 0.05% value of the concentration ratio of carbon at a time of 30 min. in a barrier metal with thicknesses of 10, 100, and 1000 microinches.

<u>Microinches</u>	<u>Diffusion Coefficient, Maximum Value</u>
10	2.26 x 10 <sup>-14</sup>
100	2.26 x 10 <sup>-12</sup>
1000	2.26 x 10 <sup>-10</sup>

The concentration ratio,  $\frac{C}{C_0}$ , represents the amount of carbon in solution at a given point in the metal relative to the amount the metal can dissolve at that temperature. From the above table it can be seen that tungsten appears to be the only metal (of those for which data are available), in which D for carbon would limit the carbon concentration to a maximum of 0.05% of saturation, at 3000°F in 30 min, with a thickness of about 100 microinches for the barrier metal.

In order to complete this carbon diffusion study, another literature survey was pursued to devise a method of bonding the selected barrier to the graphite. Of particular interest was previous work conducted in welding and brazing of tantalum, tungsten, molybdenum, columbium, and graphite. Some of the more specific areas considered in this survey included: metal shim brazing; resistance brazing with metal fibers; electron-beam welding; tungsten arc welding; and other related techniques. The information obtained on these subjects indicated that rather elaborate systems of procedures and apparatuses were required in bonding refractory metals and graphite, and most of these systems were presently experimental. Information pertaining to the brazing of high temperature metals indicated that operating temperatures of the brazes were limited near the upper temperature range desired under this program.

Previous experience had proved that molybdenum could be successfully vapor deposited onto graphite. Vapor depositions of molybdenum onto graphite were performed by the molybdenum pentachloride method. The  $\frac{1}{2}$  inch diameter graphite specimens, approximately  $\frac{1}{8}$  inch thick, were heated inductively in a "Vycor" chamber with various openings and attachments for controlling the system pressures and temperatures. A considerable amount of difficulty was experienced in controlling the parameters involved in obtaining uniform thicknesses, mechanical bonding, deposition rates, controlled grain structures and smooth finishes. Figure 22 is a photomicrograph showing the deposition of molybdenum onto graphite (specimen No. 1). Observe the nonuniform thickness and large grain structure; also the surface of the graphite is well defined, indicating poor mechanical bonding.

Since the results of the literature survey conducted on carbon diffusion rates indicated that tungsten would be the best barrier material, it was decided to attempt vapor depositions of this metal. The descriptions of the apparatus and procedure utilized for the tungsten and molybdenum depositions are included in the Appendix. Figure 23 is a photomicrograph showing the results of the deposition by the tungsten hexachloride method. A very uniform thickness of approximately 4.77 mils was obtained along with a

very smooth surface, uniform grain structure and apparently good bonding. The remainder of this specimen (specimen No. 10), after being sectioned for the above photomicrograph, was thermally cycled to approximately 3000°F three times in argon for a period of five minutes each. Figure 24 shows the results of the three exposures in which the grains have grown and an interface layer formed. The cycling also tended to cause a rougher surface on the deposited tungsten but did not cause cracking or separation of the materials.

A considerable amount of difficulty was experienced in controlling the thickness of the tungsten vapor depositions applied by the powdered tungsten hexachloride method, which required approximately four hours to deposit a layer between 0.001 inch and 0.005 inch thick on a  $\frac{1}{2}$  inch diameter graphite disc. After 44 graphite discs had been coated by this method, the apparatus was modified for depositions using tungsten hexafluoride gas as the reactive compound. A needle valve was used to control the gas flow and the required deposition time was reduced to approximately 15 minutes for each disc. The tungsten hexafluoride deposition method also virtually eliminated the necessity of cleaning the apparatus after each coating, as had been experienced with the tungsten hexachloride method.

Fifty-five graphite discs  $\frac{1}{2}$  inch diameter and  $\frac{1}{8}$  inch thick were coated with tungsten, using the tungsten hexafluoride method. On the first 30 specimens, the coating was applied on successive series of 5 to 10 discs. After each series, photomicrographs were taken on approximately one-half of the discs prepared. From the photomicrographic evaluation, tungsten layer thickness was measured and the interfacial bond inspected. Minor adjustments were then made on the system pressure, flows and temperatures in an attempt to obtain a tungsten thickness of approximately 0.0025 inch. Table 13 shows the results of measurements made of the tungsten layers on seven sectioned graphite discs. As can be seen from the table, a 15 minute time period was required to obtain the desired thickness. The remainder of the graphite discs, approximately 25, were then coated using the same conditions for periods of 15 minutes and were very similar in physical appearance.

A review of the physical appearance and the photomicrographic evaluation of the specimens indicated that the vapor deposition of tungsten on to graphite was the most practical and effective application of the diffusion barrier. The photomicrograph of Figure 24 illustrates the apparent

effectiveness of the barrier after thermal cycling, since no evidence of carbon contamination could be found. With the carbon diffusion barrier successfully applied, the next step in the development of the sensing element was the attachment of the thermocouple.

#### Attachment and Protection of the Thermocouple

Several different methods were considered and attempted in attaching a thermocouple to the diffusion barrier material. An attempt was made to attach the platinum/platinum-10 rhodium thermocouples to the tungsten layer by applying a second deposition over the surface and thermocouple. The second deposition caused the thermocouple wires to become coated and embrittled since it was impossible to deposit over the junction without also affecting the leads.

The feasibility of flash-welding the thermocouple wires to tungsten was first investigated using unalloyed tungsten cleaned with fluoric and nitric acids and degreased in trichlorethylene. A capacitance discharge flash welder was employed. The welding schedule was set by selecting the number of capacitors and resistance in the circuit. Each of the 0.005 inch diameter wires was welded individually to the tungsten by touching the wire to the tungsten with the circuit closed and causing the capacitors to discharge. An argon purge was directed onto the target area to minimize oxidation.

Since welding the thermocouple wires individually to the tungsten produced a thermocouple with an intermediate metal, an attempt was made to weld a preformed junction to the tungsten. The junction was made between the two wires by twisting them together and welding with an arc from an ac Powerstat. The bead was then welded to the tungsten with the flash welder. This procedure simplified the assembly since only one weld junction was required.

Initially, sensing assemblies of three types were evaluated in the emittance apparatus in an argon atmosphere; Figure 25 shows the designs of the sensors. The first type, shown in Figure 25a, had the thermocouple wires individually welded to the tungsten barrier with the leads perpendicular to the surface. The second type, shown in Figure 25b, also had the thermocouple wires welded individually to the tungsten; however, the leads were insulated in an alumina tube and situated parallel to the surface covered with a back face disc of graphite properly slotted for the alumina tube. The third type, Figure 25c, had the same configuration as the second type except a preformed thermocouple bead was welded to the tungsten.

The first two sensor assemblies evaluated were of the type shown in Figure 25a and had preoxidized graphite surfaces. Figure 26 and Table 14 show the results of the slow and rapid cycling of one such specimen. The output from the thermocouple decreased noticeably with each cycle to about 2700°F (1482°C). During the sixth cycle, the thermocouple was indicating temperatures approximately 90°F (50°C) lower than those obtained during the first cycle. This specimen was heated slowly over the first two cycles and, even though the output dropped after each of these cycles, increasing the maximum temperature of exposure appeared to have a much greater effect on the output of the thermocouple during subsequent cycles. The other sensor of this type (specimen 23) was evaluated in a similar manner, except it was heated slowly through only one cycle and the maximum exposure temperature was lower than that used for specimen 22; these results are shown in Figure 27 and Table 15. The thermoelectric properties of this assembly did not appear to be affected as much as those of specimen 22, probably because of the lower maximum exposure temperatures.

Specimen Nos. 25 and 26 were also of the type shown in Figure 25a and were evaluated in the same manner as specimens 22 and 23, except the graphite surfaces were not preoxidized. Some supplementary evaluations showed that ATJ graphite finished with medium grit paper after heating for five minutes in the argon atmosphere of the emittance apparatus had the same emittance as did the graphite finished with a 400 grit paper heated in air.

Specimen No. 25 was heated to an indicated temperature of 2500°F (1371°C) during the first cycle, which caused the output of the thermocouple to drop quite noticeably during the next cycle; see Figure 28 and Table 16. The other sensor (No. 26) was cycled to about 2400°F (1316°C) during the first exposure and this appeared to have a negligible effect on the second cycle; see Figure 29 and Table 17. However, after the sensor was heated to 2500°F during the second cycle, it indicated lower output during the next cycle, and the output progressively decreased on each succeeding cycle. Therefore, these sensors appeared to be affected adversely by exposure temperatures in excess of 2400°F.

Figure 30 shows a comparison of the thermoelectric output from the four sensors of the type shown in Figure 25a during the first cycle for each. The two specimens which had the preoxidized graphite surfaces (specimens 22 and 23) provided the higher output, but were lower than the assemblies evaluated with the protection tubes; see Figure 21. A thermal drain was probably created near the thermocouple junction by directing the leads perpendicular from the surface.

The next two assemblies evaluated were of the type shown in Figure 25b with the leads flash-welded individually and threaded through a double-bore alumina tube. The leads were directed parallel to the tungsten surface with the alumina tube in contact with the surface. Another piece of graphite was slotted and used to cover the thermocouple and its sheathing.

The results of thermally cycling assembly No. 27 are shown in Figure 31 and Table 18. This assembly was overexposed during the first cycle, which resulted in its failure during the second cycle. Sensor No. 28 was cycled six times and the results are shown in Figure 32 and Table 19. The maximum exposure temperature was held below an observed temperature of 2400°F (1316°C) during the first five exposures. During the sixth cycle, the thermocouple appeared to be unaffected by the previous exposures and indicated a maximum temperature of 3057°F (1681°C). The indicated thermocouple temperature exhibited excellent agreement with the true surface temperature for observed surface temperatures above 2400°F. There was no apparent time-lag caused by using the alumina tube and the additional piece of graphite.

Due to the erratic behavior of many of the thermocouples formed by welding the leads individually, the third type of sensing assembly was prepared as shown in Figure 25c. The results of the evaluations on this assembly are shown in Figure 33 and Table 20. The maximum exposure temperature was increased with each cycle and appeared to have no effect on the output of the thermocouple during subsequent exposures. There was a noticeable time-lag during the rapid heating cycles which was very similar to that noticed for other specimens; the thermoelectric output was 0.30 mv to 0.40 mv lower around an observed temperature of 2100°F.

Figure 34 is a comparison of the thermoelectric outputs from the sensing element assemblies during the first cycle for each with the thermocouple leads directed from the surface in a parallel direction. The outputs from these assemblies were considerably higher than those assemblies with thermocouple leads perpendicular to the specimens surface. The change to welding the preformed junction to the tungsten also appeared to increase the repeatability between the different assemblies in that the observed calibration runs were very similar. This method was used on all future assemblies.

Due to the better performance of the sensing assemblies with the thermocouple leads parallel to the surface (Figures 25b and c), the design of the graphite sensing disc was modified further in an effort to bond the



double-bore alumina tube to the assembly and produce an isothermal zone around the thermocouple junction by applying a second vapor deposition to the graphite disc. Alumina cement was baked over the thermocouple junction welded to the diffusion barrier to protect it from the second deposition.

The results of cycling two sensing assemblies (No. 32 and No. 36) with the second vapor deposition over the alumina tube and thermocouple junction protected with alumina cement are shown in Figures 35 and 36, and in Tables 21 and 22. Neither of these sensors was adversely affected until an indicated temperature of 2550°F (1399°C) had been exceeded. A third sensing assembly shown in Figure 37, in which a tungsten retainer ring made from 0.025 inch diameter wire was placed on the back surface and the interior filled with tungsten powder (passing 200 mesh) prior to the second vapor deposition, was prepared and evaluated. The results of the evaluations are shown in Figure 38 and Table 23. A comparison of the outputs from each of the three sensing assemblies during the first cycle for each is shown in Figure 39. The addition of the tungsten powder on No. 40 did not increase the output from this assembly over that from No. 32 and No. 36 as the sensors did produce very similar results during the first heating cycle for each. This indicated that the addition of the tungsten powder and retainer ring produced little or no effect on the output from the thermocouple during the initial run and that an optimum had probably been reached in this design. The second tungsten deposition was very effective, however, in bonding the alumina tube, retainer ring, and powder to the disc.

After completing the thermal cycling evaluations, two of the sensing assemblies were sectioned and mounted for photomicrographs. Assembly No. 36 consisted of a tungsten vapor deposition onto graphite approximately 1.7 mils thick, a thermocouple flash-welded to the tungsten, alumina cement baked over the welded bead, and a second tungsten vapor deposition approximately 1.4 mils thick. A cross-sectional view of this assembly is shown in the photomicrograph of Figure 40. The photograph was made utilizing a polarizing light to produce more contrasting shades. The dark lines are the tungsten depositions.

The other sensing assembly that was sectioned and photographed was No. 40, which was of the type shown in Figure 37. Figure 41 shows a cross-section of this specimen with a tungsten vapor deposition on the graphite approximately 1.5 mils thick, tungsten powder, and the 0.025 inch diameter tungsten retainer ring. A good bond was obtained between the powder, ring, and graphite by a second vapor deposition over the entire assembly. In both

photomicrographs the tungsten deposition appeared quite uniform in thickness, similar in structure, and well bonded to graphite. The second deposition over each assembly also appeared quite effective in bonding all parts of the assembly.

From the above, therefore, the design shown in Figure 37 was accepted as the type to be used in the prototype calorimeter.

### CALIBRATION AND EVALUATION OF THE SENSING DISC

Before the prototype calorimeter could be prepared, the graphite sensing elements developed above were evaluated under actual dynamic conditions to study response, sensitivity and repeatability in order to confirm feasibility for use in flight calorimeters. This was accomplished by performing typical calibrations on laboratory calorimeters utilizing the graphite discs as sensing elements. These laboratory calorimeters, shown in Figure 42, were designed for minimum heat loss from the sensing disc. The graphite disc and thermocouple leads were housed in a transite body and thermally insulated with thermatomic carbon packed in the annulus between the sensing element and transite housing. A  $\frac{1}{16}$  inch diameter double bore alumina tube was employed to electrically insulate the thermocouple wires.

The calibrations were performed by utilizing the 1 inch diameter black-body cavity developed under this task order and described in Part II of this report. Several calibration runs were made by situating the calorimeter at certain distances from the aperture of the blackbody at various temperatures. The irradiance of the blackbody was calibrated for temperature and distance by employing standard copper calorimeters fully described in Part II. The calibrations of the laboratory calorimeters with the graphite sensing element were performed as follows:

1. The calorimeter was subjected to various known heat flux densities and the resulting millivolt output (temperature) vs time curves were recorded on an x-y recorder.
2. The slopes ( $^{\circ}\text{F}/\text{sec}$ ) of the various temperature versus time curves were measured at several temperature levels over the entire temperature range of the graphite sensing element.
3. With the above, calibration curves were prepared by plotting heat flux density versus slope for the selected temperature levels of the sensing element.

Three laboratory calorimeters with the graphite discs, numbered 38, 105 and 106, were successfully calibrated over a wide range of heat flux densities.

The temperature-time curves and resulting calibration curves for calorimeter 38 are shown in Figures 43 and 44 for various heat flux densities ranging up to 12 Btu/ft<sup>2</sup>/sec. This was considerably below the maximum design heat flux density; however, the results were consistent and demonstrated sufficient sensitivity in this low range for practical use.

The other laboratory calorimeter, No. 106, was calibrated over the higher heat flux density range up to a maximum of 90 Btu/ft<sup>2</sup>/sec with graphite disc temperatures reaching 1800°F. The calibration curves for this unit are shown in Figure 45. The response again was consistent and fairly linear except at heat flux densities above 75 Btu/ft<sup>2</sup>/sec. The calibration did demonstrate the feasibility of a graphite slug calorimeter that would operate at temperatures up to 2000°F, which far exceeds the limits of conventional calorimeters.

The above evaluations indicated conclusively the feasibility and the many advantages of a calorimeter employing a graphite sensing element. The next phase in this program, therefore, was to design, build, and calibrate a prototype unit to be sent to NASA that approached the design required for flight conditions.

### THE PROTOTYPE CALORIMETER

The prototype calorimeter to be made and sent to NASA was to represent a unit that would be suitable for flight; however, it was not necessary to meet all specifications required for flight. Also, the design was not to consider installation requirements.

It was decided to make the prototype a total rather than a radiation calorimeter since the total calorimeter is usually subjected to conditions of higher heat flux densities and slug temperatures that are more suited to a graphite slug. However, the graphite element could be employed in either type.

## Design and Fabrication

In the design of a flight calorimeter, the main problem is the trade off necessary between rigid structural design and efficient thermal design. During flight, the calorimeter is subjected to excessive mechanical loads, primarily vibration. Therefore, the mounting of the sensing element and thermocouple leads must be extremely rigid. A rigid construction, however, always provides a thermal drain from the sensing element.

The prototype was designed incorporating the structural features of sensors presently being used. However, it was not tested for mechanical strength, and therefore it is not certified to meet NASA flight specifications. However, the design is considered a close approach to an acceptable flight unit which fulfills the requirements under the scope of this task order. The design is such to conclusively confirm the feasibility of using graphite sensing elements in future flight units.

The design of the prototype is shown in Figure 46. The graphite sensing element, which was preoxidized on the top surface, is mounted in the stainless steel housing with three 4-40 set screws, the ends of which have been turned down to  $\frac{1}{32}$  diameter pins for minimum area of contact between the graphite and set screw. The thermocouple leads, insulated with alumina tubing, are run along the back surface of the graphite element to the edge, at which point they are folded back toward the center and brought out through the back of the assembly. Powdered thermatomic carbon is tightly packed in the annulus between the sensing element and the housing. The graphite element is insulated from the closely surrounding reflective shield with zirconia cement, which also acts as a barrier to contain the thermatomic carbon. The .005 inch diameter thermocouple leads are soldered to the larger 28 gage lead wire of platinum/platinum-10 rhodium and the low temperature transition zone is potted with epoxy cement.

Since the calorimeter is a total calorimeter with the ATJ graphite element exposed, it can only be used and calibrated in a nonoxidizing atmosphere (or for short duration in an oxidizing atmosphere) to protect the surface of the sensing element from excessive oxidation.

The thermatomic carbon surrounding the sensing element was employed since it is a very effective insulator ( $k \approx 0.1$  Btu/hr/ft<sup>2</sup>/°F/in.) and it also eliminates radiant heat loss from the back face of the graphite disc. The elimination of radiant heat transfer from the disc is particularly important for this unit in comparison to conventional sensors due to the higher temperature capability of the graphite sensing element.

Originally, the epoxy potting was to be placed at two locations to support the wire. The first location was in the sleeve immediately behind the therm-atomic carbon packing where the wire insulation changed from the alumina tube to the Teflon and Refrasil sleeving. This was to secure the wire from twisting. The second potting location was in the sleeve at the end of the flexible conduit to secure the solder junction. Inadvertently, however, in the assembly, the epoxy potting also filled the area within the flexible conduit. Since this would not affect the performance or structural integrity of the prototype, it was accepted.

### Calibration

The calibration of the prototype calorimeter was performed with the 1 inch diameter blackbody cavity utilizing the methods discussed previously. Several runs in an argon atmosphere were made over a range of heat flux densities from 40 Btu/ft<sup>2</sup>/sec to 90 Btu/ft<sup>2</sup>/sec and maximum sensing element temperature of 2300°F. The calibration was performed on two separate days to confirm the repeatability of the calorimeter after the temperature of 2300°F was obtained on the graphite disc.

Some typical temperature versus time curves are shown in Figure 47, and the resulting calibration curves included in Figure 48. As can be seen from the figures, the results were very consistent and repeatable. Also shown in Figure 48 is a plot of the laboratory calorimeter No. 106 (Figures 42 and 45) discussed previously.

The comparison of the two calibrations illustrates the approximate amount of heat lost in the prototype due to its sturdier construction. At a sensing element temperature of 1000°F, approximately 8 to 12 Btu/ft<sup>2</sup>/sec is lost assuming perfect insulation for calorimeter No. 106.

In comparing the performance of the prototype with the Fenwall No. 026 total calorimeter, the sensitivity (temperature vs time slope) and response are greater for the prototype due to the smaller mass of the sensing element. Since the temperature limit of the smaller graphite element of the prototype calorimeter is considerably higher than the larger copper element in the Fenwall calorimeter, the duration time before destruction temperature is about the same for both units. This demonstrates the advantage of a graphite sensing element in that greater sensitivity and response can be obtained for the same, or greater, period of operation. Also, the calorimeter sensing element can be designed so its temperature matches that of the surrounding insulation thus giving a direct reading of input heat flux density.

### RECOMMENDATIONS FOR FUTURE WORK

Under this task order, the feasibility and specific advantages in employing graphite sensing discs in slug calorimeters have been demonstrated. However, some development still remains. The following are recommended areas for future development.

1. Provide better oxidation resistance for the sensing element. This can probably be accomplished with JTA graphite or coated graphite.
2. Study effects of size and shape of the sensing disc on the performance of the sensor. The maximum and minimum size limits can be determined here.
3. Study the feasibility of employing other types of thermocouples to extend the temperature limit.
4. Build several prototypes (both total and radiation types) to incorporate the above features and to meet NASA's flight specifications and installation requirements.

REFERENCES

1. Willhelm, Jost, Diffusion in Solids, Liquids and Gases.
2. Power and Doyle, "Diffusion of Interstitial Solutes in Group V Transition Metals," Journal of Applied Physics, Vol. 30, April 1959, p 514.

First Run —○—  
Second Run —□—

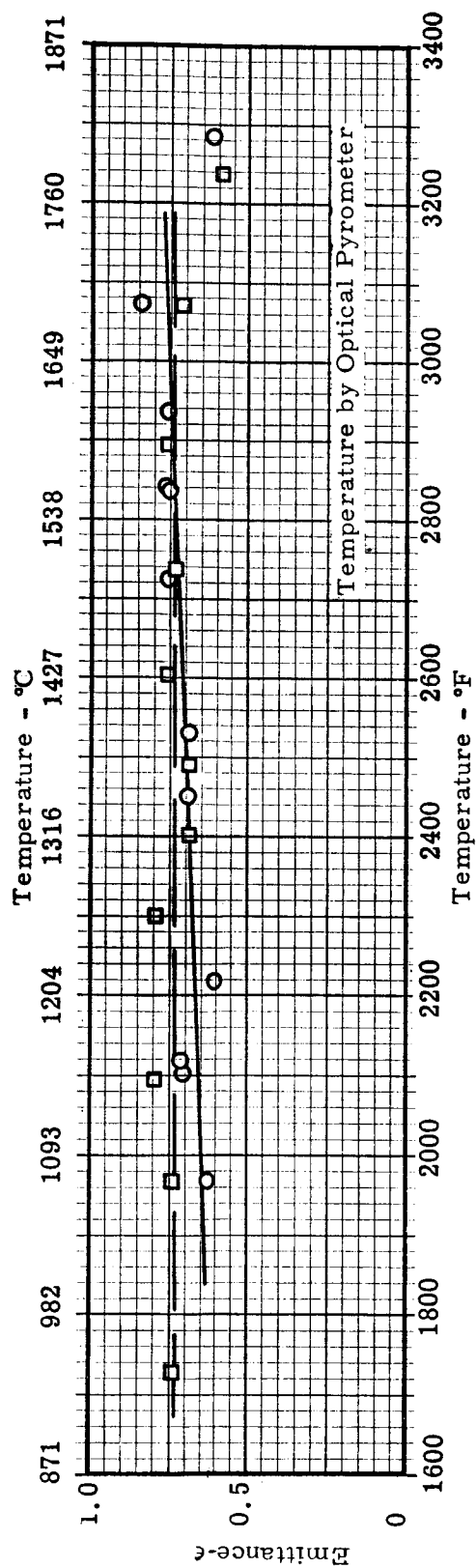


Figure 1. Change in the Emittance of ATJ Graphite Finished with "4/0" Grit Paper Run in Argon (Specimen No. 1)



Specimen No. 1 \_\_\_\_\_  
 Specimen No. 4 -----

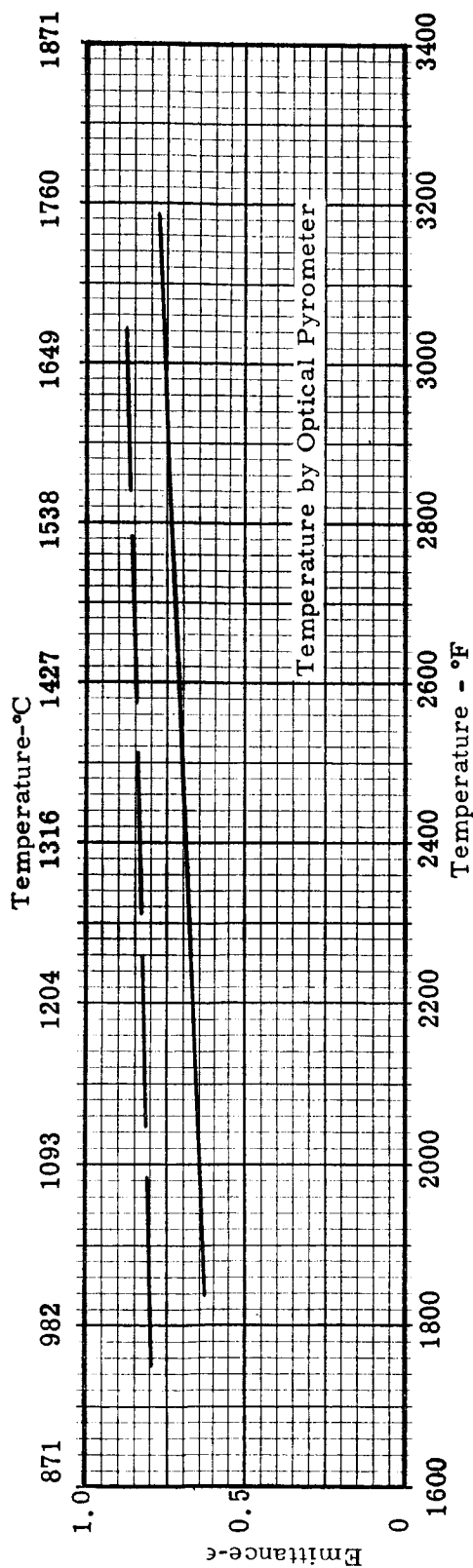


Figure 2. Comparison of the Emittances of Two ATJ Graphite Specimens Finished with "4/0" Grit Paper During the First Run for Each in Argon

First Run - O  
 Second Run - □  
 Third Run - Δ

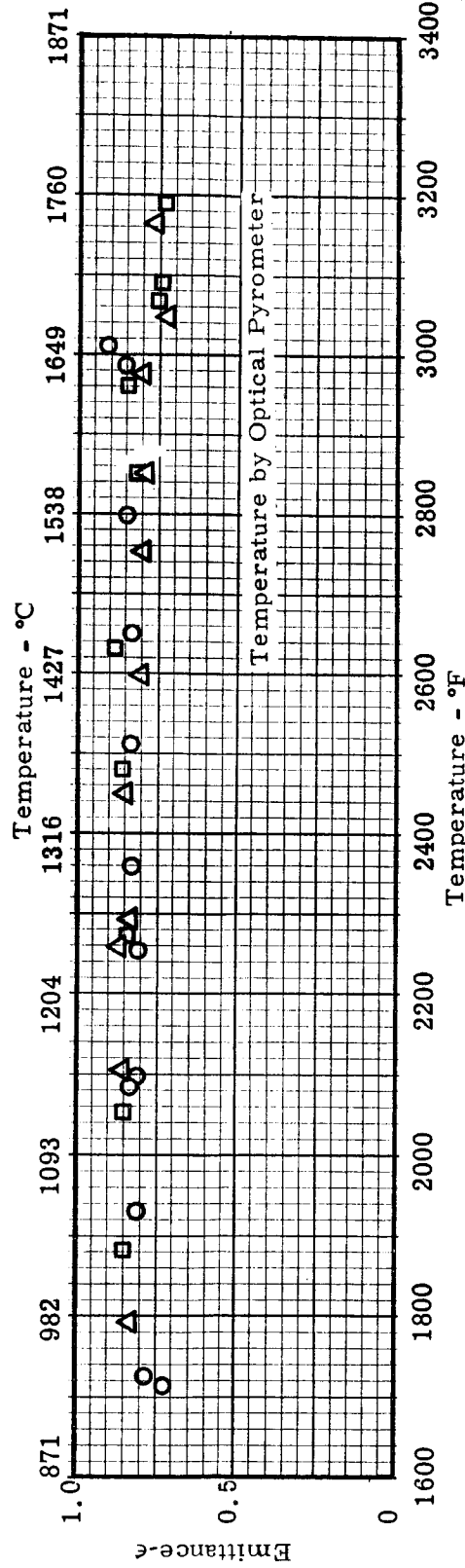


Figure 3. Stability of the Emittance of ATJ Graphite Finished with "4/0" Grit Paper, Heat Soaked at 1500°F in Air and Run in Argon (Specimen No. 3)

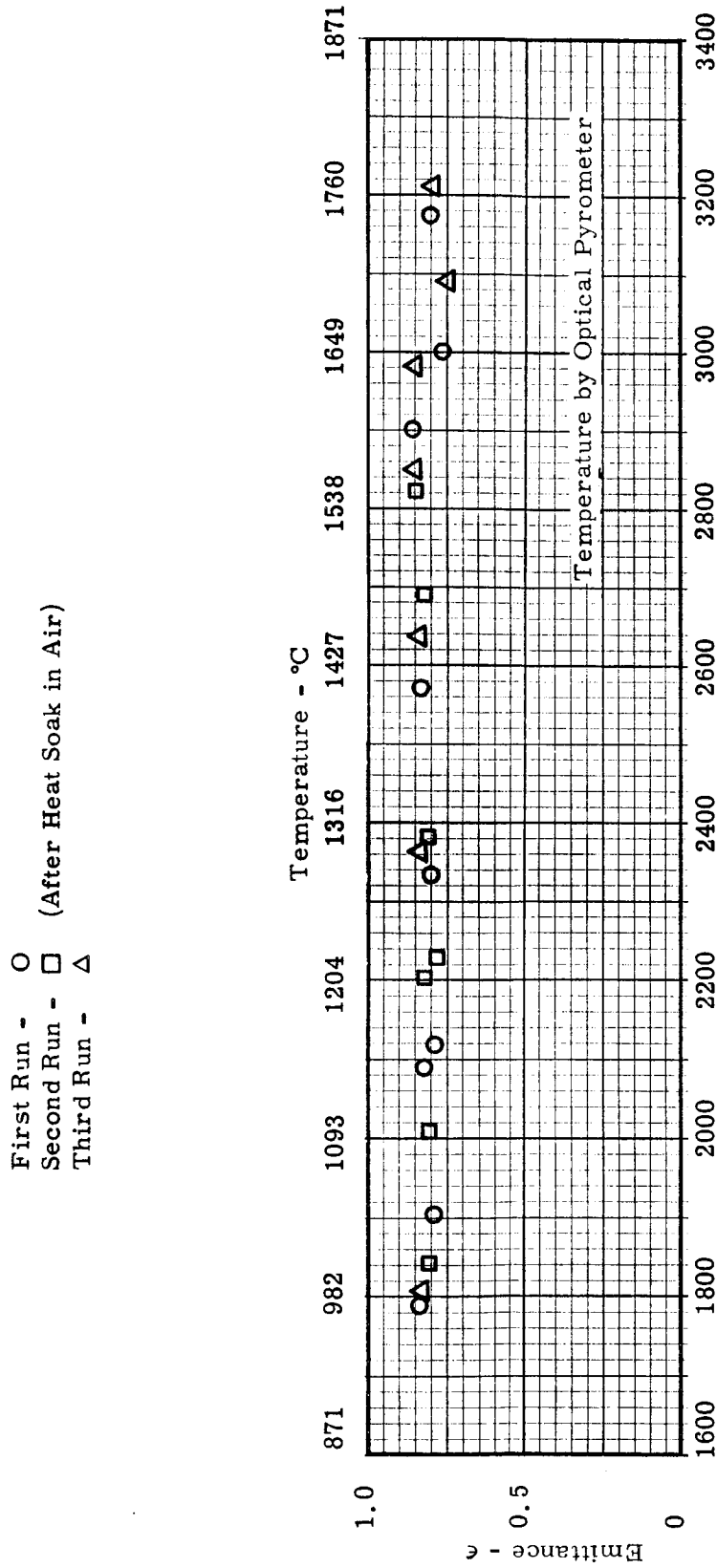


Figure 4. Stability of the Emittance of ATJ Graphite Finished with "4/0" Grit Paper Run in Argon; Specimen Heat Soaked in Air After the First Run (Specimen No. 4)

Specimen No. 3 \_\_\_\_\_  
Specimen No. 4 \_\_\_\_\_

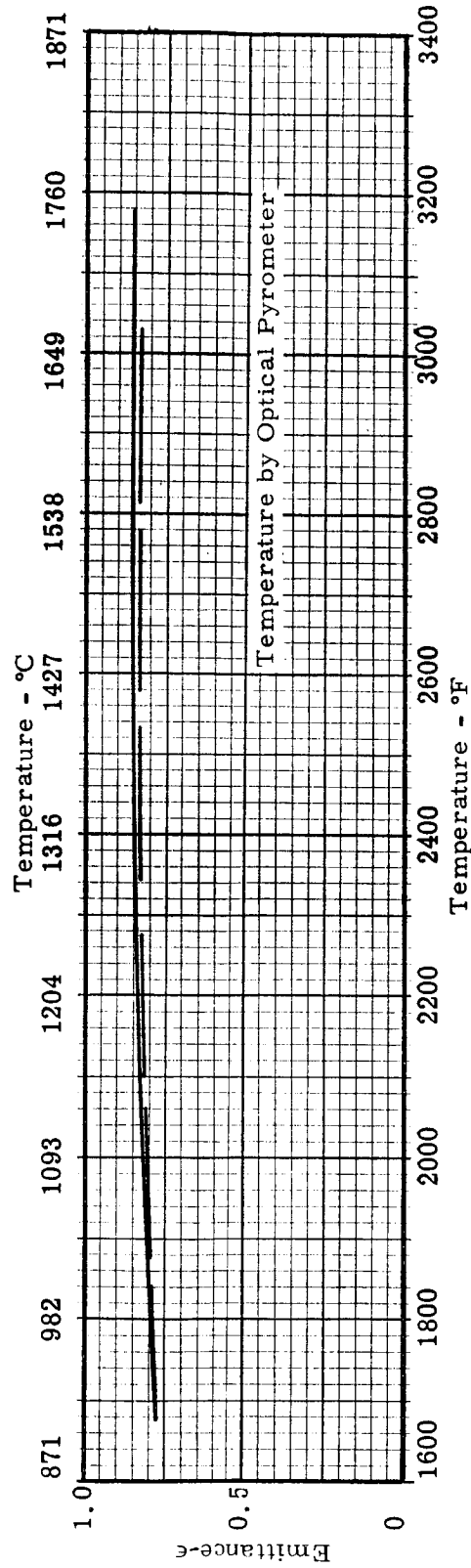


Figure 5. Comparison of the Emittances of Two "4/0" ATJ Graphite Specimens Finished with "4/0" Grit Paper; First Run for Each in Argon with Prior Heat Soak in Air

Specimen No. 3 \_\_\_\_\_  
Specimen No. 4 \_\_\_\_\_

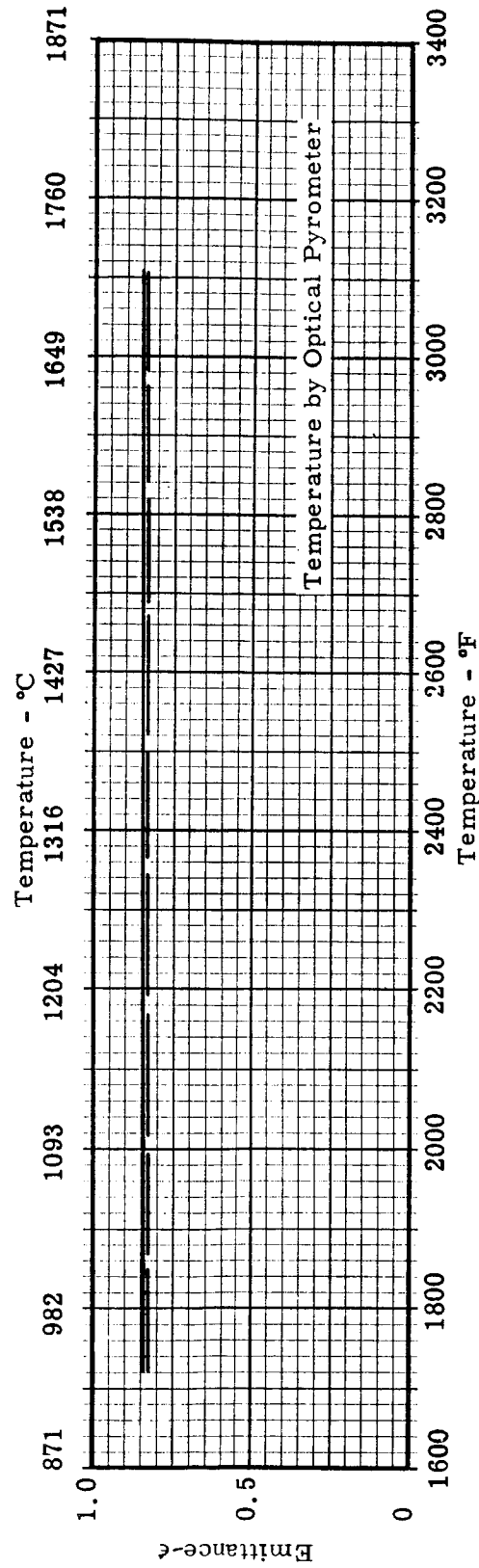


Figure 6. Comparison of the Emittances of Two ATJ Graphite Specimens Finished with "4/0" Grit Paper During the Second Run for Each in Argon with Prior Heat Soak in Air

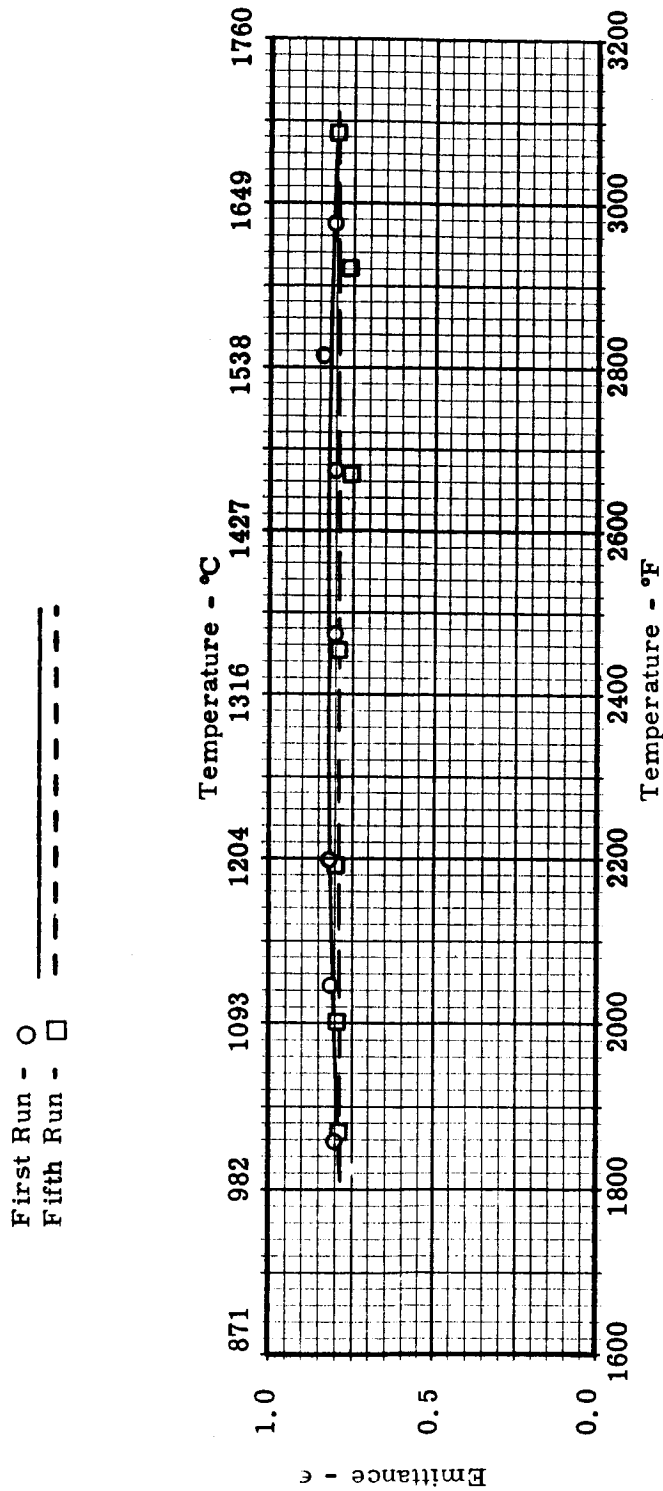


Figure 7. Emittance of ATJ Graphite During the First and Fifth Runs in Argon with Prior Heat Soak in Air (Specimen 5)

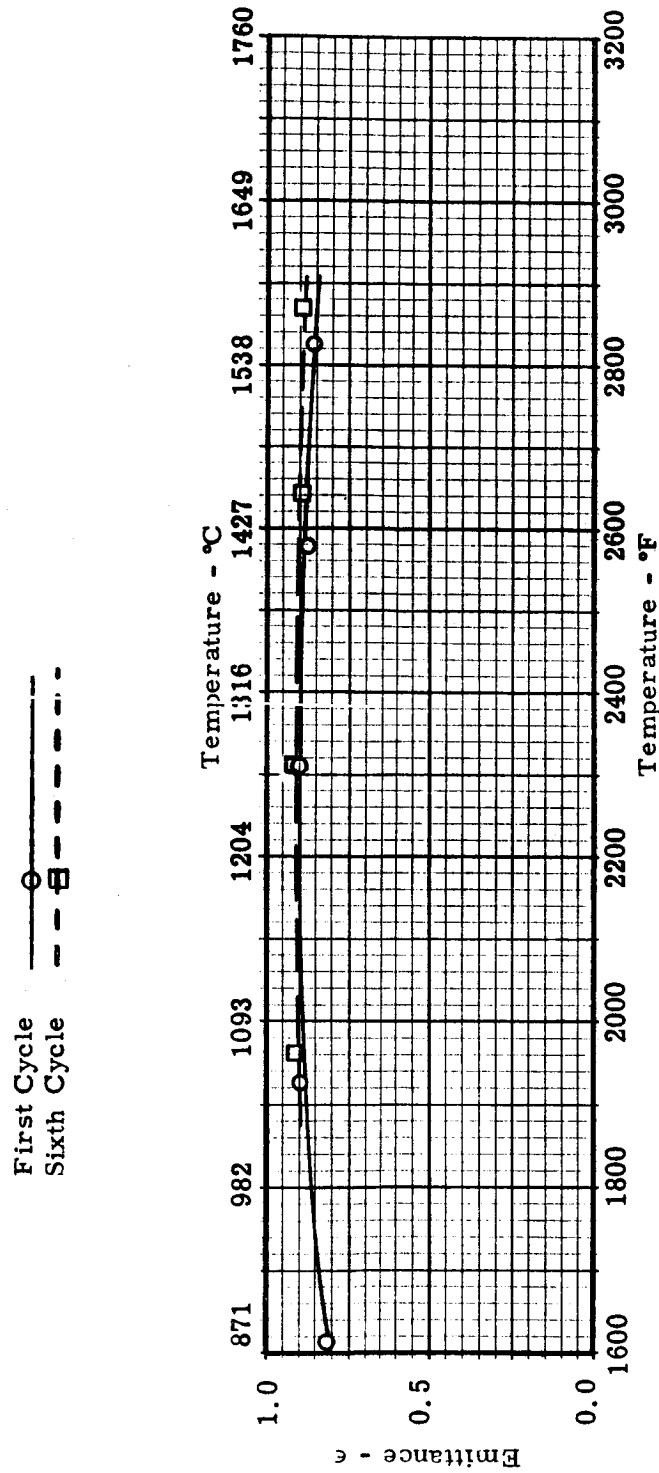


Figure 8. Emittance of ATJ Graphite During the First and Sixth Runs in Argon with Prior Heat Soak in Air (Specimen No. 2)

First Cycle  
Sixth Cycle

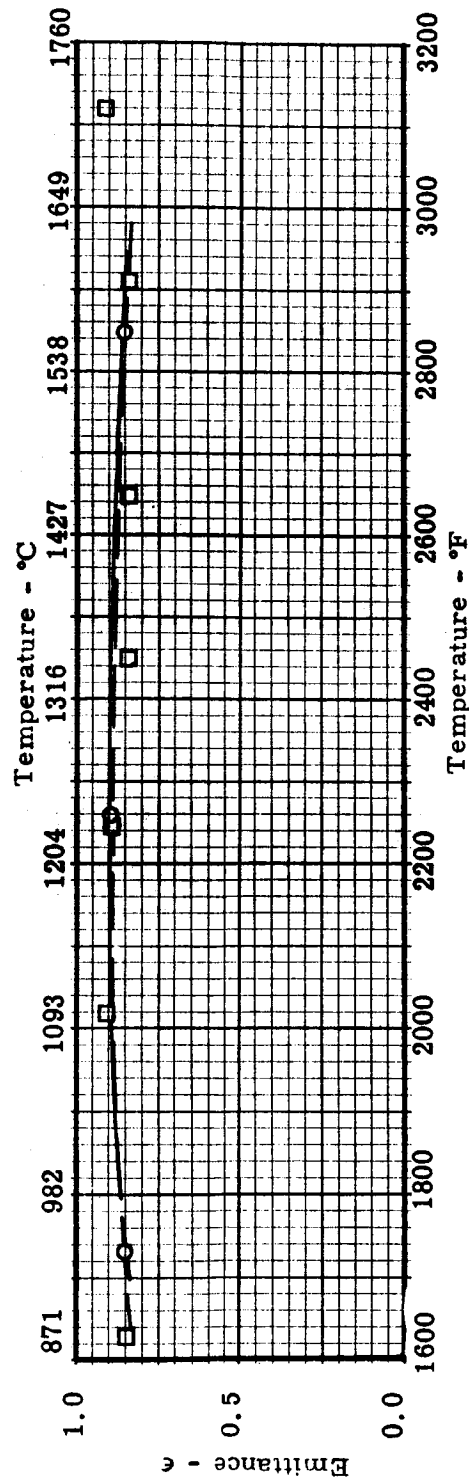


Figure 9. Emittance of ATJ Graphite During the First and Sixth Runs in Argon with Prior Heat Soak in Air (Specimen No. 3)



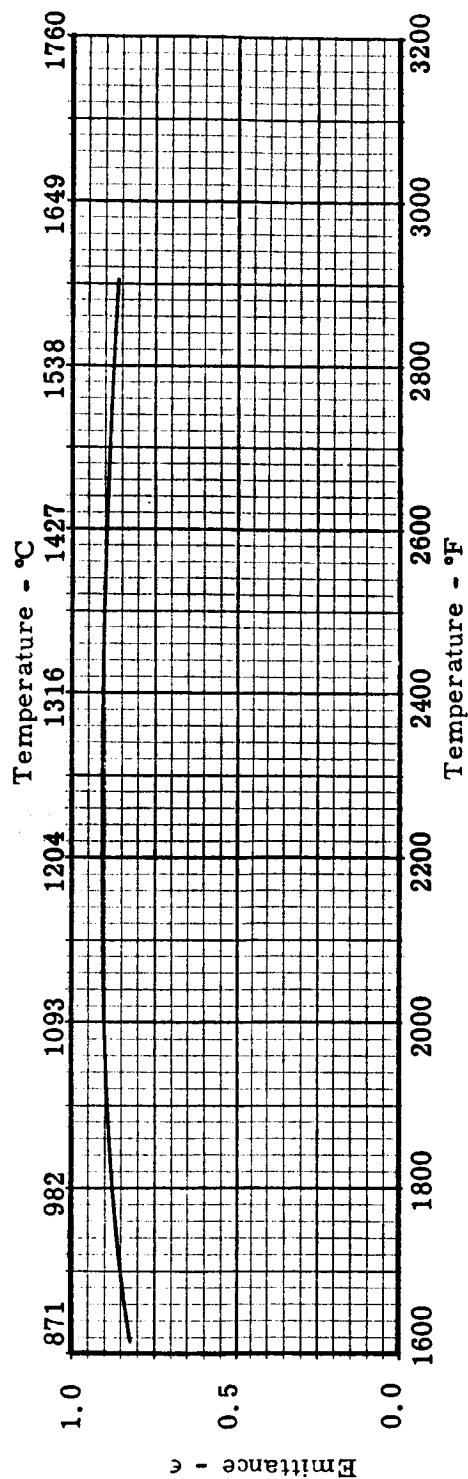


Figure 10. Emittance of Two ATJ Graphite Specimens During the First Run for Each in Argon with Prior Heat Soak in Air (Specimens No. 2 and 3)

Specimen No. 2 ———  
 Specimen No. 3 - - - - -

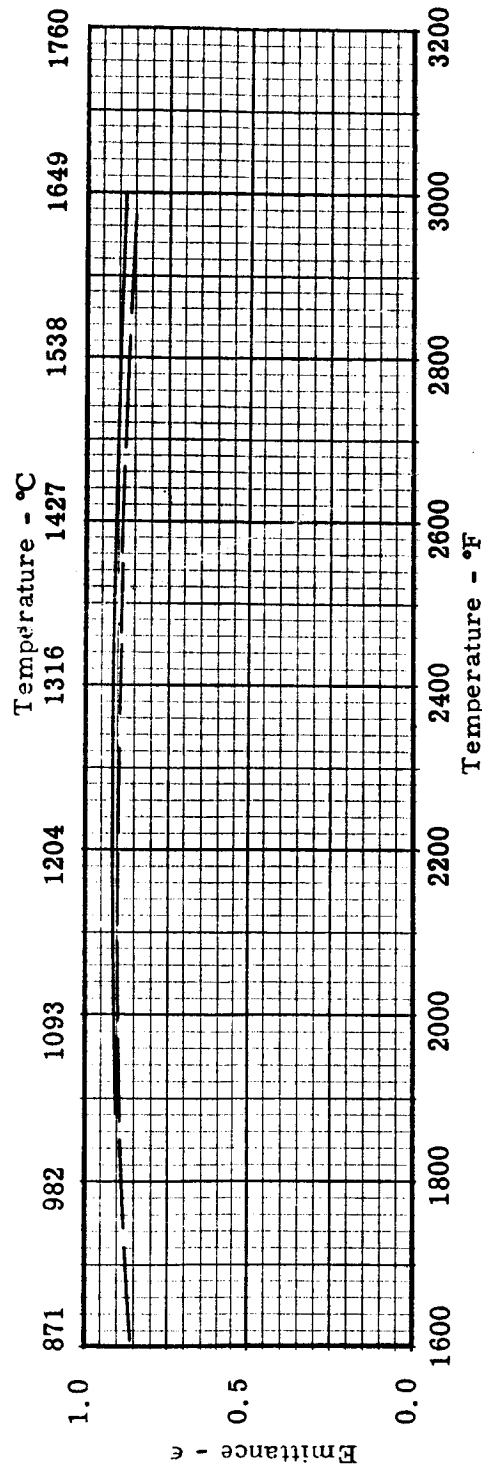


Figure 11. Comparison of the Emittances of Two ATJ Graphite Specimens During the Sixth Run for each in Argon; Specimens Were Heat Soaked in Air Prior to the First Run in Argon

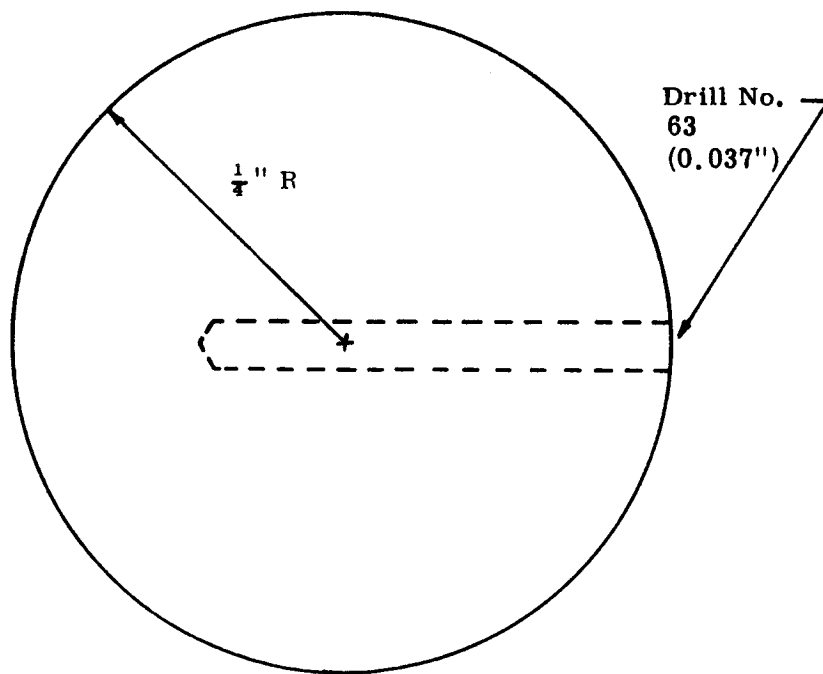
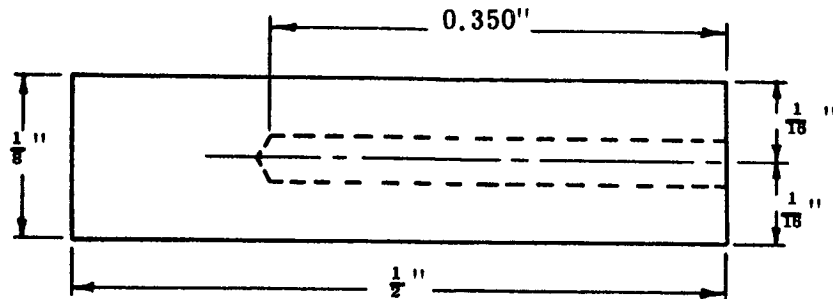


Figure 12. Drawing Showing the Location of the Thermocouple Well in the  $\frac{1}{2}$ " Diameter Graphite Specimen

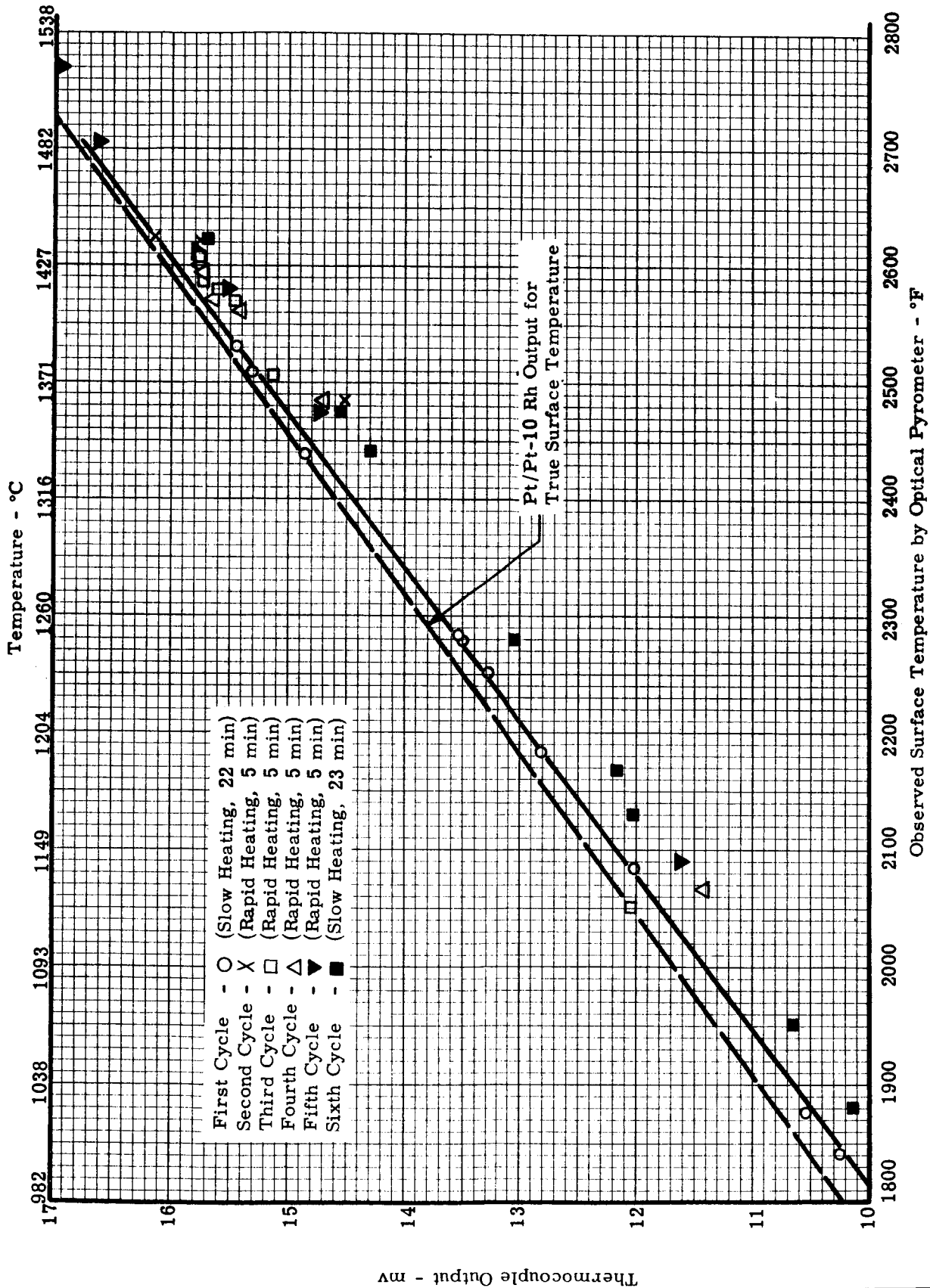


Figure 13. Effect of Slow and Rapid Thermal Cycling on an Unprotected Pt/Pt-10 Rh Thermocouple in a Graphite Specimen (Specimen No. 1)

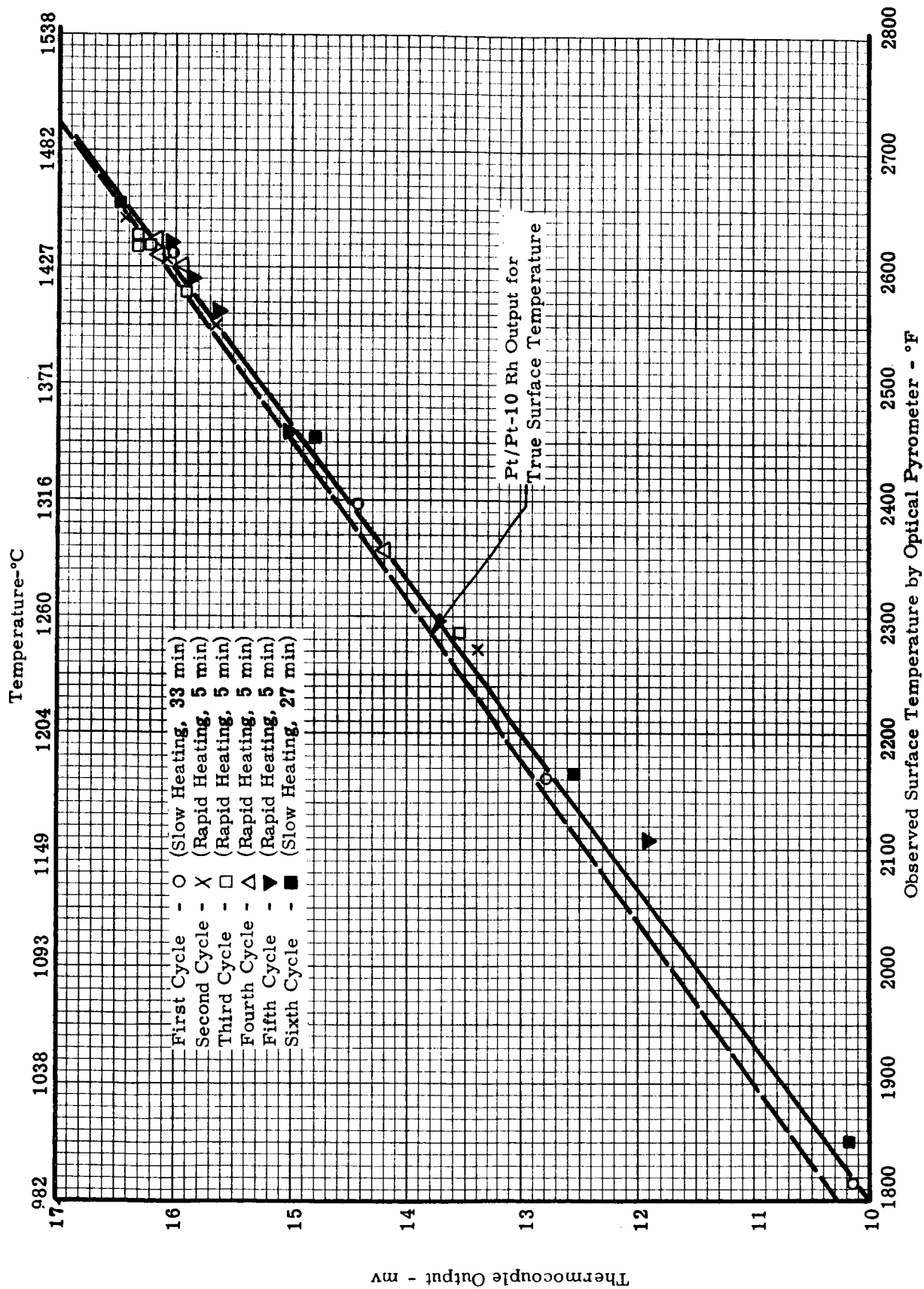


Figure 14. Effect of Slow and Rapid Thermal Cycling on an Unprotected Pt/Pt-10 Rh Thermocouple in a Graphite Specimen (Specimen No. 2)

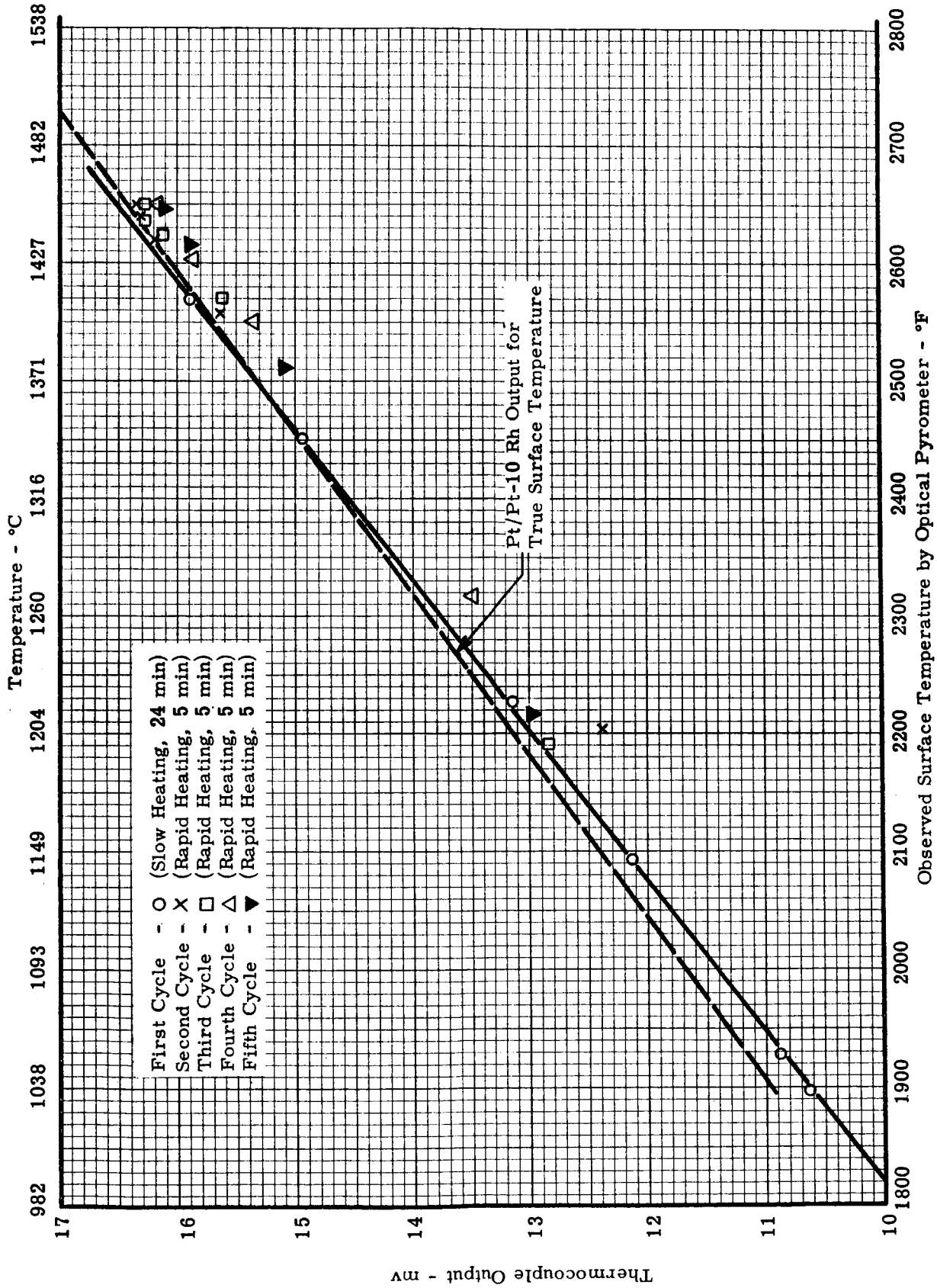


Figure 15. Effect of Slow and Rapid Thermal Cycling on an Unprotected Pt/Pt-10 Rh Thermocouple in a Graphite Specimen (Specimen No. 3)

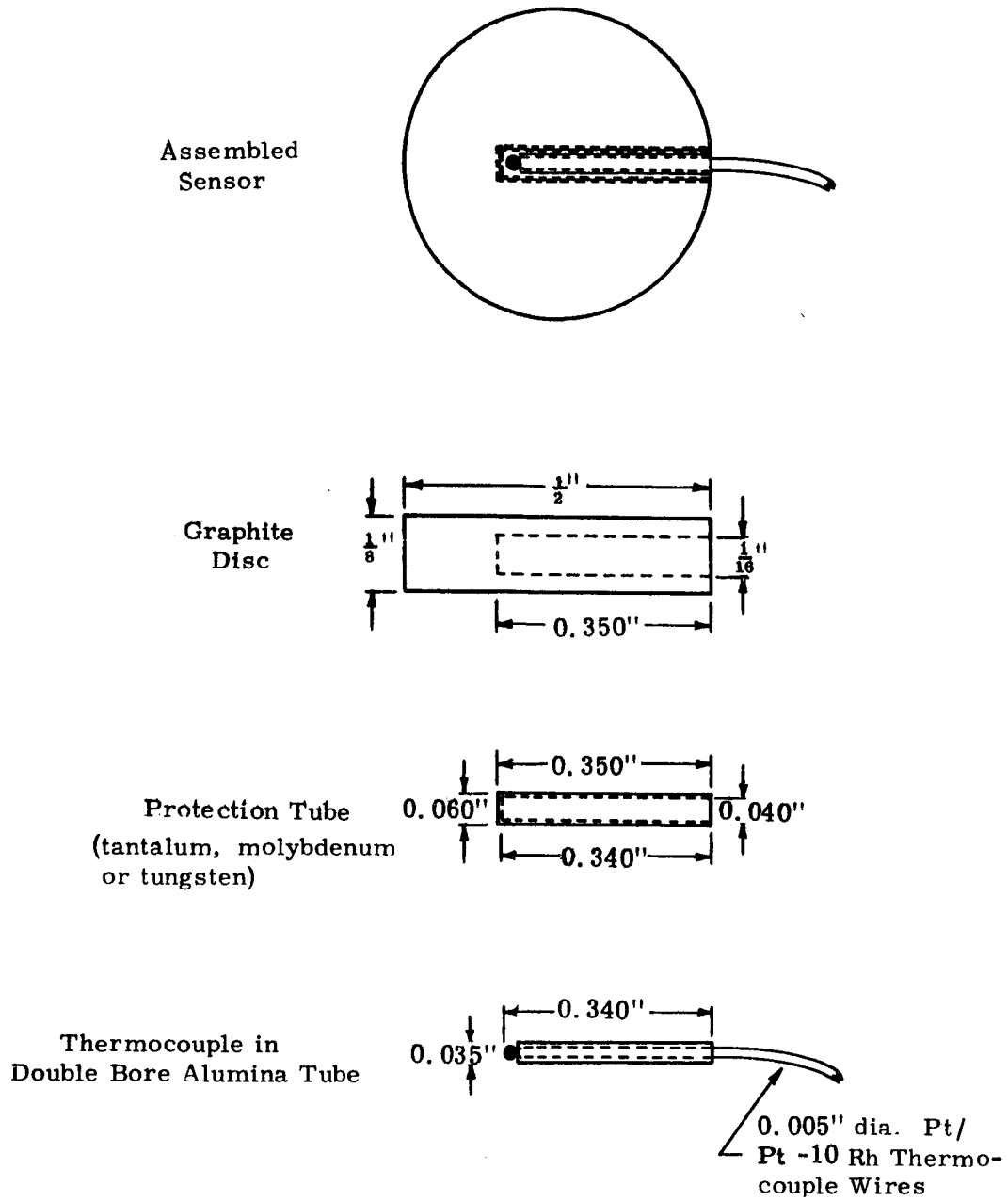


Figure 16. Configuration of Assembled Sensing Element and Components Used in Evaluating Effect of Protection Tube on Thermocouple Output

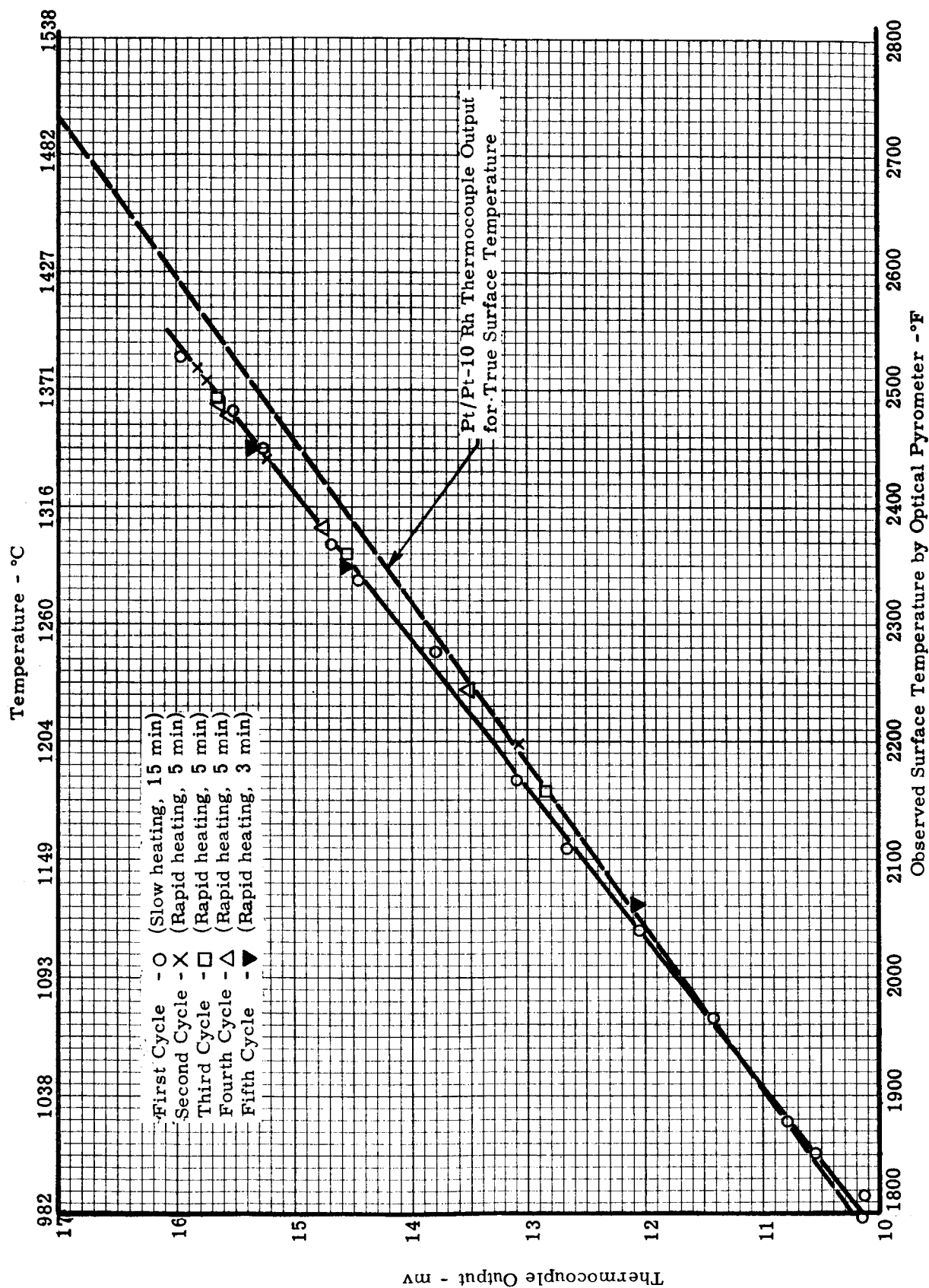


Figure 17. The Effect of Thermal Cycling on a Pt/Pt-10 Rh Thermocouple in a Molybdenum Protection Tube (Specimen No. 1)



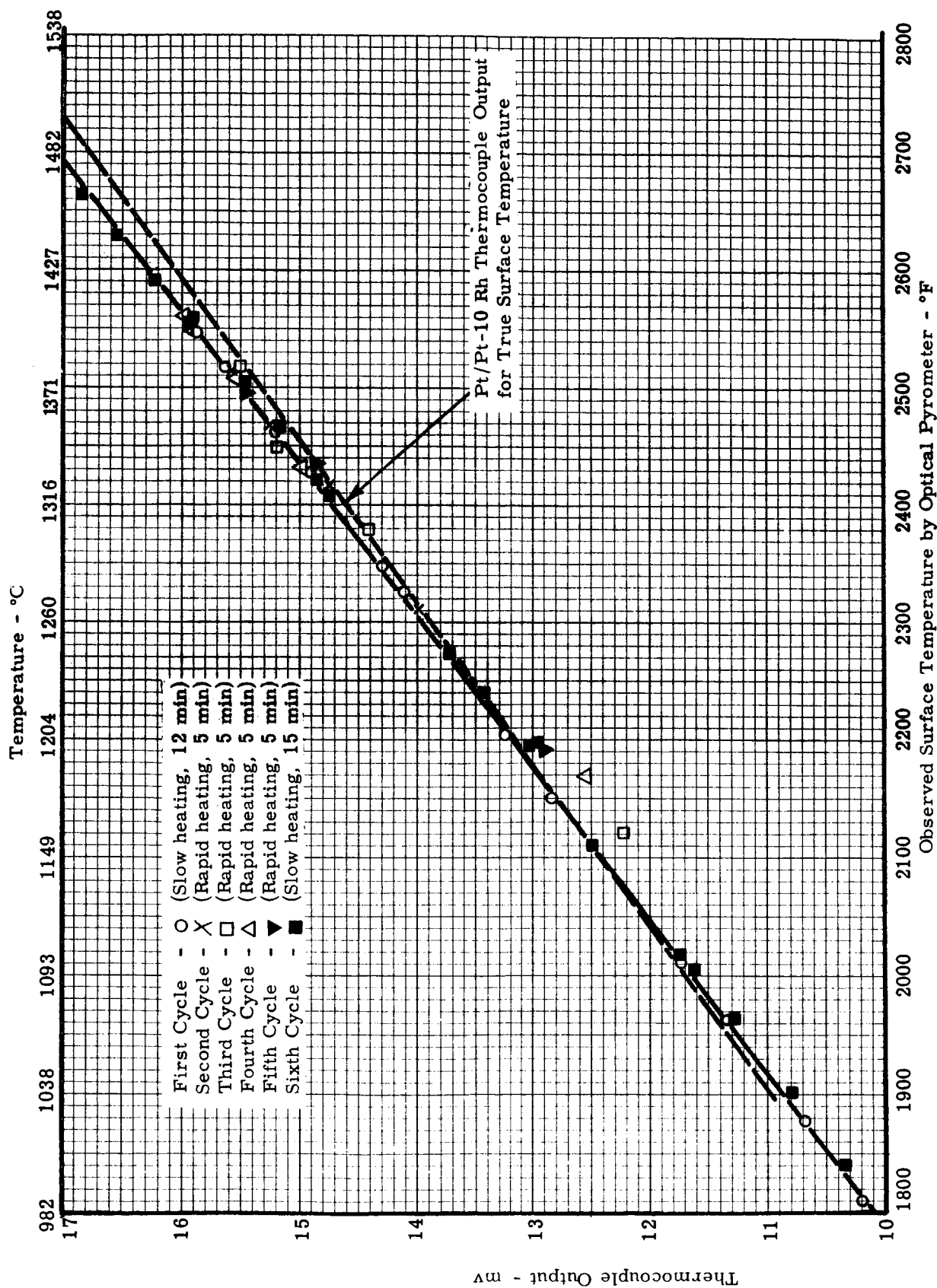


Figure 18. The Effect of Thermal Cycling on a Pt/Pt-10 Rh Thermocouple in a Molybdenum Protection Tube (Specimen No. 2)

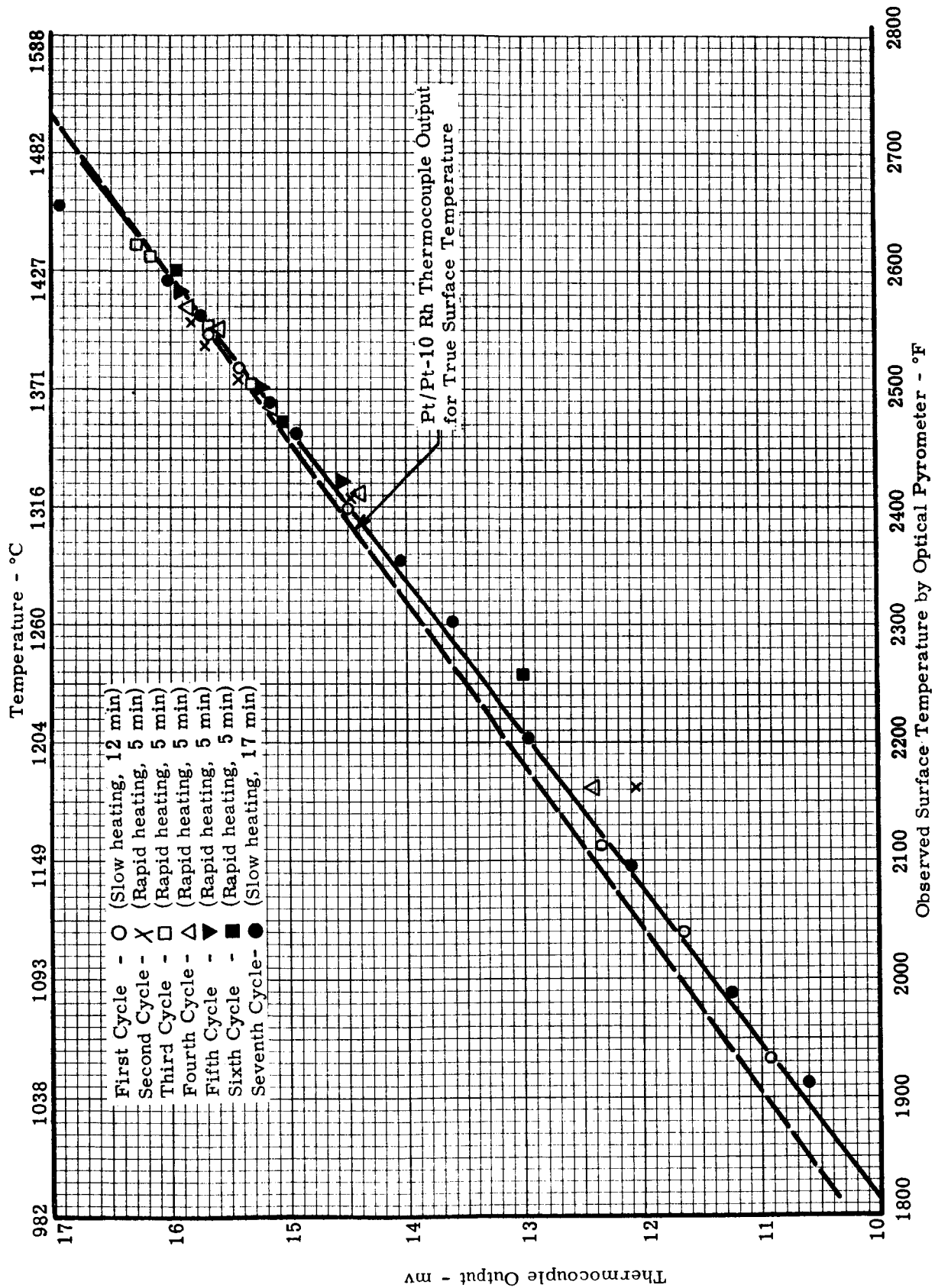


Figure 19. The Effect of Thermal Cycling on a Pt/Pt-10 Rh Thermocouple in a Tantalum Protection Tube (Specimen No. 2)

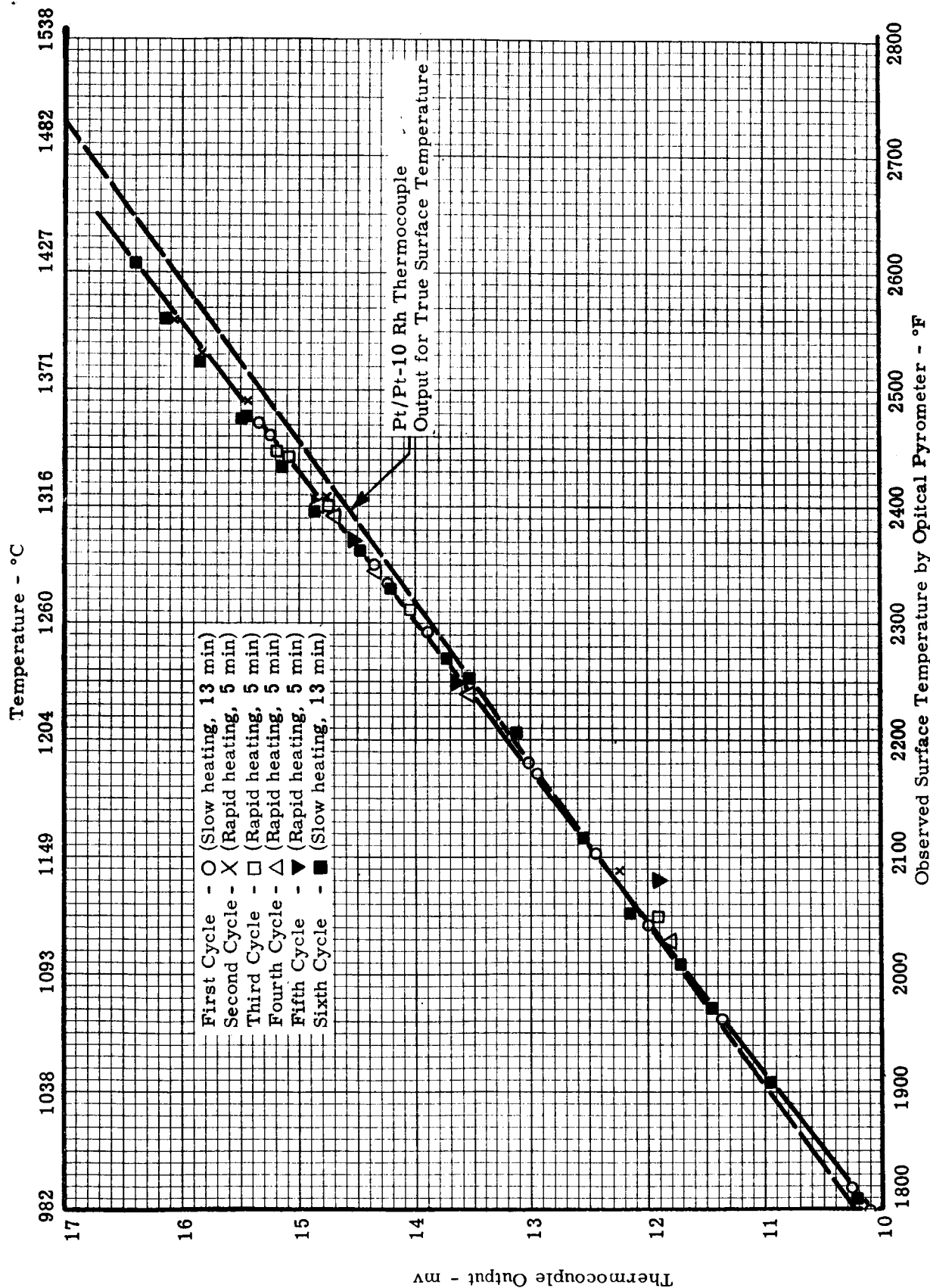


Figure 20. The Effect of Thermal Cycling on a Pt/Pt-10 Rh Thermocouple in a Tungsten Protection Tube (Specimen No. 2)

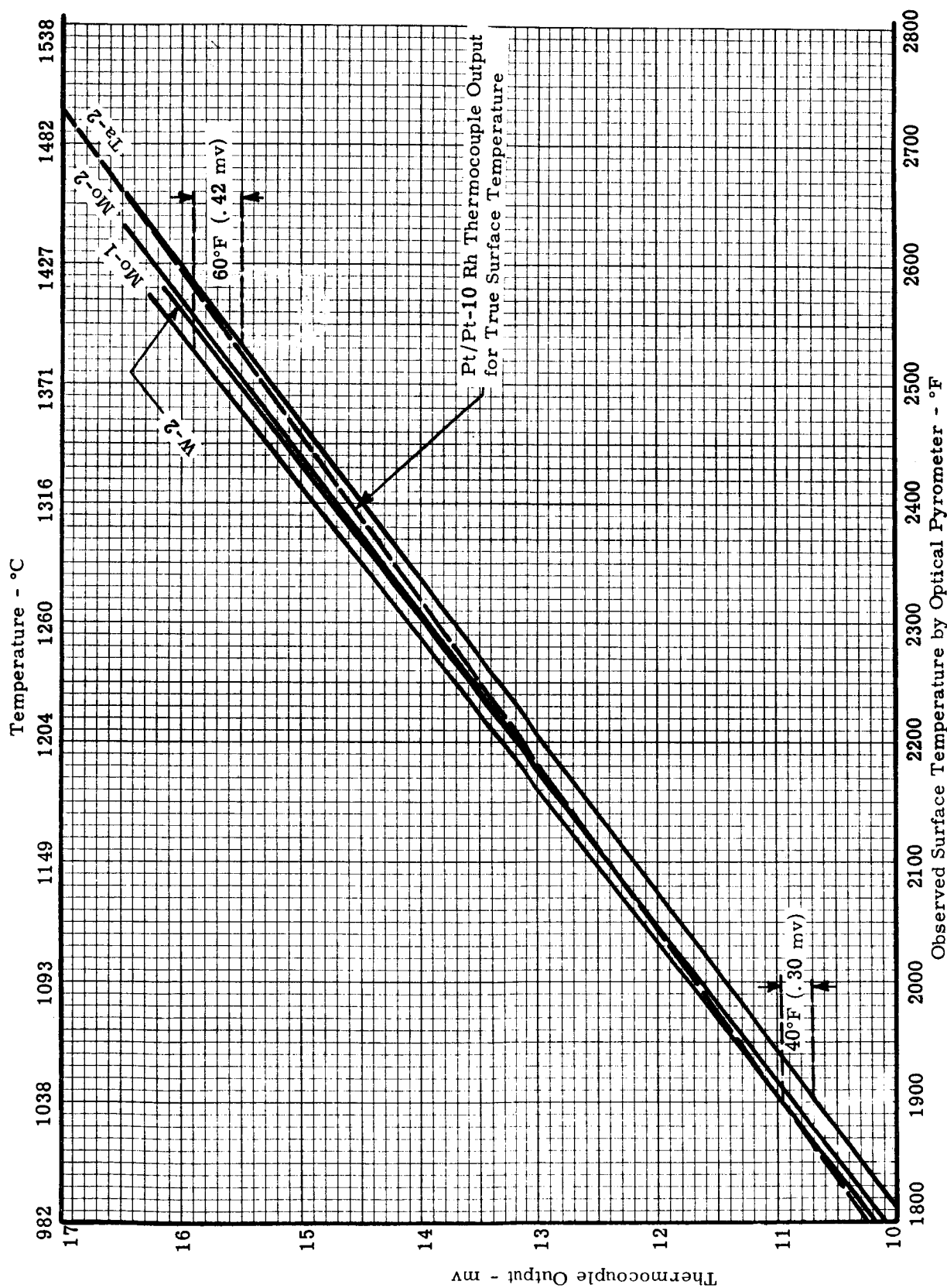


Figure 21. Comparison of the Thermoelectric Output from Four Pt/Pt-10 Rh Thermocouples During the First Cycle for Each in Protection Tubes

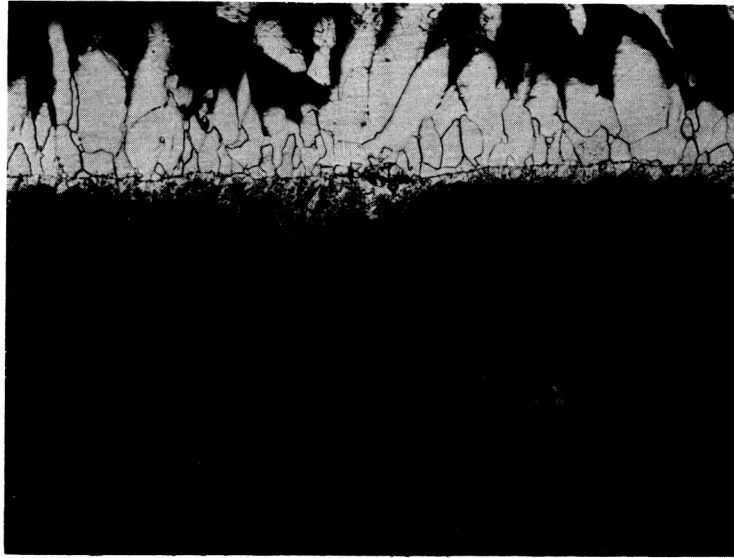


Figure 22 Photomicrograph of Molybdenum Vapor Deposited onto ATJ Graphite  
Specimen No. 1, 150X

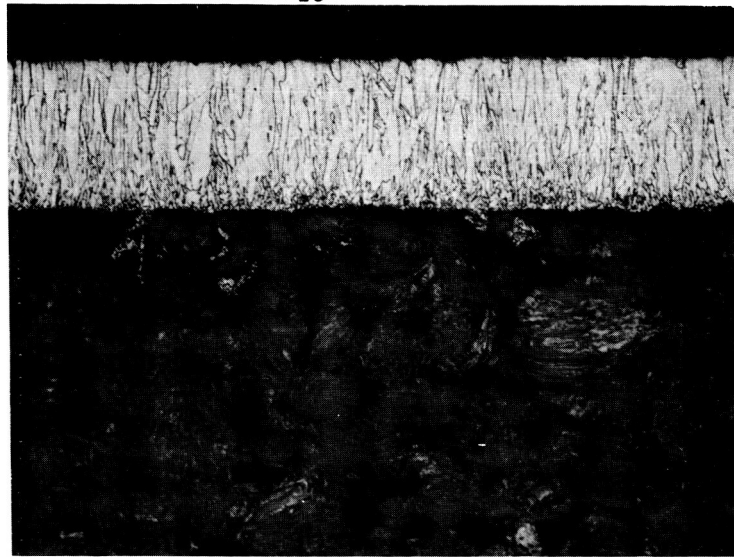
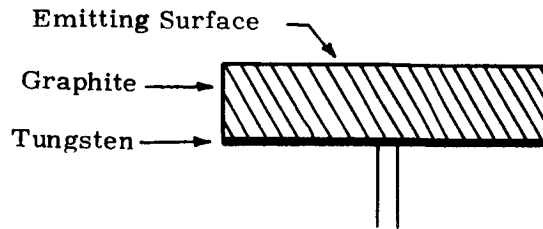


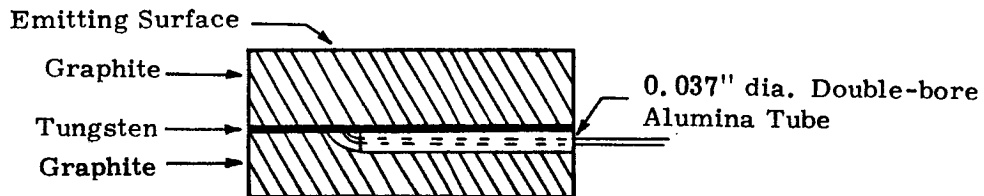
Figure 23 Photomicrograph of Tungsten Vapor Deposited onto  
ATJ Graphite Specimen No. 15, 150X



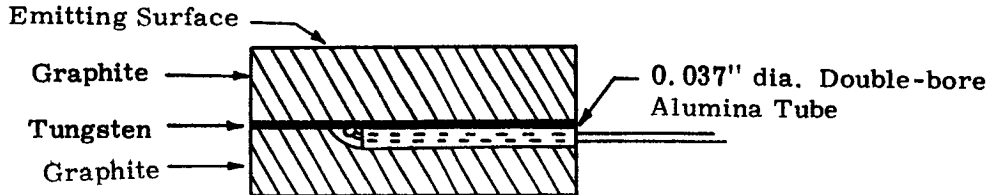
Figure 24 Photomicrograph of Tungsten Vapor Deposited onto  
ATJ Graphite Specimen No. 15 After Thermal Cycling  
to 3000°F (1649°C), 150X



- a. Pt/Pt-10 Rh thermocouple leads flash-welded individually to vapor deposited, tungsten diffusion barrier.



- b. Pt/Pt-10 Rh thermocouple wire in a double-bore alumina tube with leads flash-welded individually to vapor deposited, tungsten diffusion barrier.



- c. Pt/Pt-10 Rh thermocouple wire in a double-bore alumina tube with the thermocouple bead flash-welded to the vapor deposited, tungsten diffusion barrier.

Figure 25. The Configuration of Three Types of Sensing Element Assemblies Evaluated

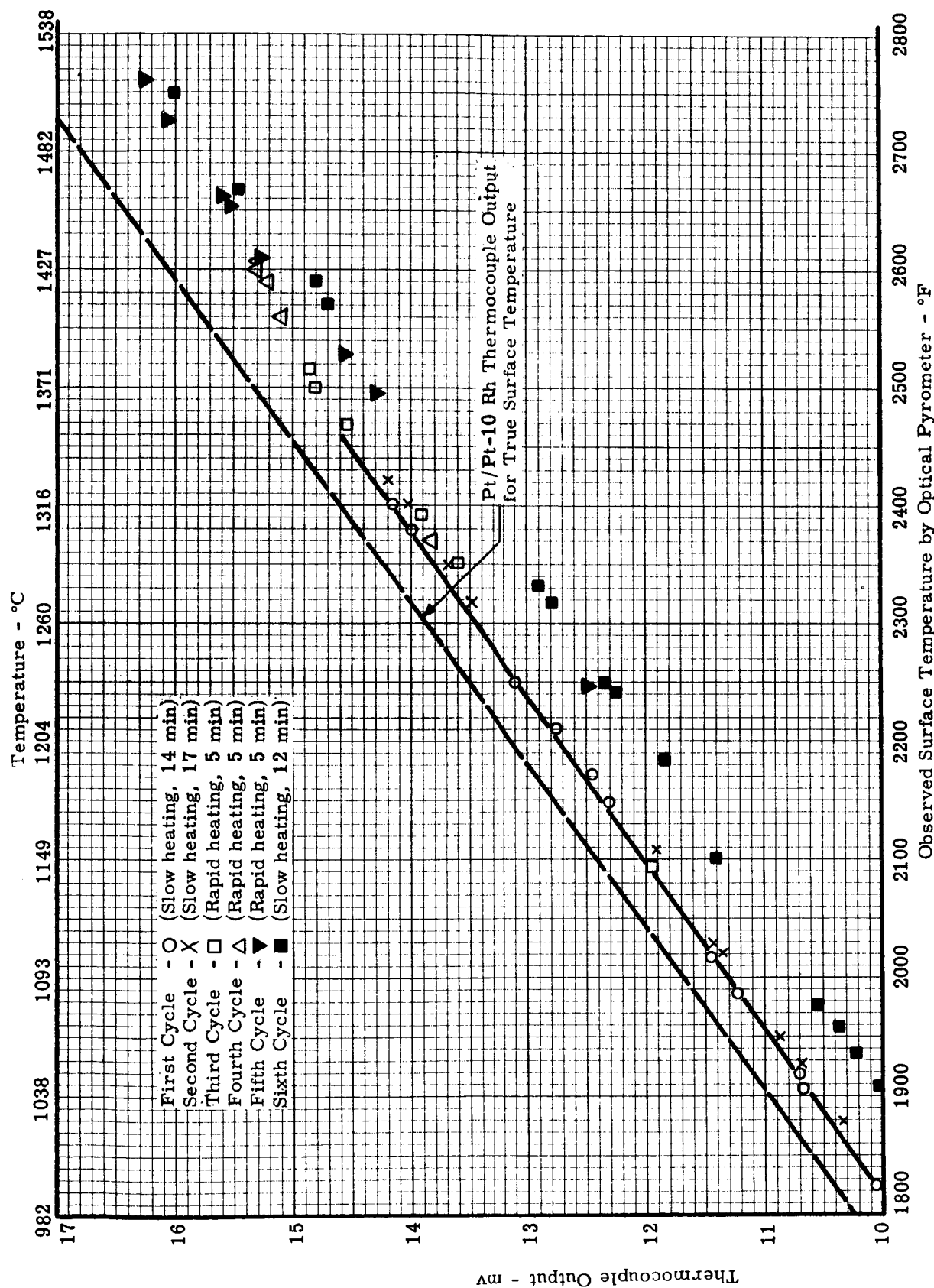


Figure 26. The Effect of Thermal Cycling on a Pt/Pt-10 Rh Thermocouple Flash-Welded to the Tungsten Diffusion Barrier on a Graphite Substrate. See Figure 25a (Specimen No. 22)(Graphite Surface was Pre-oxidized)

Tungsten Thickness = 2.32 mils



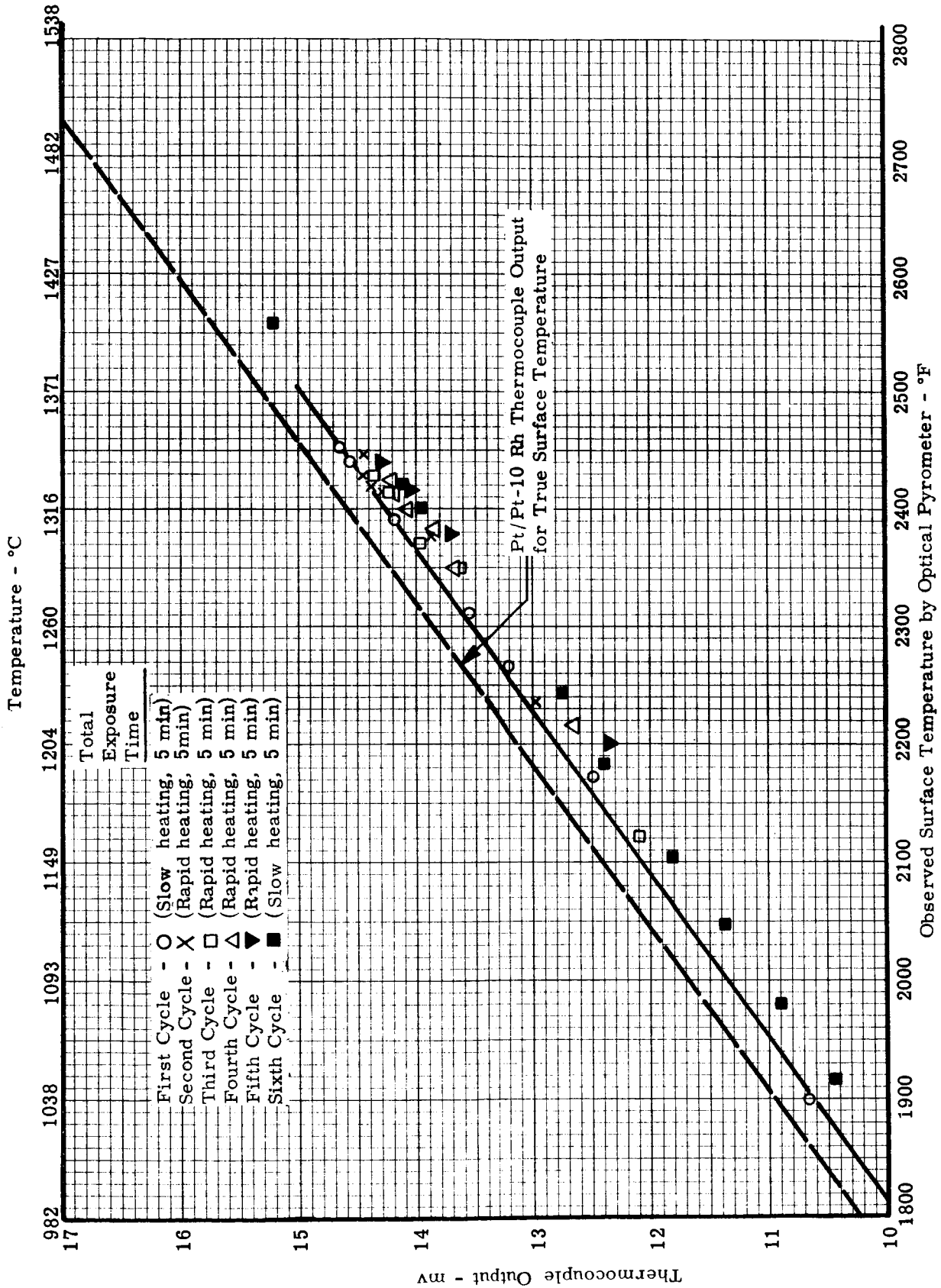


Figure 27. The Effect of Thermal Cycling on Pt/Pt-10 Rh Thermocouple Flash-Welded to the Tungsten Diffusion Barrier on a Graphite Substrate. See Figure 25a (Specimen No. 23)(Graphite Surface was Pre-oxidized.)

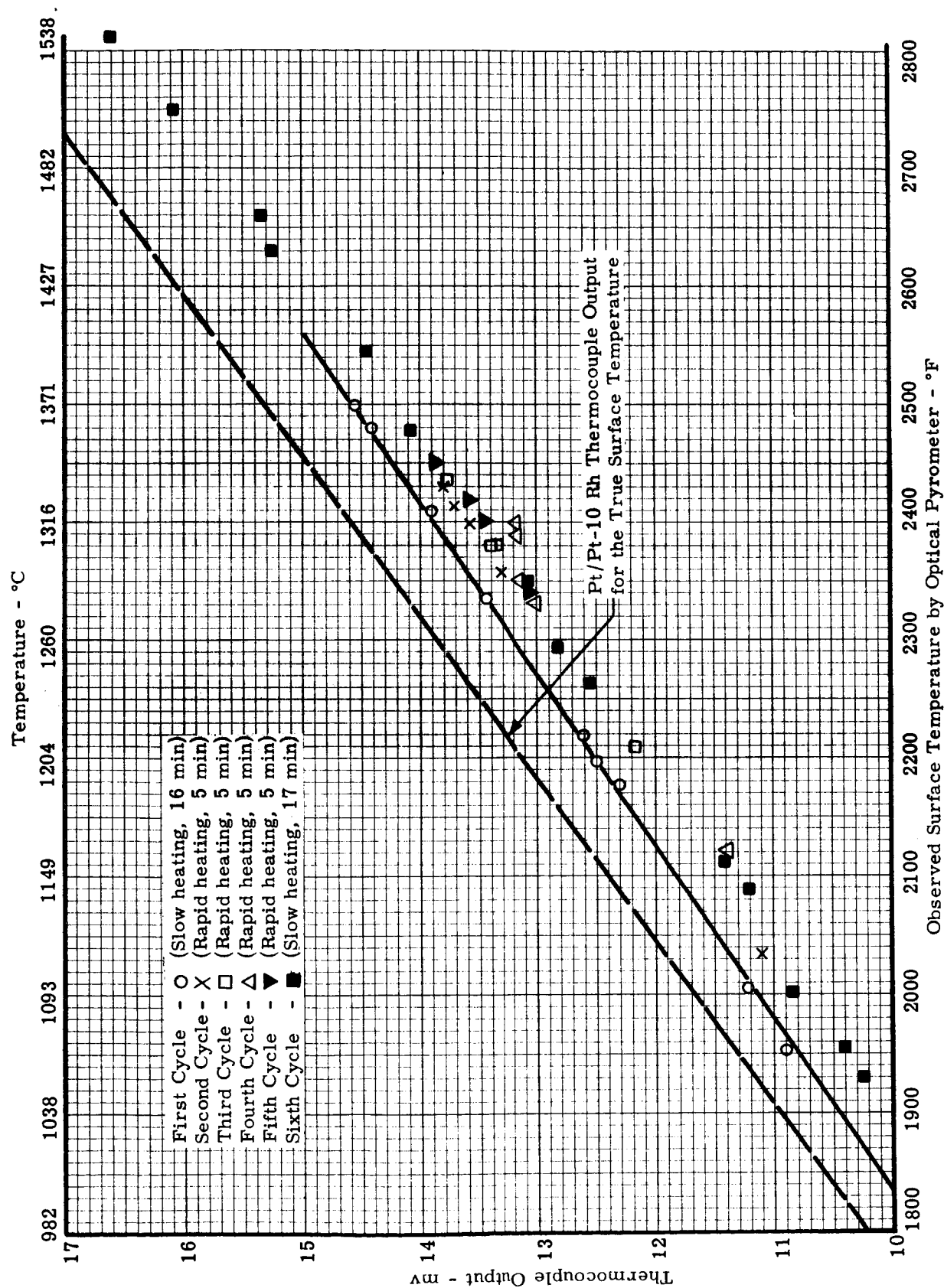


Figure 28. The Effect of Thermal Cycling on a Pt/Pt-10 Rh Thermocouple Flash-Welded to the Tungsten Diffusion Barrier on a Graphite Substrate. See Figure 25a. (Specimen No. 25)(Graphite Surface Finished with Medium Grit Paper)

Tungsten Thickness = 2.26 mils.

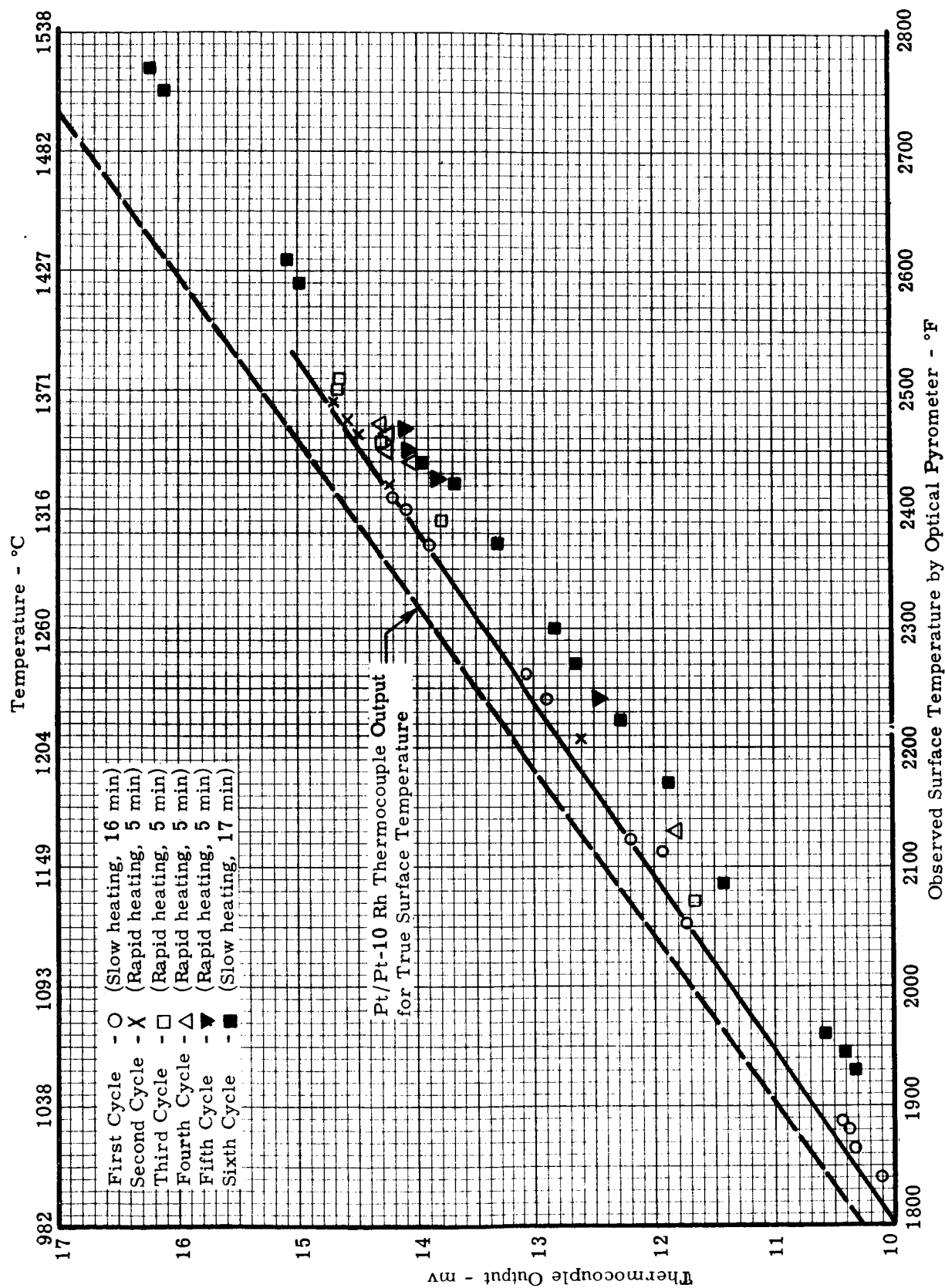


Figure 29. The Effect of Thermal Cycling on a Pt/Pt-10 Rh Thermocouple Flash-Welded to the Tungsten Diffusion Barrier on a Graphite Substrate. See Figure 25a. (Specimen No. 26)(Graphite Surface Finished with Medium Grit Paper)

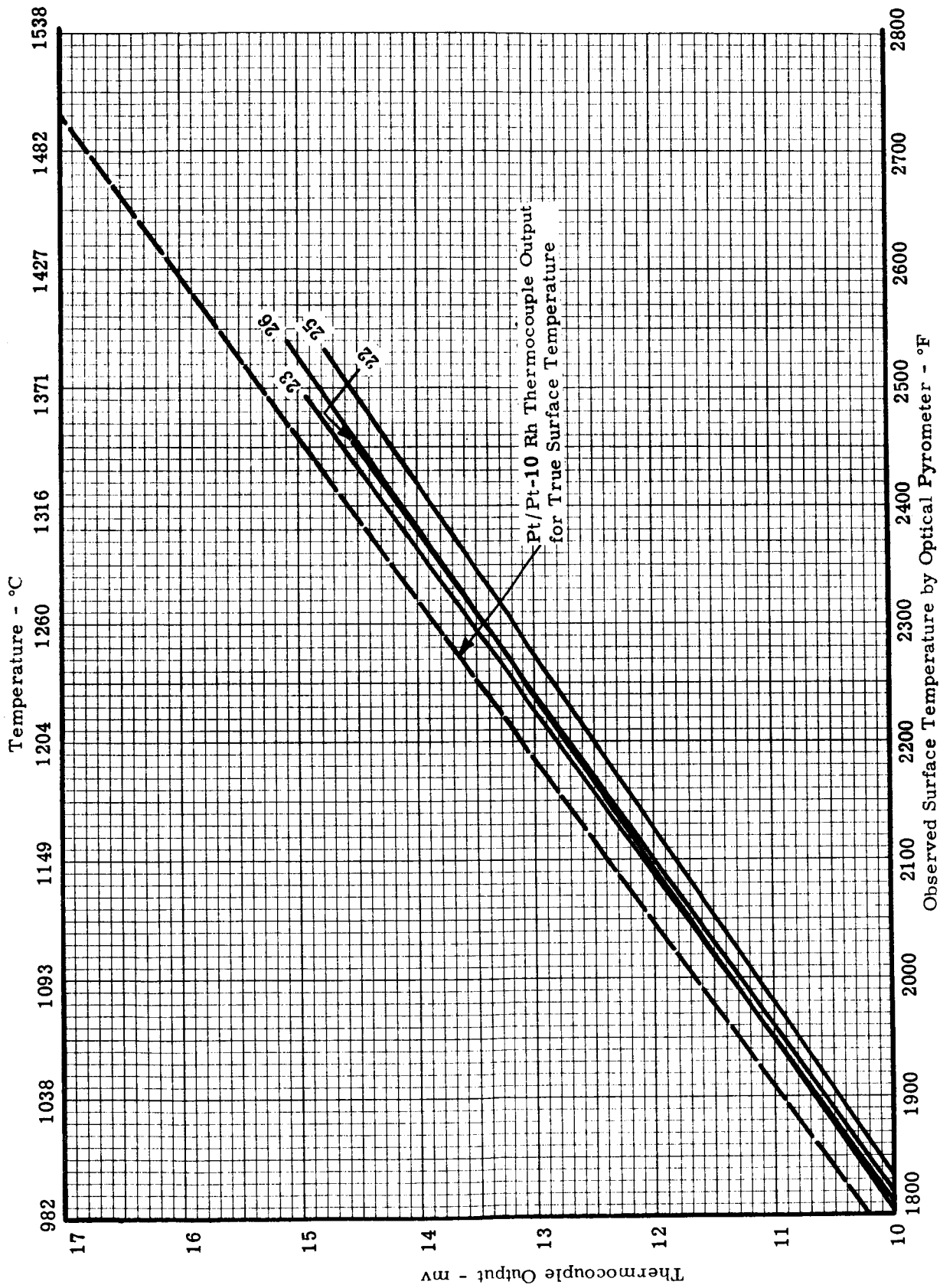


Figure 30. Comparison of the Thermoelectric Output from Four Sensor Assemblies of the Type in Figure 25a. During the First Cycle for Each

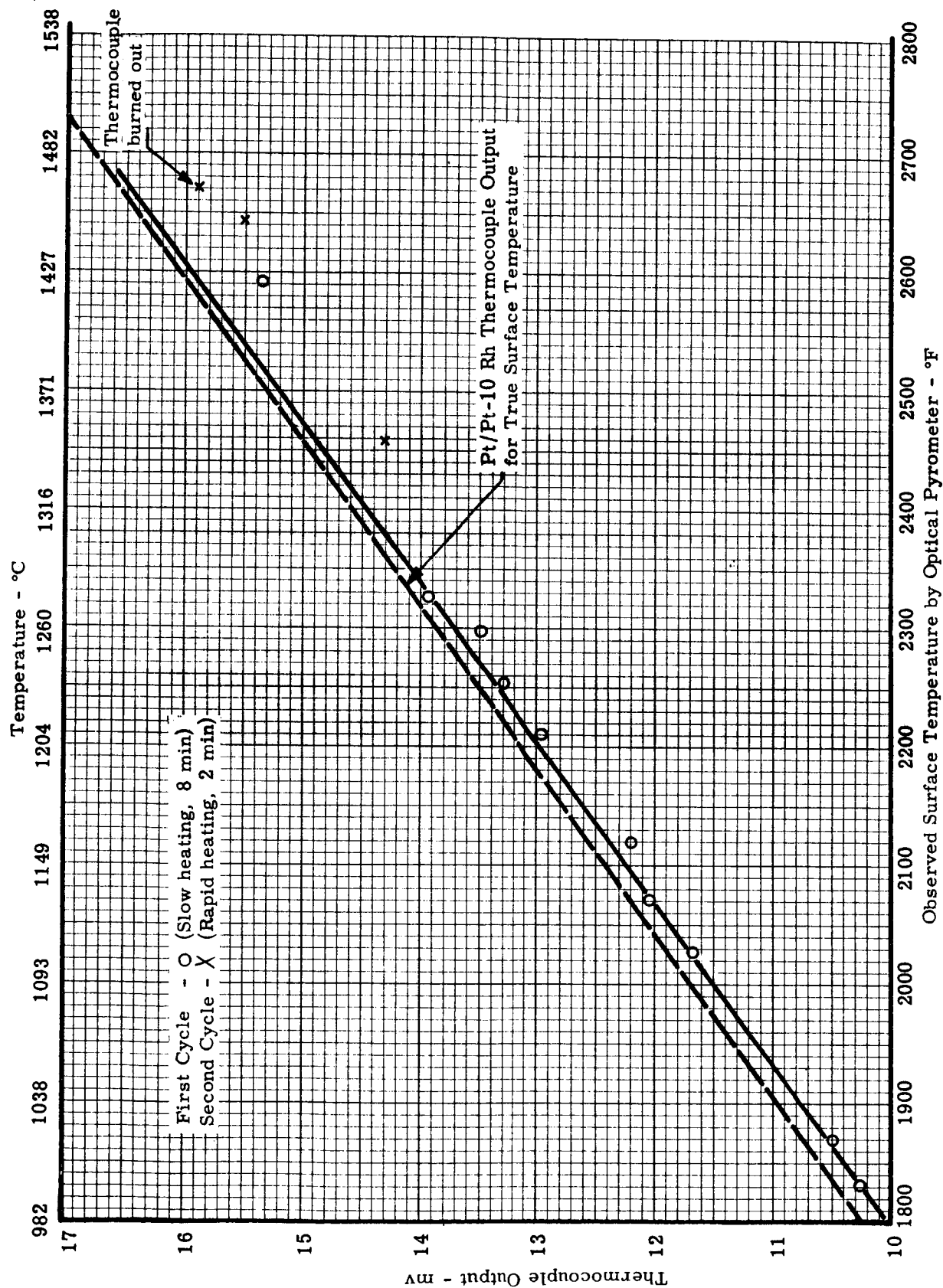


Figure 31. The Effect of Thermal Cycling on a Pt/Pt-10 Rh Thermocouple Flash-Welded to the Tungsten Diffusion Barrier on a Graphite Substrate. See Figure 25b (Specimen No. 27)

Tungsten Thickness = 5.56 mils

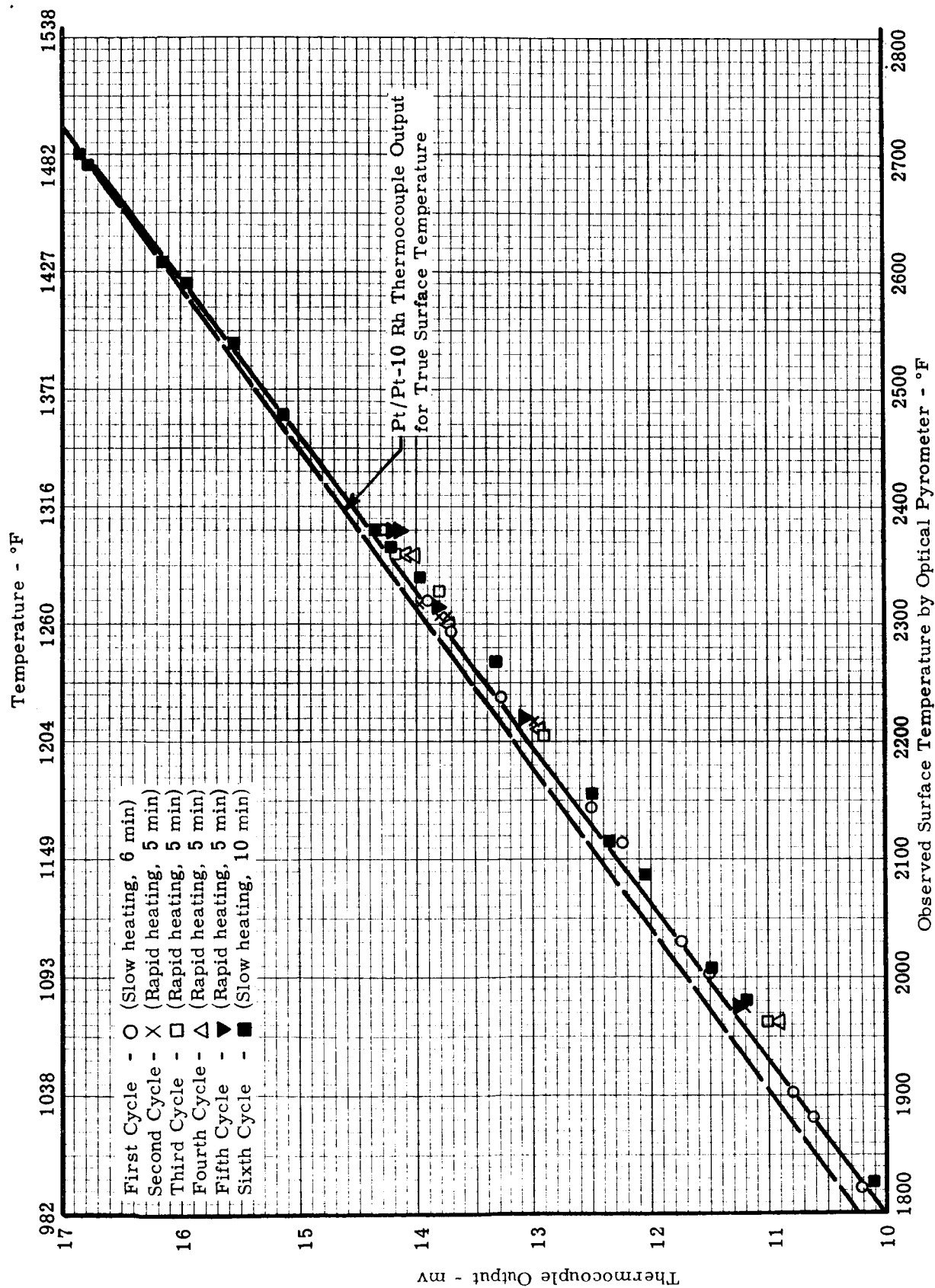


Figure 32. The Effect of Thermal Cycling on a Pt/Pt-10 Rh Thermocouple Flash-Welded to the Tungsten Diffusion Barrier on a Graphite Substrate. See Figure 25b (Specimen No. 28)

Tungsten Thickness - 6.05 mils.

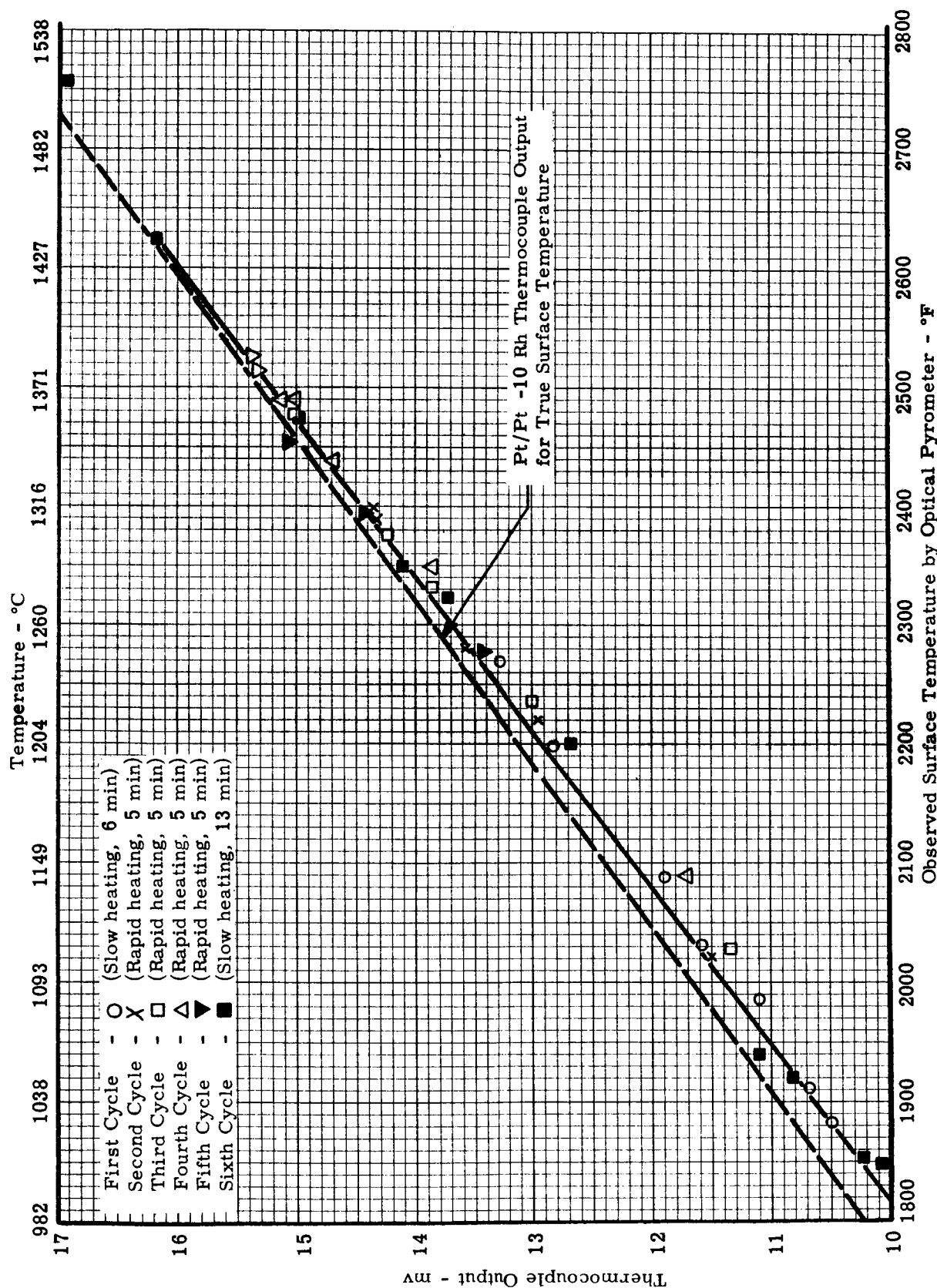


Figure 33. The Effect of Thermal Cycling on a Pt/Pt-10 Rh Thermocouple Flash - Welded to a Tungsten Diffusion Barrier on a Graphite Substrate. See Figure 25c (Specimen No. 29)

Tungsten Thickness = 1.39 mils

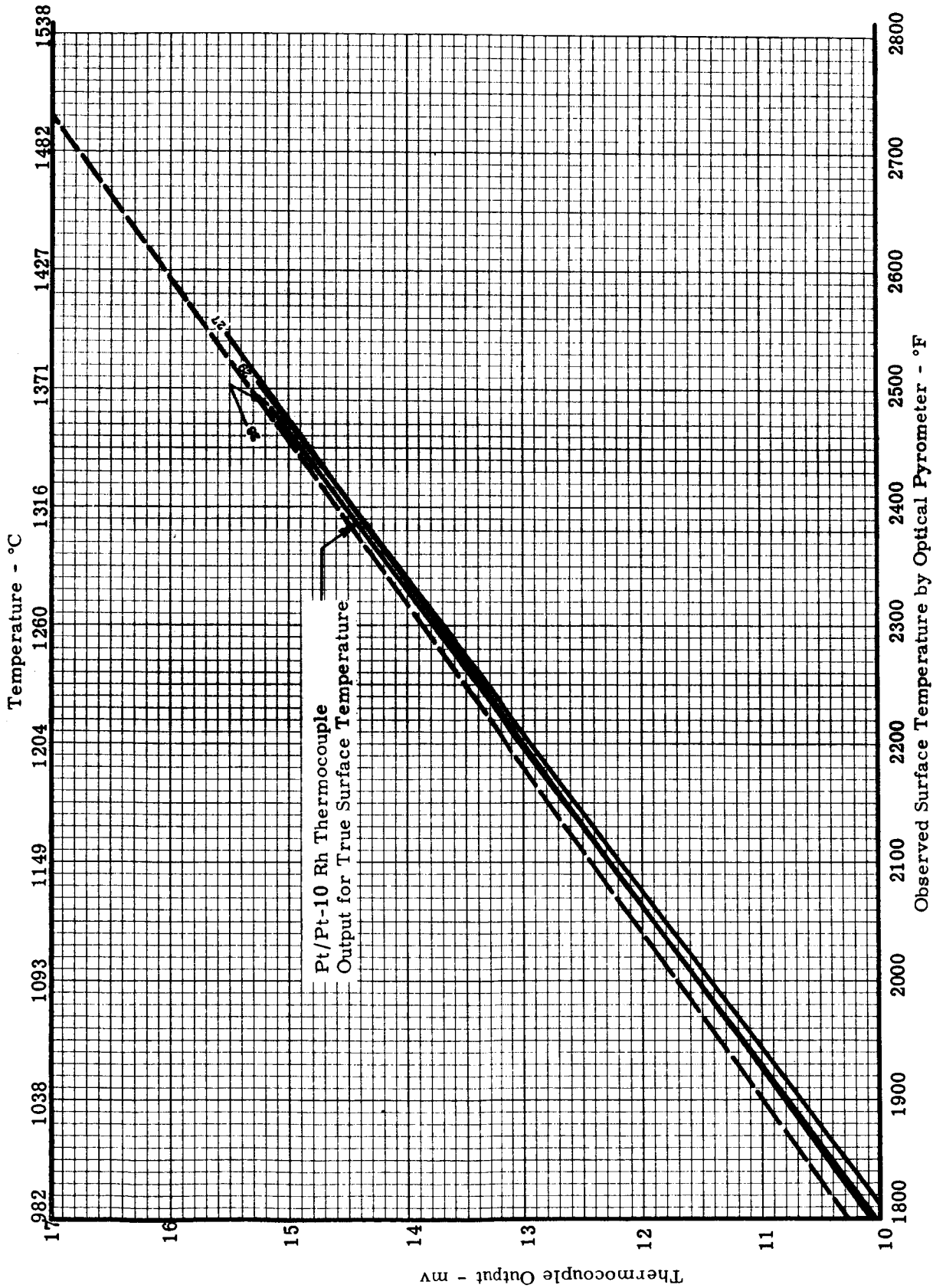


Figure 34. Comparison of the Thermoelectric Output from Three Sensor Assemblies of the Type Shown in Figure 25b and c During the First Cycle for Each.



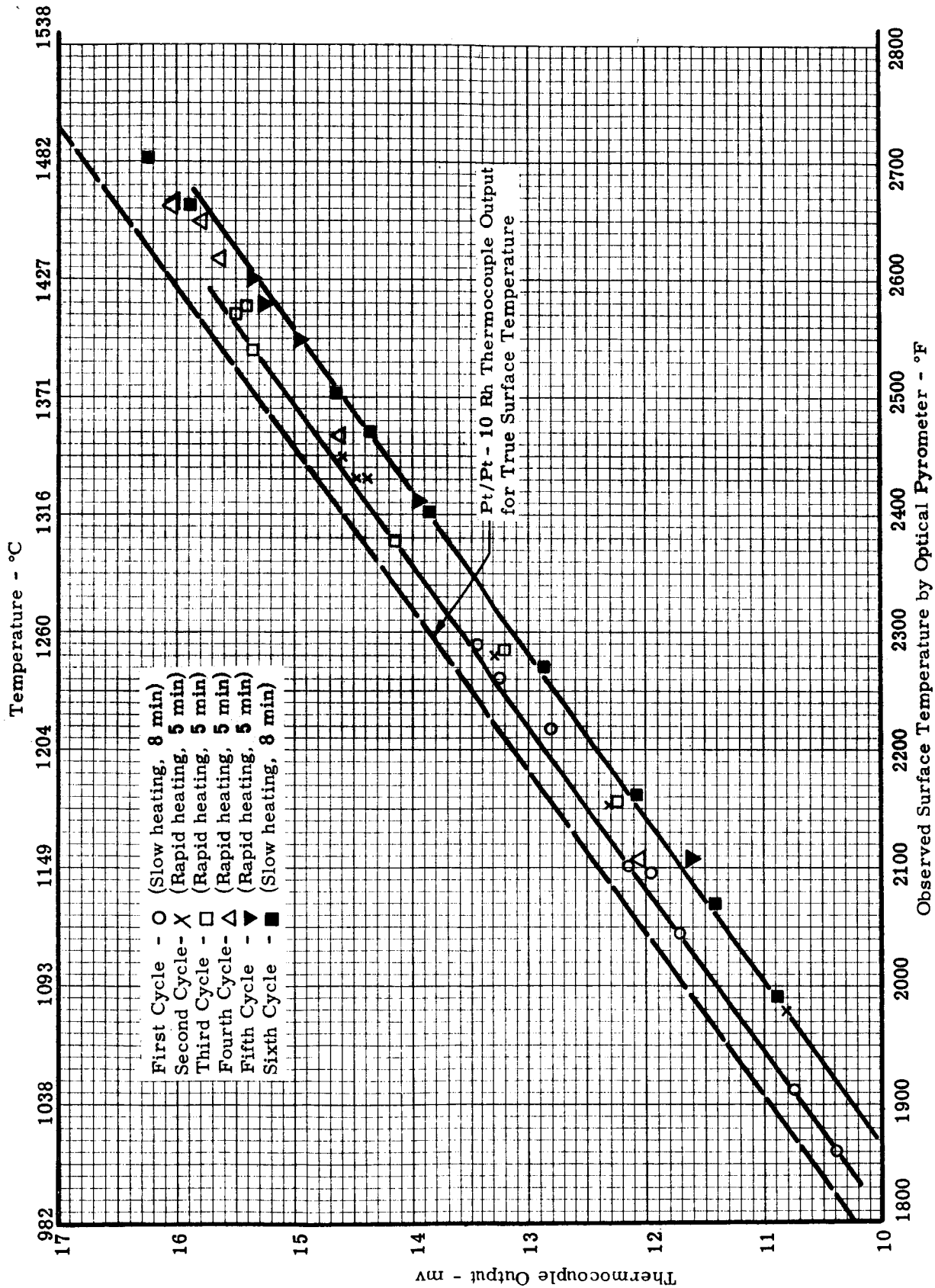


Figure 35. The Effect of Thermal Cycling on a Sensing Element with a Second Tungsten Vapor Deposition Applied over the Thermocouple Junction Protected with Alumina Cement (Specimen No. 32)

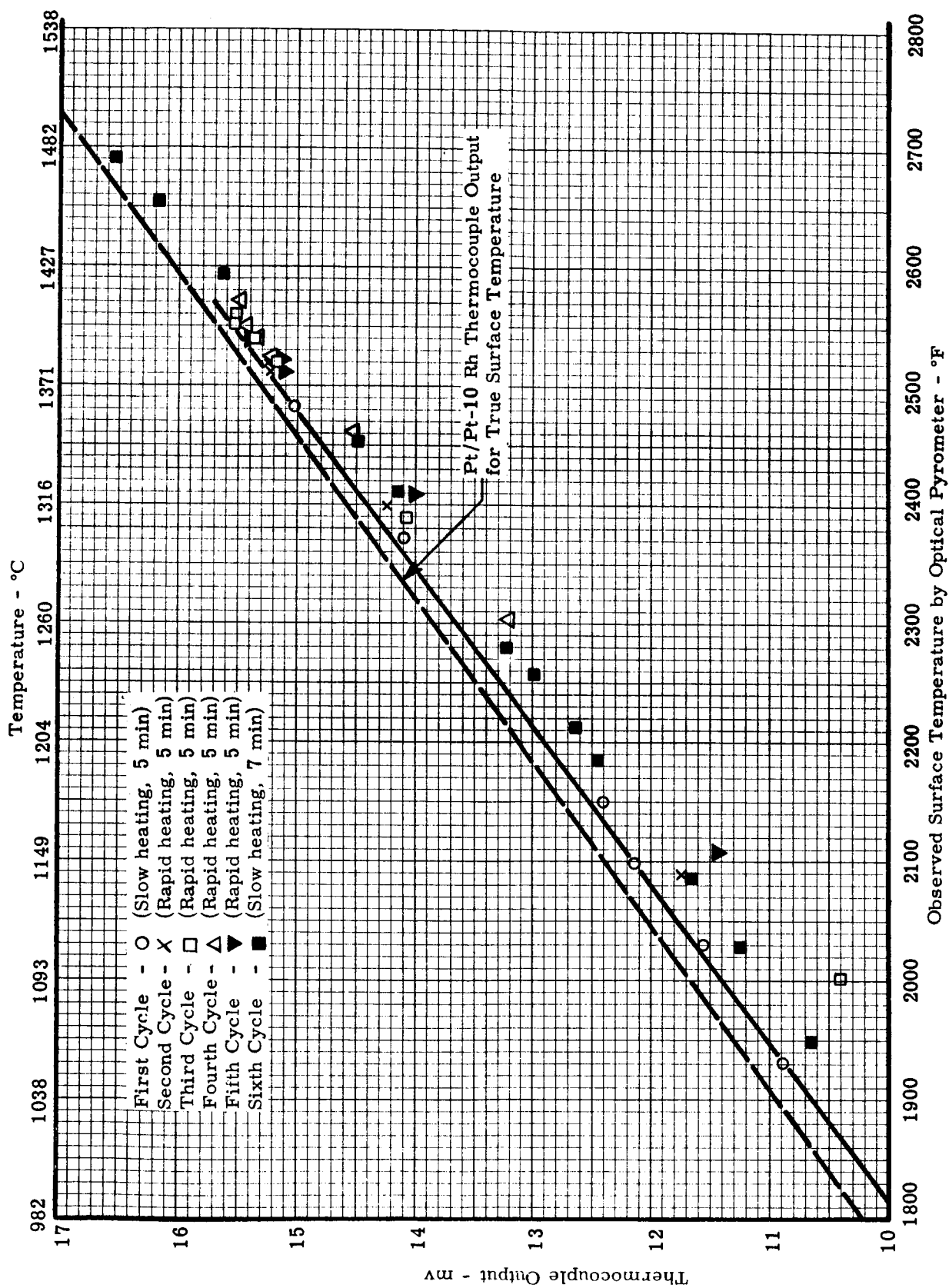


Figure 36. The Effect of Thermal Cycling on a Sensing Element Assembly with a Second Tungsten Vapor Deposition Applied over the Thermocouple Junction Protected with Alumina Cement (Specimen No 36)

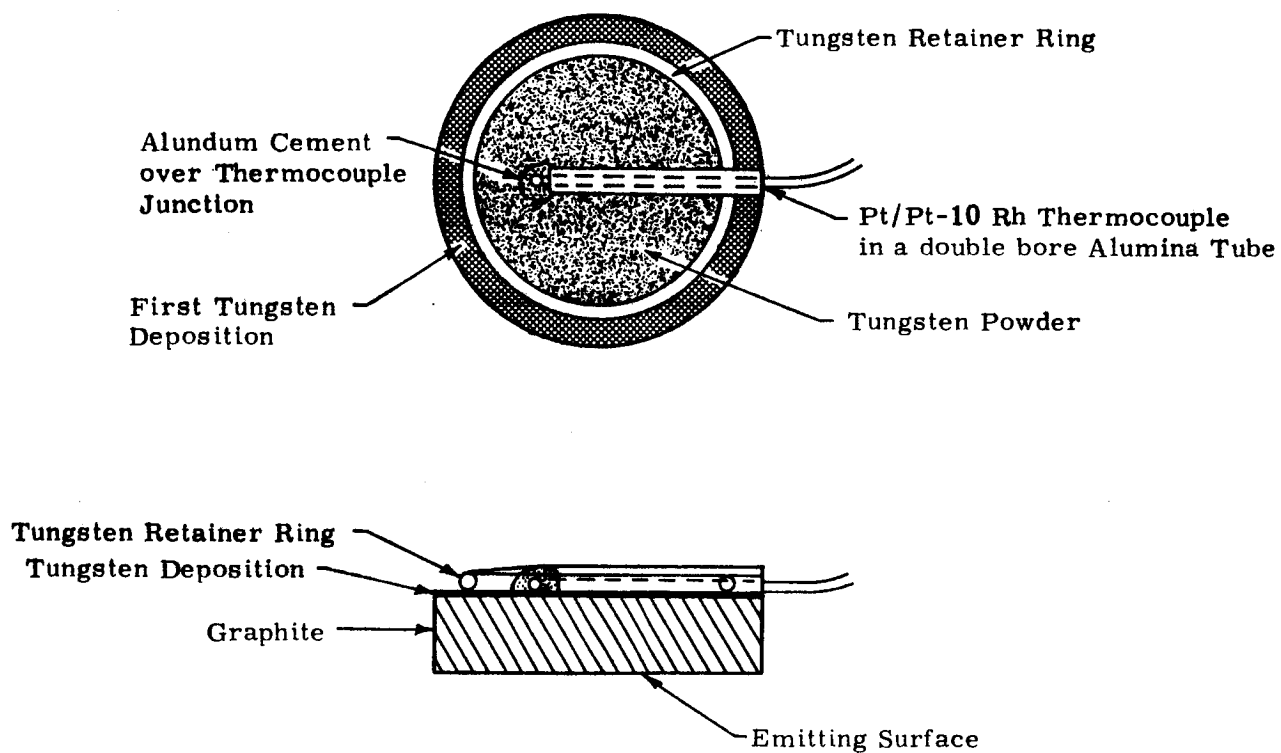


Figure 37. Diagram of Graphite Sensing Disc Prepared for a Second Tungsten Vapor Deposition

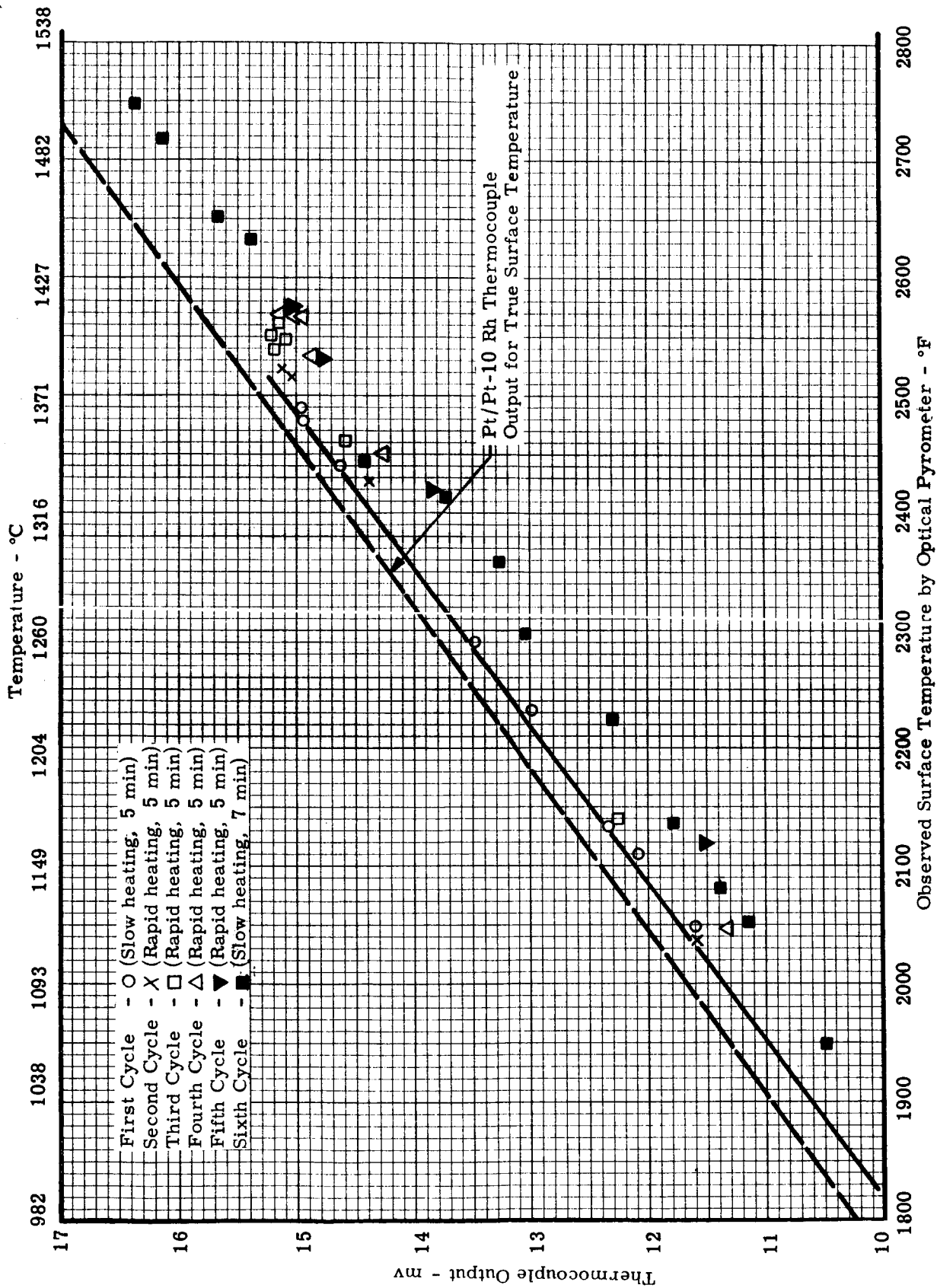


Figure 38. The Effect of Thermal Cycling on a Sensing Element Assembly of the Type Shown in Figure 37 (Specimen No. 40)

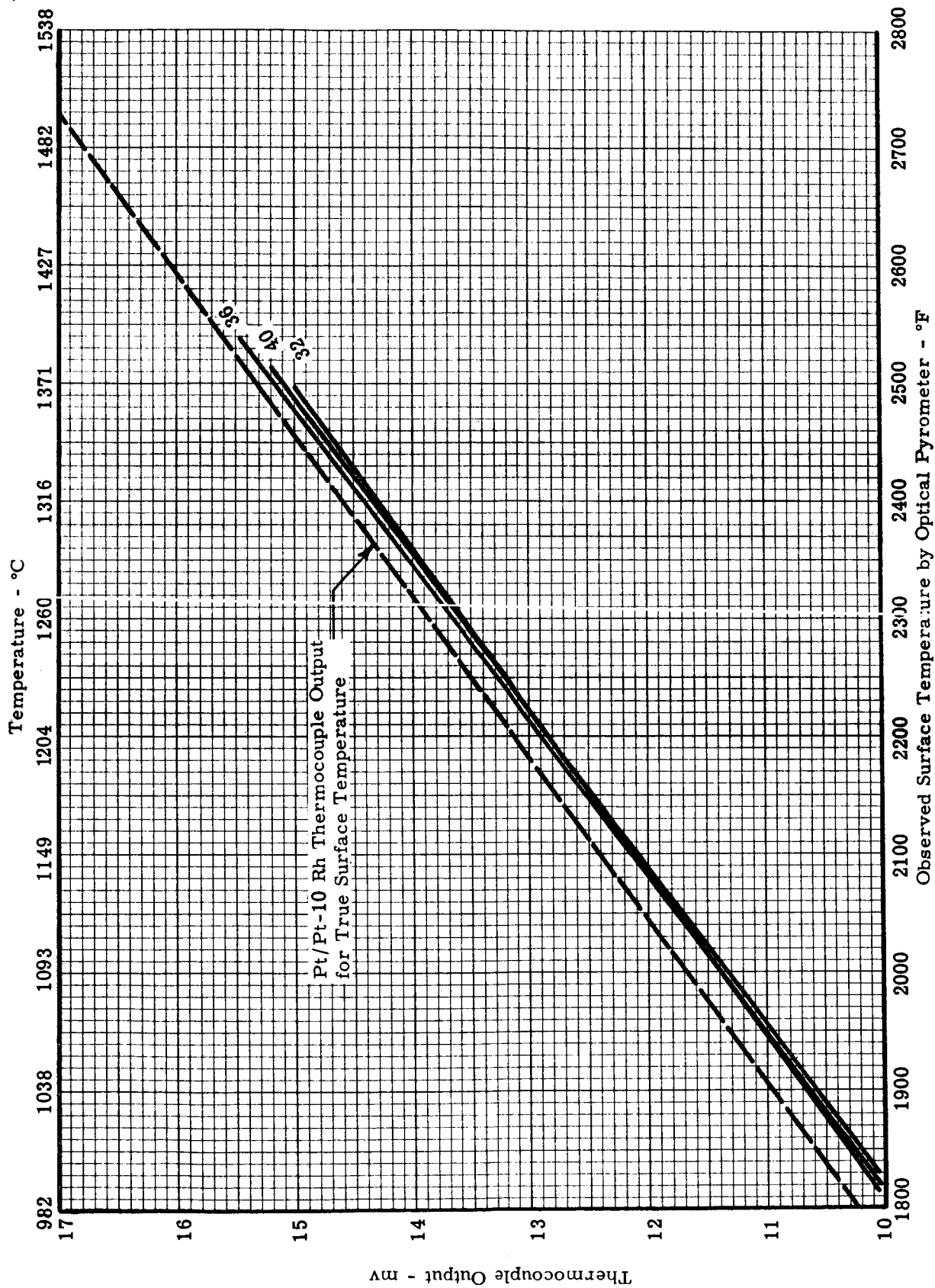


Figure 39. Comparison of the Thermoelectric Output from Three Sensing Element Assemblies with a Second Tungsten Vapor Deposition During the First Cycle for Each



Figure 40. Photomicrograph of Assembly No. 36 with Two Tungsten Vapor Depositions and the Thermocouple Bead Covered with Alundum Cement, 75X

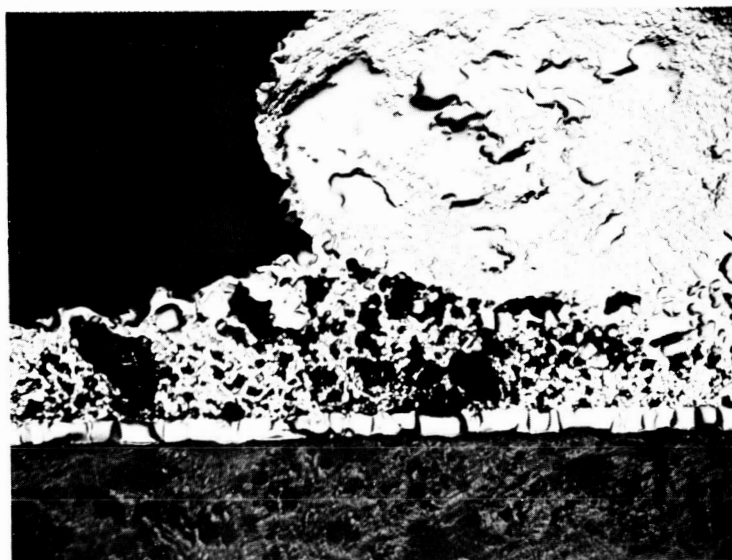
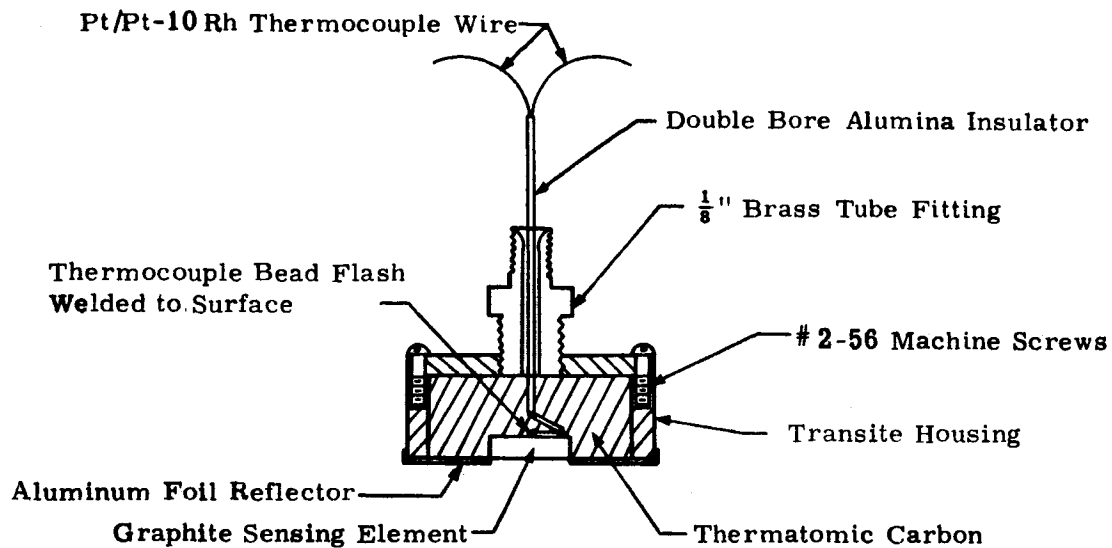
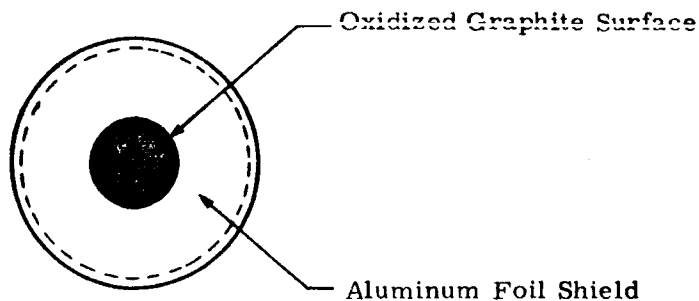


Figure 41. Photomicrograph of Assembly No. 40 with Tungsten Vapor Deposited onto Graphite, Tungsten Powder and a Tungsten Retainer Ring Bonded to the Assembly with a Second Vapor Deposition, 75X



Cross-Sectional View



Sensing Surface

Scale: 1" = 1"

Figure 42. The Laboratory Calorimeter for Calibration of the Graphite Sensing Element

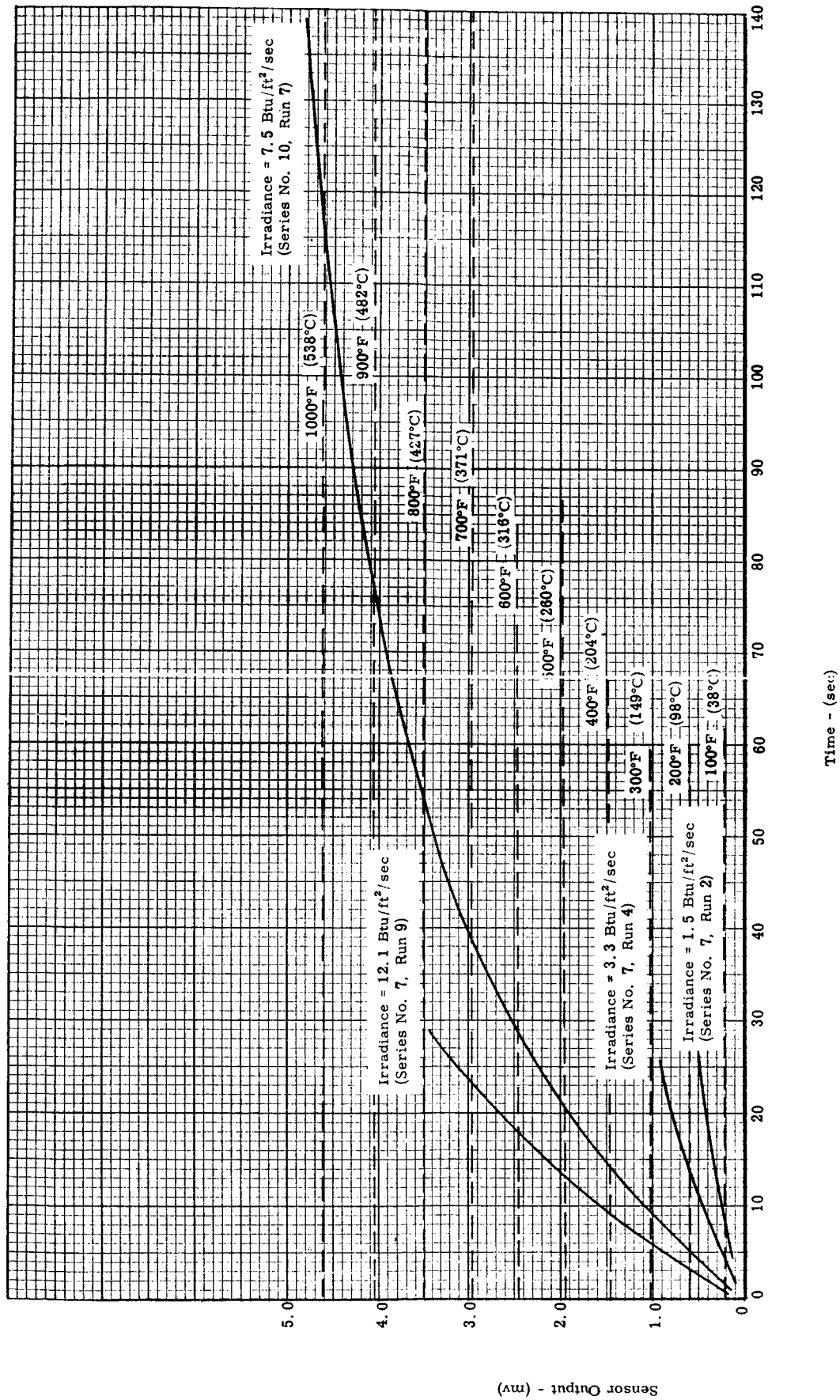


Figure 43. Millivolt Output (temperature) versus Time or Laboratory Calorimeter No. 38 with a Graphite Sensing Element, for Different Heat Flux Densities from the 1 in. Diameter Blackbody Radiation Source



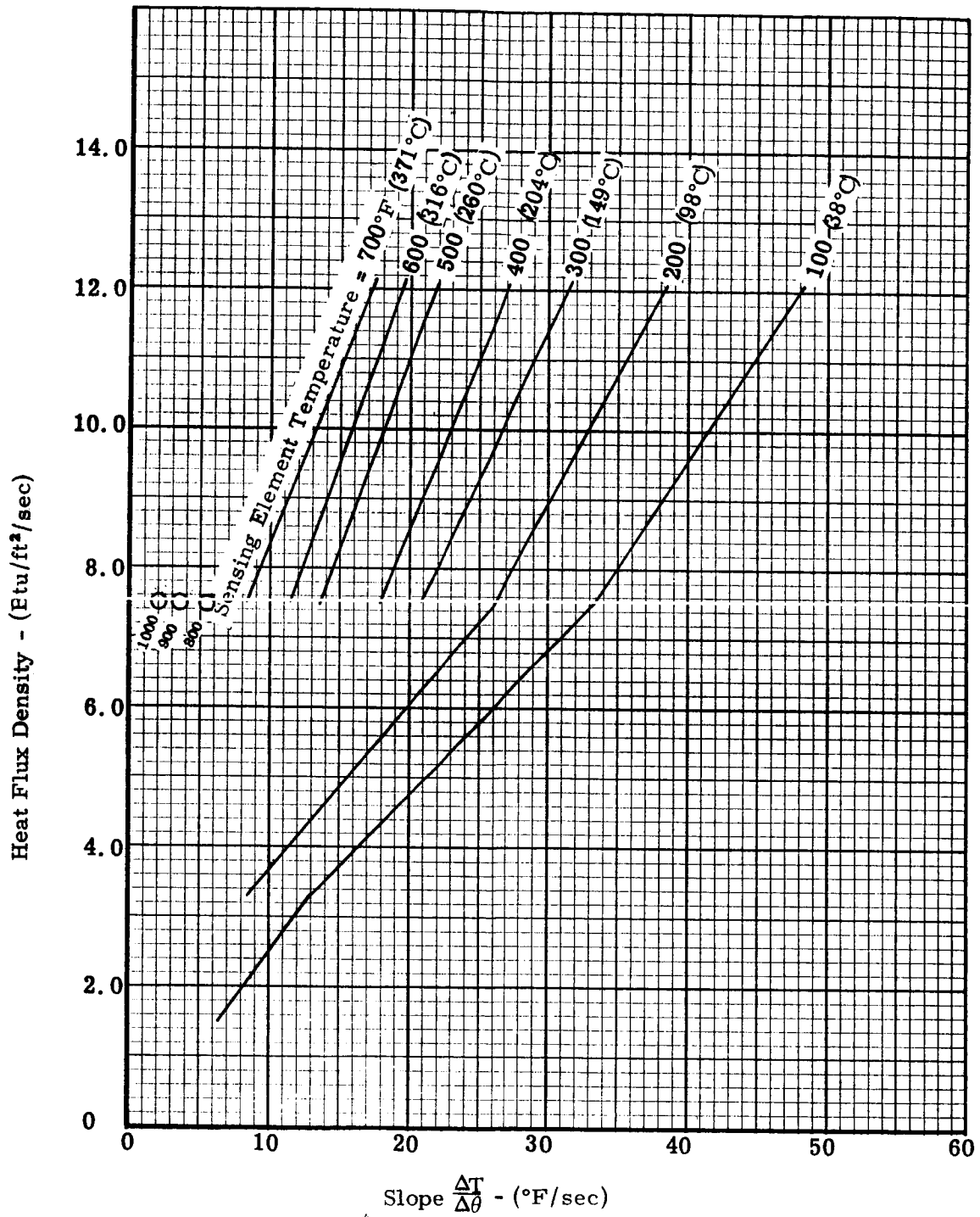


Figure 44. Calibration of Laboratory Calorimeter No. 38 with a Graphite Sensing Element for Different Heat Flux Densities and Sensing Element Temperatures

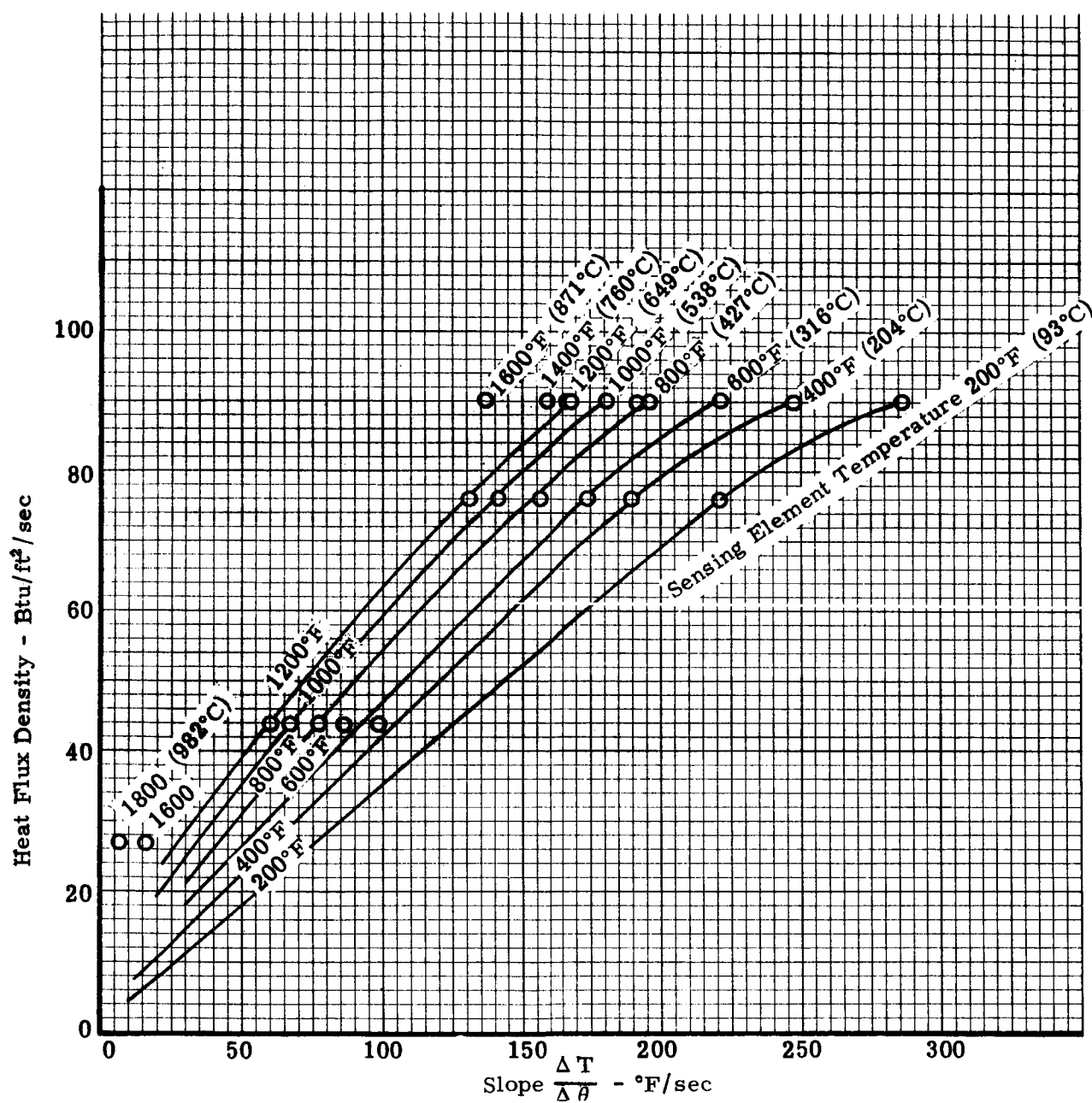
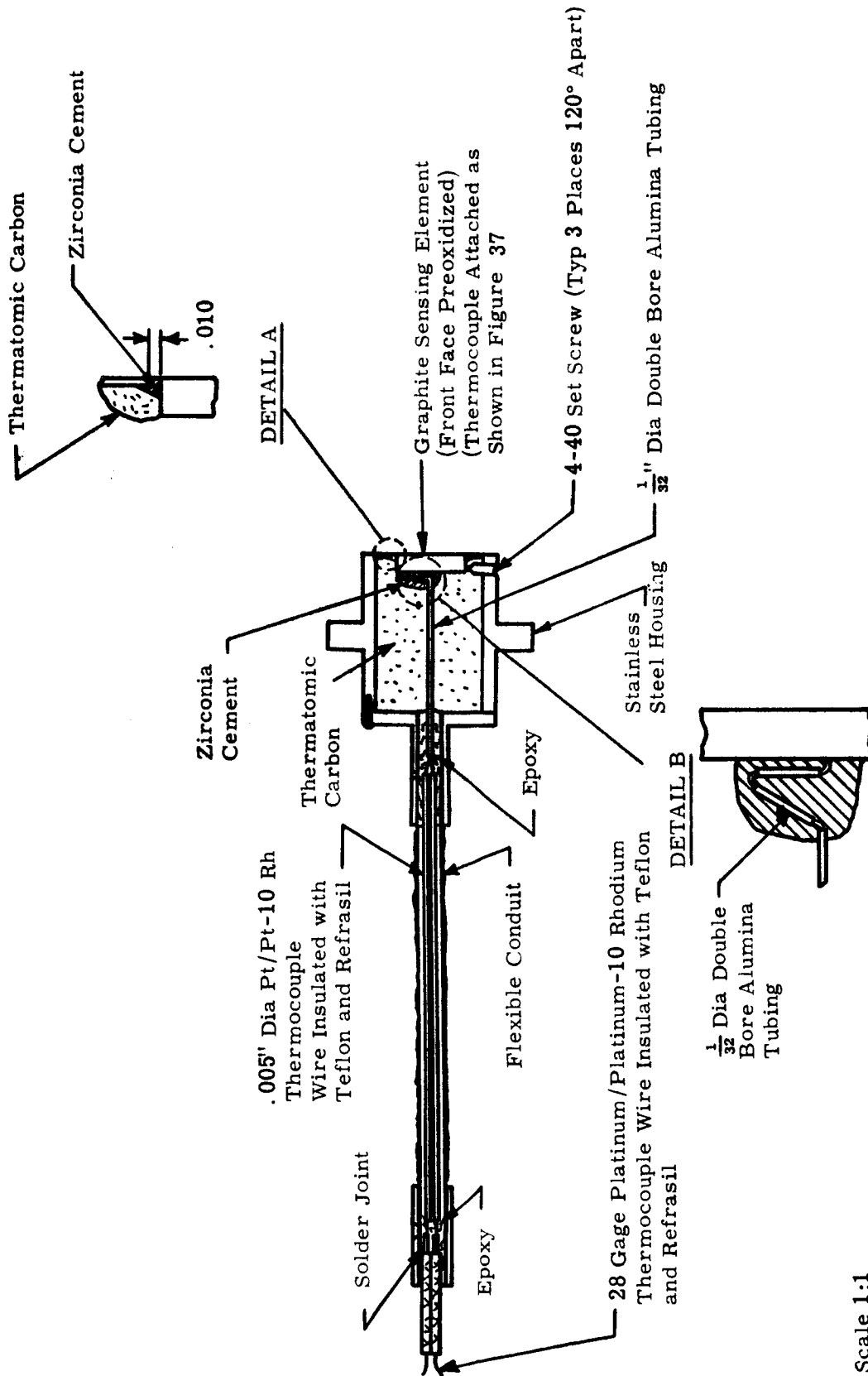


Figure 45. Calibration of Laboratory Calorimeter No. 106 with a Graphite Sensing Element for Different Heat Flux Densities and Sensing Element Temperatures



Scale 1:1

Figure 46. Prototype Total Calorimeter with Graphite Sensing Element

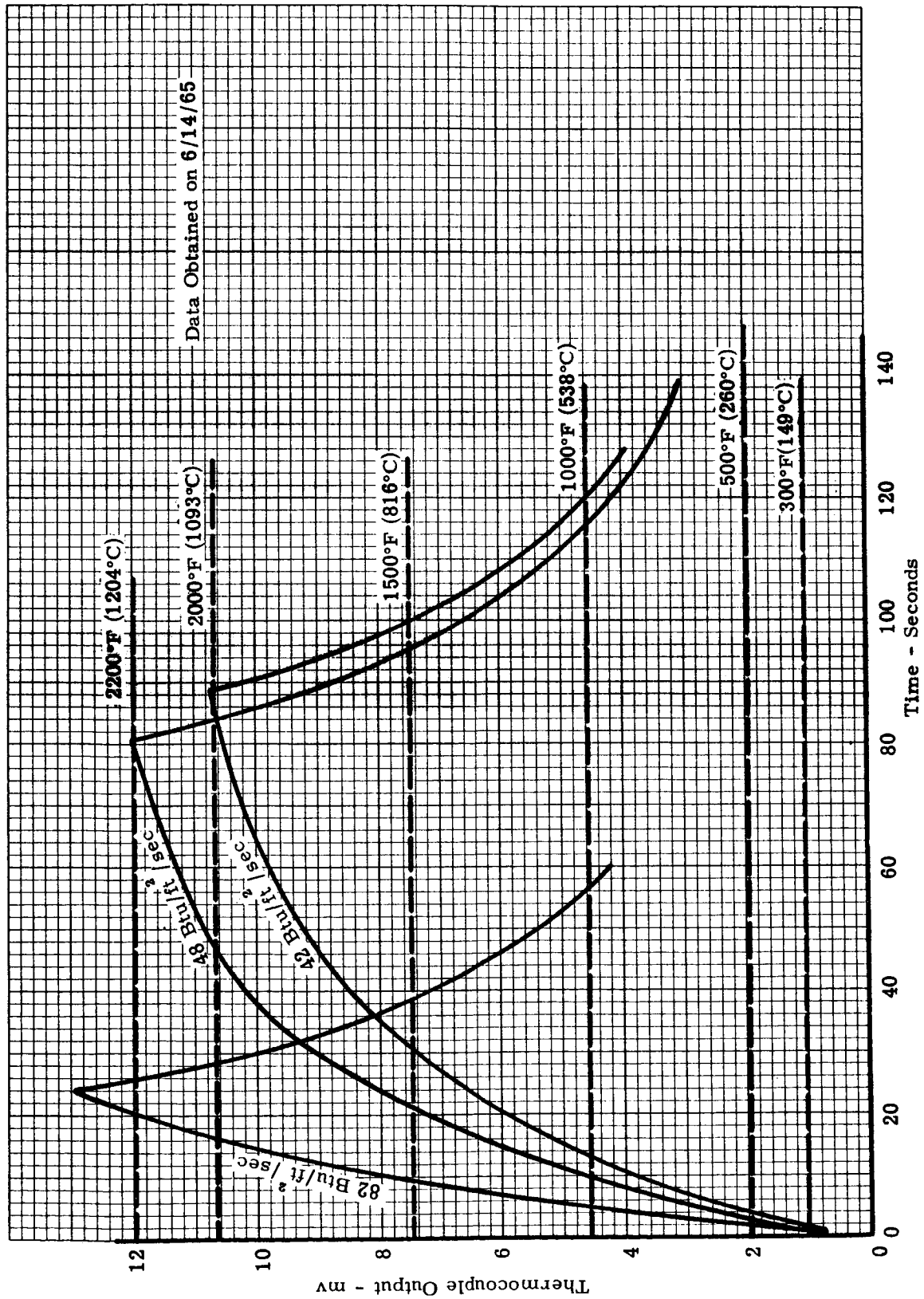


Figure 47. Millivolt Output (Temperature) versus Time Curves for the Prototype Calorimeter Subject to Three Heat Flux Densities from the 1 inch Diameter Blackbody Radiation Source

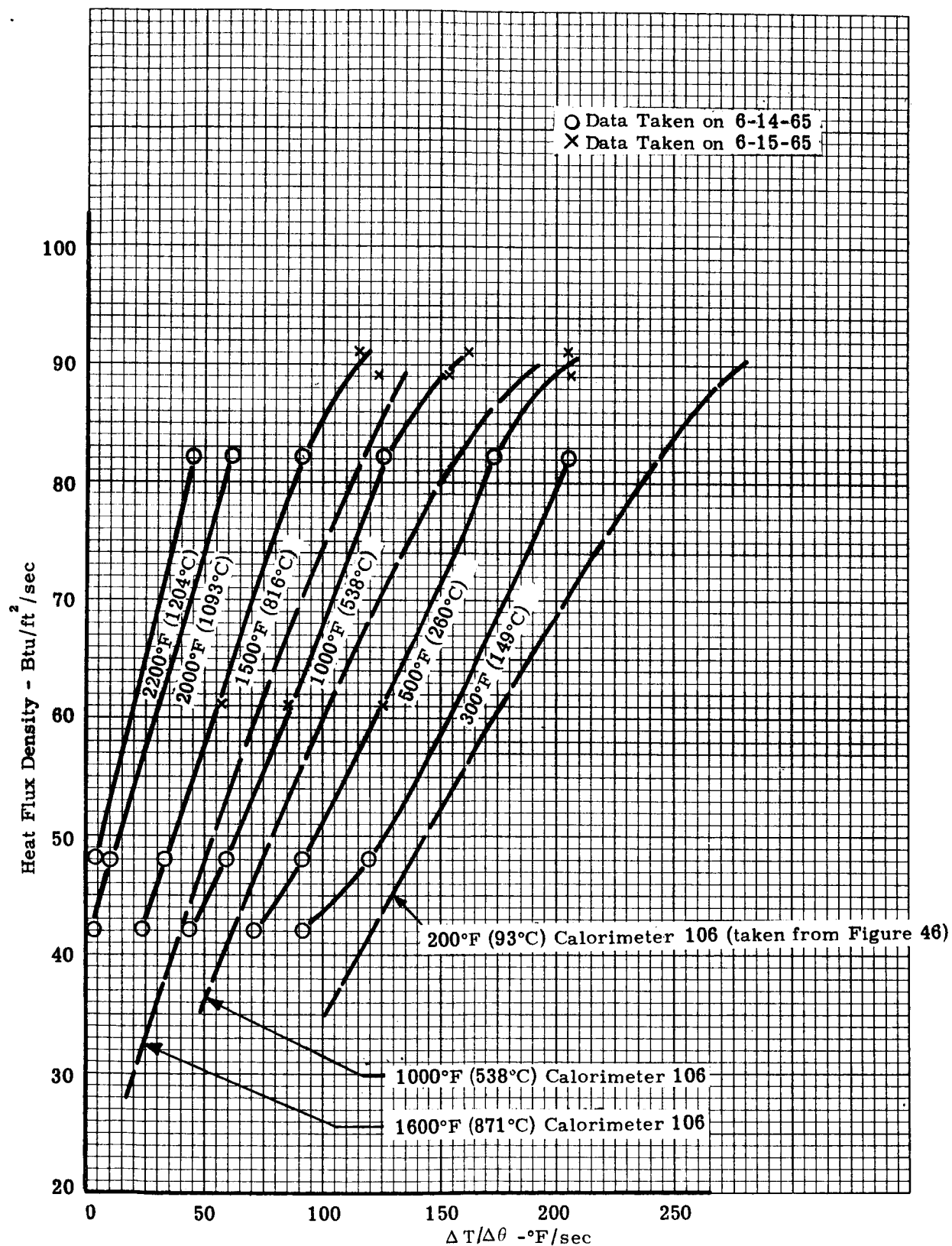


Figure 48. Calibration of the Prototype Calorimeter for Different Heat Flux Densities and Sensing Element Temperatures

Table 1  
POTENTIAL CALORIMETER HEAT SINK MATERIALS

Property	HfC	ZrC	BeO	HfO <sub>2</sub>	SiC	Graphite	HfB <sub>2</sub>
M. P. °F (°C)	7030 (3888°C)	6380 (3527°C)	4622 (2550°C)	5090 (2810°C)	4080 (D)(2249°C)	7560(S)(4182°C)	5880 (3249°C)
Density, lb ft <sup>-3</sup>	794	421	188	605	158	139	656
Sp. Ht. Btu · lb <sup>-1</sup> · °F <sup>-1</sup> mean for range of temperature	0.2 Estimation	0.2 Estimation	0.5 500-3500	0.1 500-4700	0.3 RT-2550	0.05 1000-5000	0.1 500-4500
K Btu · ft <sup>-1</sup> · hr <sup>-1</sup> · °F <sup>-1</sup> value at temperature	9 (1800) 18 (4600)	180 (?)	10 (1000) 4 (3500)	1.5 (2000-4300)	9 (2200)	33 (1500) 20 (4200)	33 (3000) 80 (3500)
$\alpha$ ft <sup>2</sup> hr <sup>-1</sup> calc. from mean values of Sp. Ht. and K	0.09	2.1	0.08	0.03	0.2	3.8	0.9
Expansion in · in <sup>-1</sup> · °F <sup>-1</sup> x 10 <sup>-6</sup>	6.9 (RT-1000)	6.7 (RT-1000)	5.9 (RT-3500)	4.0 (RT-3000)	4.4 (RT-2700)	1.6 (RT- )	4.5 (RT-4000)
Emittance	0.85 (1500) 0.95 (3000) Varies between 0.6 and 0.9 (3000-4500)	0.8 (1500) 0.8 (4000) 0.4 (4900)	0.55 (1500) 0.55 (3500)	0.85 (1500) 0.85 (4000)	0.9 (1500)	0.7 (1800)	0.4 (1000) 0.8 (2500) 0.7 (4800)
Remarks	M. P. lowered by absorbed C Volatile in vac. at 4000	M. P. lowered by absorbed C to 4400	V. P. 10 <sup>-3</sup> at 3780 Expansion unstable above 3500	Monoclinic to tetragonal at 3100. Expansion indicates instability on repeat runs and on individual runs above 3000			Expansion unstable above 4000

Note: Temperatures are in °F unless indicated otherwise.

Table 2

Change in Emittance of ATJ Graphite Finished with "4/0"  
Grit Paper, Run in Argon (Specimen No. 1)

Time	Observed Temperature °F	Radiometer Output Millivolts	True Temperature °F	Emittance	Remarks
On 8:42					
8:46	1813	0.340	1965	0.63	
8:52	1944	0.478	2101	0.71	
8:58	1960	0.501	2116	0.72	
-	2030	0.501	2221	0.61	
9:03	2247	0.796	2454	0.69	
9:09	2315	0.886	2533	0.69	
9:14	2494	1.242	2722	0.75	
9:19	2591	1.424	2835	0.75	
9:24	2596	1.448	2838	0.76	
9:28	2683	1.640	2937	0.76	
9:34	2810	1.996	3073	0.79	
Off 9:37					
On 10:15					
10:20	1619	0.263	1725	0.74	Apparatus not opened
10:25	1830	0.400	1965	0.74	
10:30	1949	0.526	2092	0.79	
10:35	2130	0.722	2297	0.79	
-	2197	0.722	2399	0.68	
10:40	2275	0.832	2486	0.69	
10:48	2390	1.065	2601	0.76	
10:53	2501	1.227	2737	0.73	
11:00	2645	1.560	2892	0.76	
11:05	2780	1.783	3069	0.71	
Off 11:09					Surface ap- peared dull and fuzzy

Table 3

Stability of the Emittance of ATJ Graphite Finished with "4/0" Grit  
Paper, Heat Soaked in Air and Run in Argon (Specimen No. 3)

Time	Observed Temperature °F	Radiometer Output Millivolts	True Temperature °F	Emittance	Remarks
On 8:41					
8:47	1466	0.171	1562	0.65	
8:52	1608	0.254	1714	0.73	
8:58	1623	0.279	1723	0.78	
9:03	1809	0.413	1930	0.81	
9:09	1949	0.548	2084	0.83	
-	1958	0.548	2097	0.81	
9:17	2097	0.700	2254	0.82	
9:24	2191	0.828	2358	0.83	
9:30	2330	1.051	2512	0.84	
9:36	2453	1.259	2652	0.84	
9:41	2586	1.552	2798	0.85	
9:47	2755	1.975	2986	0.86	
9:52	2790	2.158	3009	0.92	
Off 9:54					Apparatus not opened
On 10:08					
10:14	1454	0.209	1527	0.85	
10:20	1771	0.401	1881	0.85	
10:25	1923	0.530	2053	0.85	
10:31	2115	0.741	2269	0.84	
-	2121	0.741	2278	0.83	
10:40	2304	1.019	2480	0.86	
10:46	2447	1.295	2635	0.88	
10:52	2620	1.575	2848	0.81	
10:58	2727	1.877	2959	0.85	
10:58	2790	1.877	3065	0.75	
11:05	2810	1.925	3088	0.75	Small dark spots formed on surface
11:10	2900	2.159	3194	0.74	
Off 11:13					Apparatus not Opened.
On 1:00					
1:11	1471	0.202	1553	0.78	
1:18	1687	0.334	1789	0.83	
1:24	1969	0.581	2103	0.86	
1:30	2110	0.750	2259	0.87	
-	2130	0.750	2289	0.83	
1:37	2271	0.959	2445	0.84	Fuzzy Material on surface
1:44	2399	1.132	2598	0.81	
1:50	2528	1.367	2746	0.80	
1:59	2622	1.565	2853	0.80	
2:05	2729	1.817	2975	0.80	
-	2770	1.817	3044	0.74	
2:13	2881	2.156	3162	0.77	
Off 2:16					



Table 4

Stability of the Emittance of ATJ Graphite Finished with "4/0" Grit  
Paper, Run in Argon; Specimen Heat Soaked in Air After the  
First Run (Specimen No. 4)

Time	Observed Temperature °F	Radiometer Output Millivolts	True Temperature °F	Emittance	Remarks
On 1:57					
2:04	1687	0.335	1789	0.84	
2:10	1783	0.387	1903	0.79	
2:16	1955	0.547	2093	0.82	
-	1972	0.547	2118	0.79	
2:25	2168	0.781	2337	0.80	
2:31	2383	1.131	2574	0.83	
2:37	2680	1.775	2903	0.86	
-	2740	1.775	3002	0.76	
2:46	2903	2.275	3176	0.80	
Off 2:48					Apparatus Opened; spe- cimen heat soaked in air for 5 minutes at about 1600°F
On 8:10					
8:17	1424	0.178	1502	0.76	
8:24	1732	0.358	1842	0.81	
8:30	1880	0.475	2009	0.81	
8:36	2054	0.653	2205	0.82	
-	2073	0.653	2233	0.78	
8:46	2210	0.839	2384	0.81	
8:52	2482	1.302	2688	0.82	
8:59	2606	1.576	2825	0.84	
9:08					Power supply kicked off
On 9:42					Apparatus not opened between runs
9:50	1487	0.214	1568	0.80	
9:56	1698	0.341	1802	0.83	
10:10	2200	0.855	2365	0.84	
10:16	2437	1.220	2637	0.83	Dark looking fuzz on speci- men surface
10:22	2630	1.645	2849	0.85	
10:27	2749	1.932	2984	0.85	
-	2811	1.932	3089	0.75	
10:35	2923	2.292	3207	0.78	
Off 10:37					

Table 5

The Emittance of ATJ Graphite During the First and Fifth  
Runs in Argon with a Prior Heat Soak in Air (Specimen No. 5)

Time	Observed Temperature ° F	Radiometer Output Millivolts	True Temperature ° F	Emittance	Remarks
On 1:38					
1:44	1450	0.193	1529	0.78	
1:50	1742	0.358	1857	0.80	
1:56	1910	0.503	2043	0.82	
2:02	2048	0.645	2198	0.82	
2:07	2285	0.945	2470	0.80	
2:13	2463	1.241	2672	0.80	
2:18	2597	1.559	2814	0.84	
2:24	2720	1.799	2964	0.81	
Off 2:27					
On 2:29					
2:30	2710				
2:32	2728				
Off 2:34	2728				
On 2:35					
2:36	2726				
2:38	2739				
Off 2:40	2748				
On 2:41					
2:42	2721				
2:44	2734				
Off 2:46	2730				
On 2:55					
3:03	1420	0.175	1498	0.75	
3:10	1746	0.355	1863	0.78	
3:16	1868	0.454	2000	0.79	
3:22	2037	0.623	2189	0.80	
3:28	2268	0.910	2453	0.79	
3:34	2450	1.175	2668	0.76	
3:40	2665	1.594	2918	0.76	
3:47	2820	2.037	3082	0.80	
Off 3:50					

Table 6

Effect of Slow and Rapid Thermal Cycling on an Unprotected  
Pt/Pt-10 Rh Thermocouple in a Graphite Specimen  
(Specimen No. 2)

Time	Observed Temperature			Radiometer Output mv	True Temperature ° F	Emittance	Remarks
	Surface °F	Thermocouple					
		mv	°F				
On 9:10							
9:14	1530	7.97	1577	0.239	1615	0.82	
9:24	1814	10.14	1920	0.454	1923	0.90	
9:30	2160	12.80	2321	0.840	2309	0.90	
9:36	2396	14.44	2568	1.192	2579	0.87	
9:41	2613	16.14	2824	1.626	2825	0.86	
Off 9:43							
On 9:49	2271	13.41	2413				
-	2550	15.66	2752				
9:51	2609	16.12	2821				
Off 9:54	2641	16.44	2870				
On 9:55	2285	13.55	2434				
-	2579	15.91	2790				
9:56	2619	16.23	2838				
9:59	2620	16.32	2852				
Off 10:00	2627	16.32	2852				
On 10:02	2356	14.21	2533				
-	2599	15.93	2793				
10:03	2620	16.18	2831				
10:04	2619	16.20	2834				
Off 10:07	2610	16.16	2827				
On 10:08	2106	11.92	2190				
-	2459	15.02	2655				
-	2561	15.62	2746				
10:10	2590	15.87	2783				
10:12	2619	16.05	2811				
Off 10:13	2612	16.08	2815				
On 10:20							
10:29	1849	10.17	1925	0.492	1960	0.92	
10:38	2163	12.56	2286	0.847	2311	0.90	
10:42	2453	14.80	2622	1.315	2640	0.89	
10:45	2656	16.49	2878	1.755	2868	0.88	
Off 10:47							

Table 7

Effect of Slow and Rapid Thermal Cycling on an Unprotected  
Pt/Pt-10 Rh Thermocouple in a Graphite Specimen  
(Specimen No. 3)

Time	Observed Temperature			Radiometer Output mv	True Temperature °F	Emittance	Remarks
	Surface °F	Thermocouple mv	°F				
On 12:56							
1:03	1592	8.46	1656				
1:05	1640			0.311	1734	0.86	
1:07	1896	10.64	1997				
1:08	1926	10.88	2033				
1:09	2091	12.16	2226				
1:11	2115			0.779	2259	0.90	
1:14	2225	13.15	2374				
1:15	2450	14.95	2644				
1:16	2450	14.94	2643				
1:17	2568	15.91	2790				
1:18	2631			1.662	2847	0.86	
Off 1:20							
On 1:21	2202	12.40	2262				
--	2555	15.65	2750				
1:22	2619	16.20	2834				
1:24	2639	16.31	2850				
Off 1:26	2648	16.34	2855				
On 1:28	2189	12.86	2330				
-	2569	15.02	2746				
1:29	2622	16.13	2823				
1:31	2635	16.29	2847				
Off 1:33	2650	16.29	2847				
On 1:36	2315	13.50	2426				
-	2549	15.38	2709				
1:37	2603	15.89	2787				
1:39	2648	16.20	2834				
Off 1:41	2642	16.19	2832				
On 1:43	2215	13.00	2351				
-	2510	15.10	2667				
1:44	2615	15.90	2788				
1:46	2644	16.13	2823				
1:48	2640	16.11	2820				
Off 1:49							Thermocouple failed at approximately 17 mv output
On 1:56							
2:01	1543			0.254	1626	0.85	
2:07	1900			0.536	2018	0.91	
2:12	2103			0.762	2246	0.90	
-	2120			0.762	2271	0.87	
2:20	2273			0.956	2448	0.84	
2:26	2451			1.261	2649	0.84	
2:33	2686			1.771	2913	0.84	
2:38	2890			2.458	3120	0.92	
Off 2:40							

Table 8

Effect of Slow and Rapid Thermal Cycling on an Unprotected  
Pt/Pt-10 Rh Thermocouple in a Graphite Specimen  
(Specimen No. 1)

Time	Observed Temperature			Remarks
	Surface °F	Thermocouple mv	°F	
On 12:35				
12:41	1490	7.74	1540	
12:43	1523	7.94	1572	
12:45	1511	7.86	1559	
-	1680	9.07	1754	
-	1841	10.24	1936	
12:48	1877	10.54	1981	
12:50	2084	12.02	2205	
-	2183	12.81	2323	
-	2252	13.29	2395	
12:53	2283	13.53	2431	
12:54	2280	13.50	2426	
12:56	2439	14.86	2631	
-	2509	15.33	2702	
-	2531	15.47	2723	
Off 12:57				
On 1:02	2028	13.55	2434	
-	2483	14.54	2583	
-	2620	15.75	2765	
-	2590	15.93	2793	
1:05	2623	16.14	2824	
1:06	2610	15.93	2793	
Off 1:07	2605	15.79	2771	
On 1:12	2051	12.05	2209	
-	2506	15.12	2670	
-	2570	15.49	2726	
1:14	2580	15.62	2746	
1:16	2589	15.74	2764	
Off 1:17	2605	15.77	2768	
On 1:20	2085	11.43	2116	
-	2482	14.73	2611	
-	2561	15.43	2717	
-	2571	15.65	2750	
1:22	2595	15.74	2764	
1:23	2599	15.78	2770	
Off 1:25	2599	15.73	2762	
On 1:30	2089	11.62	2145	
-	2475	14.74	2613	
-	2561	15.88	2785	
1:32	2581	15.56	2737	
1:34	2601	15.74	2764	
1:35	2608	15.79	2771	
1:36	2706	16.63	2899	
Off 1:37	2770	16.98	2952	
On 2:55	1430	6.98	1414	
3:02	1442	7.09	1432	
3:03	1556	7.85	1558	
3:05	1664	8.59	1677	
3:06	1732	9.06	1752	
3:08	1769	9.35	1798	
3:09	1789	9.51	1823	
3:10	1880	10.13	1919	
3:12	1949	10.66	2000	
3:13	2130	12.02	2205	
3:14	2168	12.18	2229	
3:15	2280	13.04	2357	
3:16	2440	14.30	2546	
3:17	2474	14.56	2586	
Off 3:18	2621	15.71	2759	

Table 9

Effect of Thermal Cycling on a Pt/Pt-10 Rh Thermocouple  
in a Molybdenum Protection Tube (Specimen No. 1)

Time	Observed Temperature			Remarks
	Surface °F	Thermocouple mv	°F	
On 1:19				Graphite oxidized prior to evaluation
1:24	1544	8.30	1631	
1:26	1794	10.14	1920	
1:27	1813	10.24	1935	
1:27	1850	10.55	1983	
1:28	1877	10.79	2019	
1:28	1963	11.41	2113	
1:29	2038	12.04	2208	
1:30	2108	12.65	2299	
1:30	2166	13.08	2363	
1:31	2277	13.79	2470	
1:31	2338	14.45	2569	
1:32	2368	14.65	2599	
1:33	2450	15.24	2688	
1:33	2481	15.51	2729	
1:34	2519	15.83	2777	
1:34	2528	15.96	2797	
Off 1:35				
On 1:37	2197	13.09	2365	Thermocouple Failed
-	2441	15.25	2690	
1:38	2509	15.73	2762	
1:40	2517	15.80	2773	
Off 1:42	2500	15.65	2750	
On 1:44	2156	12.84	2327	
-	2358	14.56	2586	
1:45	2442	15.26	2691	
1:47	2492	15.66	2752	
Off 1:49	2498	15.66	2752	
On 1:51	2241	13.50	2426	
-	2382	14.74	2613	
1:52	2448	15.26	2691	
1:54	2476	15.53	2732	
Off 1:56	2483	15.63	2747	
On 1:59	2050	12.05	2209	
-	2348	14.54	2583	
2:00	2450	15.34	2703	
Off 2:02				

Table 10

Effect of Thermal Cycling on a Pt/Pt-10 Rh Thermocouple  
in a Molybdenum Protection Tube (Specimen No. 2)

Time	Observed Temperature			Remarks
	Surface ° F	Thermocouple mv	° F	
On 3:10				Graphite oxidized prior to evaluation
3:13	1676	9.16	1768	
3:15	1809	10.20	1929	
3:16	1876	10.68	2003	
3:16	1962	11.34	2103	
3:17	2010	11.73	2161	
3:18	2150	12.83	2326	
3:18	2204	13.26	2390	
3:19	2204	13.11	2368	
3:19	2328	14.10	2516	
3:20	2349	14.29	2545	
3:20	2429	14.91	2638	
3:21	2463	15.21	2684	
3:21	2518	15.63	2747	
Off 3:22	2548	15.87	2783	
On 3:25	2311	13.99	2500	
-	2418	14.76	2616	
3:26	2469	15.25	2690	
3:28	2511	15.51	2729	
Off 3:30	2515	15.55	2735	
On 3:32	2120	12.21	2233	
-	2379	14.41	2563	
3:33	2450	15.20	2682	
3:35	2519	15.51	2729	
Off 3:37	2510	15.51	2729	
On 3:39	2168	12.54	2283	
-	2430	14.95	2644	
3:40	2508	15.53	2732	
3:42	2550	15.89	2786	
Off 3:44	2561	15.96	2797	
On 3:50	2191	12.90	2336	
-	2431	14.90	2637	
3:51	2496	15.45	2720	
3:53	2549	15.87	2783	
Off 3:55	2554	15.93	2793	
On 4:00				
4:03	1725	9.50	1821	
4:05	1787	9.97	1894	
4:05	1839	10.33	1949	
4:06	1900	10.80	2021	
4:06	1961	11.29	2095	
4:07	2003	11.62	2145	
4:07	2016	11.74	2163	
4:08	2110	12.50	2277	
4:08	2193	12.91	2338	
4:09	2193	13.01	2353	
4:09	2240	13.44	2417	
4:10	2271	13.72	2459	
4:11	2408	14.75	2614	
4:11	2421	14.88	2634	
4:12	2465	15.21	2684	
4:12	2504	15.48	2724	
4:13	2560	15.95	2796	
4:13	2591	16.23	2838	
4:14	2630	16.55	2887	
4:14	2667	16.85	2932	
4:15	2705	17.14	2977	
Off 4:15				Thermocouple burned out

Table 11

Effect of Thermal Cycling on a Pt/Pt-10 Rh Thermocouple in  
a Tantalum Protection Tube (Specimen No. 2)

Time	Observed Temperature			Remarks
	Surface °F	Thermocouple mv	°F	
On 8:00				Graphite oxidized prior to evaluation
8:05	1583	8.39	1645	
8:07	1737	9.51	1823	
8:08	1932	10.91	2038	
-	2039	11.66	2151	
8:09	2112	12.36	2256	
8:10	2398	14.51	2578	
-	2519	15.43	2717	
8:11	2547	15.70	2758	
Off 8:12				
On 8:16	2150	12.06	2211	
-	2409	14.47	2572	
8:17	2509	15.43	2717	
8:19	2539	15.71	2759	
Off 8:21	2558	15.82	2776	
On 8:23	2503	15.31	2699	
8:24	2553	15.69	2756	
8:26	2612	16.19	2832	
Off 8:28	2622	16.29	2847	
On 8:32	2160	12.41	2263	
-	2411	14.41	2563	
8:33	2486	15.16	2676	
8:35	2550	15.66	2752	
Off 8:37	2570	15.84	2779	
On 8:40	2421	14.56	2586	
-	2503	15.26	2691	
8:41	2549	15.65	2750	
8:43	2584	15.94	2794	
Off 8:45	2584	15.94	2794	
On 8:47	2257	13.00	2351	
-	2472	15.07	2662	
8:48	2551	15.65	2750	
8:50	2600	15.95	2796	
Off 8:52	2568	15.82	2776	
On 8:54				
8:59	1911	10.60	1990	
9:00	1988	11.25	2089	
9:01	2094	12.11	2218	
9:02	2203	12.98	2348	
9:03	2302	13.62	2444	
9:04	2355	14.07	2512	
9:05	2462	14.94	2643	
9:06	2489	15.19	2681	
9:07	2562	15.75	2765	
9:08	2591	16.03	2808	
9:09	2707	16.95	2948	
9:10	2712	17.09	2969	
Off 9:11	2811	17.30	3001	



Table 12

Effect of Thermal Cycling on a Pt/Pt-10 Rh Thermocouple in  
a Tungsten Protection Tube (Specimen No. 2)

Time	Observed Temperature			Remarks
	Surface °F	Thermocouple mv	°F	
On 9:24				Graphite oxidized prior to evaluation
9:27	1682	9.29	1788	
9:31	1798	10.10	1914	
9:31	1818	10.26	1939	
9:32	1961	11.36	2106	
9:32	2041	11.99	2200	
9:33	2102	12.46	2271	
9:33	2170	12.93	2341	
9:34	2180	13.01	2353	
9:34	2292	13.90	2486	
9:35	2334	14.23	2536	
9:35	2350	14.35	2554	
9:36	2403	14.79	2620	
9:36	2461	15.25	2690	
Off 9:37	2472	15.36	2706	
On 9:39	2088	12.25	2239	
-	2408	14.79	2620	
9:40	2490	15.46	2721	
9:42	2530	15.84	2779	
Off 9:44	2560	16.10	2818	
On 9:46	2048	11.90	2187	
-	2311	14.06	2510	
9:47	2399	14.75	2614	
9:49	2446	15.19	2681	
Off 9:51	2441	15.10	2667	
On 9:59	2028	11.80	2172	
-	2239	13.54	2432	
10:00	2342	14.34	2552	
10:02	2390	14.70	2607	
Off 10:04	2402	14.84	2628	
On 10:09	2079	11.90	2187	
-	2249	13.65	2449	
10:12	2371	14.53	2581	
Off 10:14	2404	14.85	2629	
On 10:16				
10:18	1622	8.83	1716	
10:21	1789	10.06	1908	
10:21	1810	10.21	1931	
10:22	1908	10.95	2044	
10:22	1971	11.46	2121	
10:23	2008	11.72	2160	
10:23	2052	12.16	2226	
10:24	2118	12.56	2286	
10:24	2207	13.11	2368	
10:25	2252	13.56	2435	
10:25	2269	13.73	2461	
10:25	2331	14.24	2537	
10:26	2362	14.49	2575	
10:26	2400	14.85	2629	
10:27	2434	15.16	2676	
10:27	2477	15.46	2721	
10:28	2475	15.49	2726	
10:28	2583	15.86	2782	
10:29	2560	16.15	2826	
10:29	2609	16.90	2940	
Off 10:30				

Table 13

Thickness of Tungsten Diffusion Barrier  
on Sectioned Graphite Discs

Series and Discs No.	Depositioned Time (min)	Thickness (in)
1-74	30	0.0086
1-75	30	0.0085
1-76	30	0.0076
1-77	30	0.0076
2-79	30	0.0045
2-80	45	0.0066
2-81	15	0.0023

Disc Temperature = 1292°F (700°C)

Argon Flow = 1% - 3 $\frac{1}{2}$ %

WF1<sub>6</sub> = ~2%

Hydrogen Flow = 12% - 14%

Table 14

Effect of Thermal Cycling on a Pt/Pt-10 Rh Thermocouple  
Flash-Welded to the Tungsten Diffusion Barrier  
on a Graphite Substrate. (See Figure 25a)(Gra-  
phite Surface was Preoxidized)(Specimen No. 22)

Time	Observed Temperature			Remarks
	Surface °F	Thermocouple mv	Thermocouple °F	
On 2:38			%	Graphite oxidized prior to evaluation. Thermocouple wires flash-welded individually.
2:42	1826	10.06	1908	
2:43	1906	10.66	2000	
2:44	1920	10.69	2004	
2:45	1988	11.21	2083	
2:45	2018	11.46	2121	
2:46	2150	12.31	2248	
2:46	2173	12.46	2271	
2:47	2212	12.76	2315	
2:48	2251	13.11	2368	
2:49	2381	14.00	2501	
2:51	2403	14.17	2527	
Off 2:52				
On 2:55				
2:58	1880	10.34	1951	
2:59	1927	10.71	2007	
3:01	1950	10.90	2036	
3:03	2020	11.39	2110	
3:03	2030	11.44	2118	
3:04	2020	11.36	2106	
3:07	2108	11.92	2190	
3:08	2217	12.75	2314	
3:08	2319	13.51	2428	
3:09	2353	13.68	2453	
3:09	2339	13.60	2441	
3:11	2401	14.06	2510	
Off 3:12	2422	14.22	2534	
On 3:17	2095	11.95	2194	
-	2353	13.61	2443	
3:18	2393	13.91	2488	
3:19	2470	14.56	2586	
3:20	2500	14.81	2623	
Off 3:22	2517	14.86	2631	
On 3:26	2371	13.85	2479	
-	2561	15.10	2667	
3:27	2590	15.23	2687	
3:28	2589	15.26	2691	
3:30	2602	15.31	2699	
Off 3:31	2608	15.31	2699	
On 3:35	2246	12.50	2277	
-	2497	14.29	2545	
3:36	2530	14.57	2587	
3:37	2612	15.29	2696	
3:37	2657	15.56	2736	
3:38	2663	15.61	2744	
3:39	2729	16.08	2815	
3:39	2762	16.29	2847	
Off 3:40	2750	16.19	2832	
On 3:45				
3:49	1910	10.03	1903	
3:49	1936	10.22	1932	
3:50	1960	10.35	1952	
3:50	1979	10.53	1980	
3:50	2101	11.41	2113	
3:51	2184	11.83	2176	
3:52	2243	12.26	2241	
3:52	2250	12.35	2254	
3:52	2319	12.80	2321	
3:53	2333	12.91	2338	
3:53	2572	14.72	2610	
3:54	2591	14.80	2622	
3:54	2669	15.46	2721	
3:55	2751	16.02	2806	
3:55	2810	16.41	2865	
3:57	2875	16.42	2867	
Off 3:57	2929	16.68	2907	Tungsten thickness = 2.32 mils

Table 15

Effect of Thermal Cycling on a Pt/Pt-10 Rh Thermocouple  
Flash-Welded to the Tungsten Diffusion Barrier  
on a Graphite Substrate. (See Figure 25a) (Gra-  
phite Surface was Preoxidized)(Specimen No. 23)

Time		Observed Temperature			Remarks
		Surface mv	Thermocouple mv	°F	
On	2:04				Graphite oxidized prior to evaluation. Thermocouple wires flash-welded individually.
	2:05	1610	8.56	1672	
	2:05	1899	10.66	2000	
	2:06	2126	10.81	2022	
	2:06	2171	12.49	2275	
	2:07	2266	13.21	2383	
	2:07	2311	13.56	2435	
	2:08	2390	14.18	2528	
	2:08	2439	14.57	2587	
Off	2:09	2452	14.65	2599	
On	2:11	2234	13.00	2351	
	-	2397	14.10	2510	
	2:12	2415	14.28	2543	
	2:13	2420	14.39	2560	
	2:15	2445	14.45	2569	
Off	2:16	2429	14.48	2574	
On	2:18	2121	12.05	2209	
	-	2350	13.62	2444	
	2:19	2370	13.96	2495	
	2:21	2413	14.24	2537	
Off	2:23	2427	14.35	2554	
On	2:30	2214	12.65	2299	
	-	2350	13.70	2456	
	2:31	2382	13.86	2480	
	2:32	2400	14.09	2515	
	2:33	2411	14.19	2530	
	2:34	2430	14.11	2518	
Off	2:35	2424	14.21	2533	
On	2:39	2199	12.35	2254	
	-	2378	13.71	2458	
	2:40	2415	14.05	2509	
	2:42	2438	14.31	2548	
Off	2:44	2438	14.29	2545	
On	2:47				
	2:48	1916	10.46	1969	
	2:48	1980	10.89	2035	
	2:49	2047	11.38	2109	
	2:49	2103	11.81	2173	
	2:50	2182	12.40	2262	
	2:50	2242	12.75	2314	
	2:50	2400	13.98	2498	
	2:51	2420	14.11	2518	
	2:51	2558	15.21	2684	
Off	2:52	2557	15.19	2681	Tungsten thickness = 1.82 mils.

Table 16

Effect of Thermal Cycling on a Pt/Pt-10 Rh Thermocouple  
Flash-Welded to the Tungsten Diffusion Barrier  
on a Graphite Substrate. (See Figure 25a)(Gra-  
phite Surface Finished with Medium Grit Paper)  
(Specimen No. 25)

Time	Observed Temperature			Remarks
	Surface °F	Thermocouple mv	°F	
On 8:44				Medium grit finish on graphite surface. Thermocouple wires flash-welded individually.
8:46	1743	9.45	1813	
8:49	1953	10.90	2036	
8:50	2006	11.21	2083	
8:51	2177	12.29	2245	
8:52	2195	12.49	2275	
8:53	2221	12.60	2292	
8:55	2335	13.43	2416	
8:56	2411	13.90	2486	
8:57	2481	14.41	2563	
8:57	2500	14.54	2583	
8:58	2491	14.34	2552	
Off 9:00				
On 9:03	2036	11.10	2066	
-	2360	13.29	2395	
9:04	2400	13.58	2438	
9:06	2414	13.71	2458	
Off 9:08	2430	13.80	2471	
On 9:11	2210	12.15	2224	
-	2379	13.39	2410	
9:12	2436	13.76	2465	
9:14	2432	13.79	2470	
Off 9:16	2379	13.36	2405	
On 9:19	2120	11.39	2110	
-	2331	13.00	2350	
9:20	2350	13.16	2375	
9:22	2389	13.16	2375	
Off 9:24	2398	13.16	2375	
On 9:32	2341	13.05	2359	
-	2402	13.46	2420	
9:33	2420	13.59	2440	
9:35	2436	13.76	2465	
Off 9:37	2450	13.88	2483	
On 9:41				
9:43	1929	10.23	1934	
9:43	1955	10.39	1958	
9:45	2002	10.82	2024	
9:48	2089	11.20	2081	
9:49	2112	11.39	2110	
9:49	2264	12.54	2283	
9:49	2294	12.80	2321	
9:50	2350	13.07	2362	
9:51	2331	13.05	2359	
9:53	2478	14.08	2513	
9:53	2545	14.46	2570	
9:54	2630	15.26	2691	
9:55	2660	15.35	2705	
9:55	2750	16.10	2818	
9:56	2813	16.60	2894	
9:56	2827	16.55	2887	
9:57	2894	16.95	2948	
Off 9:58				Tungsten thickness = 2.26 mils

Table 17

Effect of Thermal Cycling on a Pt/Pt-10 Rh Thermocouple  
Flash-Welded to the Tungsten Diffusion Barrier  
on a Graphite Substrate. (See Figure 25a)(Gra-  
phite Surface Finished with Medium Grit Paper )  
(Specimen No. 26)

Time	Observed Temperature			Remarks
	Surface °F	Thermocouple mv	°F	
On 12:52				Medium grit finish on graphite surface. Thermocouple wires flash-welded individually.
12:54	1839	10. 11	1916	
12:54	1863	10. 30	1945	
12:55	1880	10. 35	1952	
12:56	1886	10. 41	1962	
12:58	2051	11. 74	2163	
12:59	2122	12. 20	2232	
1:00	2112	11. 92	2190	
1:03	2240	12. 89	2335	
1:03	2262	13. 07	2362	
1:04	2371	13. 90	2486	
1:04	2401	14. 10	2516	
1:05	2411	14. 20	2531	
Off 1:07				
On 1:10	2206	12. 62	2294	
-	2422	14. 24	2537	
1:11	2464	14. 50	2576	
1:13	2473	14. 59	2590	
Off 1:15	2491	14. 71	2608	
On 1:18	2070	11. 65	2149	
-	2391	13. 79	2470	
1:19	2455	14. 30	2546	
1:21	2502	14. 67	2602	
Off 1:23	2509	14. 65	2599	
On 1:25	2129	11. 80	2172	
-	2440	14. 05	2509	
1:26	2471	14. 31	2548	
1:28	2449	14. 26	2540	
Off 1:30	2464	14. 24	2537	
On 1:35				
-	2241	12. 45	2269	
1:36	2426	13. 85	2479	
1:38	2451	14. 08	2513	
Off 1:40	2469	14. 11	2518	
On 1:43				
1:45	1931	10. 30	1945	
1:46	1944	10. 40	1960	
1:47	1960	10. 54	1981	
1:49	2086	11. 40	2112	
1:50	2171	11. 88	2184	
1:51	2224	12. 27	2242	
1:53	2270	12. 65	2299	
1:53	2299	12. 82	2324	
1:54	2372	13. 43	2416	
1:54	2421	13. 69	2455	
1:55	2439	13. 98	2498	
1:58	2590	14. 99	2650	
1:59	2610	15. 09	2665	
1:59	2751	16. 13	2823	
2:00	2770	16. 26	2843	
2:00	2848	16. 81	2926	
Off 2:01	2870	16. 89	2939	Tungsten thickness = 5.79 mils

Table 18

Effect of Thermal Cycling on a Pt/Pt-10 Rh Thermocouple Flash-  
Welded to the Tungsten Diffusion Barrier on a Graphite  
Substrate (See Figure 25b)(Specimen No. 27)

Time		Observed Temperature		Remarks
		Surface °F	Thermocouple mv °F	
On	8:01			Medium grit finish on graphite surface. Thermocouple wires flash-welded individually.
	8:03	1831	10.24	
	8:04	1869	10.49	
	8:04	2027	11.67	
	8:05	2070	12.05	
	8:06	2117	12.20	
	8:06	2210	12.96	
	8:06	2253	13.30	
	8:07	2297	13.50	
	8:07	2326	13.94	
Off	8:09	2592	15.36	Thermocouple erratic
On	8:11	2460	14.30	
	-	2644	15.50	
	8:12	2672	15.90	
Off	8:13			Thermocouple burned out. Tungsten thickness - 5.56 mils

Table 19

Effect of Thermal Cycling on a Pt/Pt-10 Rh Thermocouple  
Flash-Welded to the Tungsten Diffusion Barrier  
on a Graphite Substrate (See Figure 25b)  
(Specimen No. 28)

Time	Observed Temperature			Remarks
	Surface °F	Thermocouple mv	°F	
On 2:44				Medium grit finish on graphite surface. Thermocouple wires flash-welded individually.
2:46	1823	10.21	1931	
2:46	1882	10.63	1995	
2:47	1902	10.80	2021	
2:47	2002	11.50	2127	
2:48	2030	11.74	2163	
2:48	2115	12.24	2238	
2:48	2144	12.51	2278	
2:49	2238	13.30	2396	
2:49	2294	13.71	2458	
2:49	2320	13.91	2488	
Off 2:50				
On 2:52	1976	11.21	2083	
-	2219	13.01	2353	
2:53	2309	13.83	2476	
2:55	2318	13.95	2494	
Off 2:57	2309	13.81	2473	
On 2:59	1963	11.01	2053	
-	2206	12.92	2339	
3:00	2328	13.80	2471	
3:02	2360	14.20	2531	
Off 3:04	2380	14.30	2546	
On 3:06	1962	10.94	2042	
-	2210	12.96	2345	
3:07	2300	13.71	2458	
3:09	2359	14.06	2510	
Off 3:11	2359	14.09	2515	
On 3:13	1976	11.21	2083	
-	2220	13.07	2362	
3:14	2314	13.81	2473	
3:16	2379	14.17	2527	
Off 3:18	2380	14.20	2531	
On 3:23				
3:26	1829	10.11	1916	
3:26	1978	11.19	2080	
3:27	2005	11.50	2127	
3:27	2087	12.07	2212	
3:28	2115	12.33	2251	
3:28	2156	12.50	2277	
3:28	2269	13.33	2401	
3:28	2340	13.97	2497	
3:29	2366	14.22	2534	
3:29	2378	14.35	2554	
3:30	2479	15.13	2672	
3:30	2539	15.56	2736	
3:31	2590	15.96	2797	
3:31	2608	16.16	2827	
3:32	2690	16.81	2926	
3:32	2699	16.88	2937	
3:32	2801	17.66	3056	
Off 3:33	2820	17.66	3056	Tungsten thickness = 6.05 mils



Table 20

Effect of Thermal Cycling on a Pt/Pt-10 Rh Thermocouple  
Flash-Welded to the Tungsten Diffusion Barrier on a  
Graphite Substrate. (See Figure 25c)  
(Specimen No. 29)

Time	Observed Temperature			Remarks
	Surface °F	Thermocouple mv	°F	
On 7:53				Thermocouple bead formed, then flashed to the tungsten coating. Medium grit finish on graphite surface.
7:55	1883	10.50	1975	
7:55	1911	10.69	2004	
7:56	1986	11.12	2069	
7:56	2031	11.60	2142	
7:57	2088	11.90	2187	
7:58	2198	12.85	2329	
7:58	2270	13.30	2396	
Off 7:59				
On 8:01	2021	11.51	2128	
-	2221	12.98	2348	
8:02	2281	13.60	2441	
8:04	2398	14.39	2560	
Off 8:06	2392	14.34	2552	
On 8:08	2028	11.34	2103	
-	2237	13.01	2353	
8:09	2332	13.88	2483	
8:11	2377	14.26	2540	
Off 8:13	2479	15.04	2658	
On 8:15	2087	11.71	2158	
-	2349	13.87	2482	
8:16	2439	14.71	2609	
8:18	2491	15.04	2658	
Off 8:20	2490	15.15	2674	
On 8:22	2278	13.44	2417	
-	2395	14.46	2570	
8:23	2455	15.09	2665	
8:25	2513	15.35	2705	
Off 8:27	2527	15.39	2711	
On 8:31				
8:34	1847	10.09	1912	
8:34	1852	10.25	1937	
8:35	1920	10.83	2025	
8:35	1939	11.12	2069	
8:36	1990	12.19	2230	
8:39	2139	12.70	2306	
8:39	2200	12.68	2303	
8:41	2323	13.74	2462	
8:42	2350	14.31	2521	
8:43	2477	15.01	2653	
8:44	2627	16.20	2834	
8:45	2702	17.12	2974	
Off 8:45	2758	16.95	2948	
				Window in main port fogged with condensate from air.
				Fog Thermocouple burned out. Tungsten thickness = 1.39 mils.

Table 21

Effect of Thermal Cycling on a Sensing Element with  
a Second Tungsten Vapor Deposition Applied over  
the Thermocouple Junction Protected with Alumina  
Cement (Specimen No. 32)

Time		Observed Temperature			Remarks
		Surface °F	Thermocouple mv	°F	
On	8:12				Bead flash-welded to tungsten; thermocouple junction covered with Alundum cement and a second vapor deposition was applied.
	8:15	1860	10.39	1959	
	8:15	1913	10.75	2013	
	8:16	2045	11.71	2158	
	8:16	2102	12.15	2224	
	8:17	2095	11.95	2194	
	8:18	2218	12.81	2323	
	8:18	2261	13.25	2389	
Off	8:20	2290	13.45	2419	
On	8:22	1978	10.80	2021	
	-	2152	12.31	2248	
	8:23	2279	13.28	2393	
	8:24	2449	14.60	2592	
	8:25	2430	14.49	2575	
Off	8:27	2430	14.41	2563	
On	8:29	2155	12.25	2239	
	-	2285	13.20	2381	
	8:30	2378	14.15	2524	12.05 mv questionable
	8:31	2541	15.37	2708	
	8:32	2572	15.49	2726	
Off	8:34	2577	15.41	2714	
On	8:43	2105	12.05	2209	
	-	2467	14.61	2593	
	8:44	2663	16.04	2809	
	8:45	2665	16.01	2805	
	8:46	2619	15.63	2747	
Off	8:48	2649	15.79	2771	
On	8:52	2107	11.60	2142	
	-	2411	13.94	2492	
	8:53	2548	14.96	2646	
	8:54	2579	15.25	2690	
	8:55	2580	15.25	2690	
Off	8:57	2601	15.34	2703	
On	9:01				Power supply acting erratically
	9:02	1990	10.89	2035	
	9:02	2069	11.41	2113	
	9:03	2162	12.08	2214	
	9:03	2270	12.86	2330	
	9:04	2401	13.87	2480	
	9:04	2470	14.35	2554	
	9:04	2503	14.66	2601	
	9:05	2663	15.89	2787	
	9:05	2703	16.25	2841	
	9:07	2450	14.30	2546	
	9:08	2560	14.94	2643	
	9:08	2640	15.64	2749	
	9:09	2830	17.09	2969	
Off	9:09	2917	17.66	3057	

Table 22

Effect of Thermal Cycling on a Sensing Element with  
Second Tungsten Vapor Deposition Applied over the  
Thermocouple Junction Protected with Alumina Cement  
(Specimen No. 36)

Time	Observed Temperature			Remarks
	Surface °F	Thermocouple mv	°F	
On 2:19				Bead flash-welded to tungsten; thermocouple junction covered with Alundum cement and a second vapor deposition was applied.
2:21	1931	10.89	2035	
2:21	2030	11.55	2134	
2:22	2098	12.14	2223	
2:22	2149	12.41	2263	
2:23	2373	14.10	2516	
Off 2:24	2483	15.05	2659	
On 2:26	2089	11.75	2164	
-	2399	14.26	2540	
2:27	2511	15.25	2690	
2:28	2551	15.54	2733	
2:29	2550	15.55	2735	
Off 2:31	2519	15.25	2690	
On 2:33	2023	10.40	1960	
-	2387	14.10	2516	
2:34	2519	15.19	2681	
2:35	2538	15.39	2711	
2:36	2551	15.54	2733	
Off 2:38	2560	15.54	2733	
On 2:40	2302	13.23	2385	
-	2460	14.56	2586	
2:41	2520	15.23	2687	
2:42	2540	15.35	2705	
2:43	2550	15.45	2720	
Off 2:45	2570	15.52	2730	
On 2:47	2107	11.46	2121	
-	2407	14.02	2504	
2:48	2510	15.14	2673	
2:49	2542	15.41	2714	
2:50	2520	15.16	2676	
Off 2:52	2520	15.16	2676	
On 2:55				
2:56	1949	10.65	1998	
2:56	2027	11.26	2091	
2:57	2084	11.66	2151	
2:57	2183	12.48	2274	
2:58	2212	12.65	2299	
2:58	2256	13.00	2351	
2:59	2278	13.24	2387	
2:59	2410	14.17	2527	
3:00	2452	14.51	2578	
3:00	2593	15.66	2752	
3:01	2653	16.20	2834	
3:01	2690	16.56	2888	
3:01	2786	17.20	2986	
Off 3:02	2814	17.35	3009	

Table 23

Effect of Thermal Cycling on a Sensing Element Assembly  
of the Type Shown in Figure 37. (Specimen No. 40)

Time	Observed Temperature			Remarks
	Surface °F	Thermocouple mv	°F	
On 10:37				Bead flash-welded to tungsten surface; thermocouple junction covered with Alundum cement; 0.025" diameter tungsten retainer ring and tungsten powder passing 200 mesh seive placed on back surface; a second tungsten vapor deposition was applied to bond the tungsten powder and ring.
10:38	2048	11.61	2143	
10:38	2110	12.09	2215	
10:39	2133	12.26	2241	
10:39	2232	13.00	2351	
10:40	2291	13.50	2426	
10:40	2440	14.65	2599	
10:41	2479	14.95	2644	
Off 10:42	2490	14.98	2649	
On 10:44	2035	11.61	2143	
-	2426	14.40	2562	
10:45	2518	15.06	2661	
10:46	2547	15.26	2691	
10:47	2523	15.13	2672	
Off 10:49	2548	15.20	2682	
On 10:51	2139	12.26	2241	
-	2462	14.60	2592	
10:52	2539	15.20	2682	
10:53	2549	15.11	2669	
10:54	2551	15.21	2684	
Off 10:56	2561	15.16	2676	
On 10:58	2046	11.33	2101	
-	2451	14.28	2543	
10:59	2565	14.96	2646	
11:00	2568	15.06	2661	
11:01	2568	15.18	2679	
Off 11:03	2534	14.89	2635	
On 11:05	2119	11.50	2127	
-	2420	13.86	2480	
11:06	2522	14.80	2622	
11:07	2573	15.04	2658	
11:08	2574	15.05	2659	
Off 11:10	2563	15.05	2659	
On 11:12				
11:13	1948	10.49	1974	
11:13	2052	11.14	2072	
11:13	2081	11.40	2112	
11:14	2136	11.80	2172	Thermocouple wavering
11:14	2224	12.30	2247	
11:15	2297	13.05	2359	
11:15	2358	13.28	2393	
11:16	2412	13.75	2464	
11:16	2443	14.44	2568	
11:17	2632	15.40	2712	
11:17	2652	15.69	2756	
11:17	2719	16.16	2827	
11:18	2749	16.40	2864	
11:18	2830	16.94	2946	Maximum output = 17.15 mv
Off 11:19				

## PART II

### DEVELOPMENT OF A HIGH TEMPERATURE BLACKBODY SOURCE FOR CALIBRATION OF HEAT FLUX SENSORS

#### INTRODUCTION

To provide an accurate means of calibrating heat flux sensors, a high temperature blackbody radiation source was developed. The cavity was constructed of graphite, with a one-inch diameter water cooled aperture, and was inductively heated using a 25 kw Lepel unit operating at a frequency of about 400 kc. Design specifications called for a maximum irradiance of 100 Btu/ft<sup>2</sup>/sec.

The primary problems encountered during the development concerned the proper design of the cavity and load coil to eliminate thermal gradients within the cavity.

#### DEVELOPMENT OF THE BLACKBODY

The development of a blackbody with a one-inch diameter aperture was based on prior experience here with a cylindrical graphite cavity having a  $\frac{1}{2}$  inch diameter aperture and a 6:1 aspect ratio. The  $\frac{1}{2}$  inch diameter blackbody was inductively heated, using a 25 kw Lepel power supply. Since the  $\frac{1}{2}$  inch blackbody performed quite satisfactorily, its basic design features were retained in the larger one-inch blackbody. However, several problems developed in scaling up the design. These primarily involved determining the most efficient cavity design for maximum irradiance, and the proper configuration of cavity and load coil to minimize thermal gradients.

The assembled blackbody apparatus is shown schematically in Figure 1; drawings of the major components are shown in Figures 2 through 6. The blackbody consisted basically of a graphite cavity, induction heating coil, water cooled aperture and optical stop.

For thermal insulation, thermatomic carbon was used between the cavity and the load coil, and Fiberfrax was placed around the sides and bottom of the housing. For additional thermal protection, a cooling coil constructed of  $\frac{1}{8}$  inch diameter copper tubing was placed in the bottom of the housing. A zirconia disc was placed on top of this cooling coil for thermal insulation and to support the thermatomic carbon.

The water cooled aperture, shown in Figure 4, was thermally insulated from the top surface of the cavity and from the thermatomic carbon with several Grafoil and mica washers, comprising a stack approximately  $\frac{1}{8}$  inch thick. Two mica washers were placed directly beneath the aperture to electrically insulate it from the graphite cavity.

The graphite cavity, shown in Figure 2, was basically cylindrical with a conically shaped interior. This configuration was modified from the initial design, shown in Figure 8, in order to obtain better coupling with the induction coil and a more uniform temperature. The diameter of the entrance hole was increased from 1 inch to  $1\frac{1}{2}$  inches to give the maximum irradiance to a calorimeter placed directly above the aperture.

The induction coil is shown in Figure 3. It consisted of two concentric helically wound coils constructed of  $\frac{1}{4}$  inch diameter soft copper tubing. To provide electrical insulation the coil was dipped three times in General Electric Glyptal 1201 red enamel. It was then encased in alumina cement to provide structural rigidity and further thermal protection. The double wound helix was used to concentrate more power input near the top of the cavity, thereby reducing thermal gradients. With this design the maximum thermal gradient was about 300°F between top and bottom of the cavity when the temperature at the bottom was 4100°F.

The transite housing is shown in Figure 6. This housing was provided with a stainless steel flange which mated with a second stainless steel flange through which the aperture cooling coils and a water cooled optical stop were installed. The optical stop was used to shield the calorimeter from the high intensity radiation between readings. A photograph of the housing with the bottom cooling coil installed is shown in Figure 9.

The cavity was heated by means of a Lepel 25 kw induction heating unit, which operated at 250 v, three phase at a frequency of 400 kc.

### CALIBRATION OF THE BLACKBODY

Calibration curves for the blackbody were established by measuring the irradiance at various temperatures and ranges (distances from the aperture) using precalibrated heat flux sensors. The primary calibration standard employed was the copper slug calorimeter shown in Figure 10. The sensing element was a  $\frac{1}{2}$  inch diameter x  $\frac{1}{8}$  inch thick copper disc, shown in Figure 11. The sensor was installed in a transite housing insulated with thermatomic carbon ( $k \approx 0.1$  Btu/hr/ft<sup>2</sup>/°F/in.).

The exposed surface of the thermatomic carbon and the housing were covered with a reflective shield of aluminum foil. To obtain maximum emittance, the surface of copper disc was grooved as shown in Figure 11 and painted with Japalac flat black enamel. The emittance of one such disc was measured over the temperature range from 500°F to 1050°F using the apparatus described in the Appendix. The results shown in Table 1 and Figure 13, show that the emittance was constant at about 0.9 up to 800°F. Above 800°F, it decreased slightly to a value of 0.85 at 1000°F. During the calibrations, therefore, the effects of changing emittance were avoided by limiting the calorimeter temperature to 700°F.

In operation, the cavity was heated to the desired temperature while maintaining an argon purge through the housing. The calorimeter was positioned directly above the cavity at the desired distance from the aperture. The calorimeter thermocouple leads were connected to an X-Y time recorder (Mosely Model 135). The optical stop was pulled out, exposing the sensor to irradiance from the blackbody. Simultaneously, the X-Y recorder was turned on and a plot of calorimeter output in millivolts versus time obtained. The heat flux density received by the calorimeter was calculated from the initial slope of the temperature time curve using the equation

$$\frac{q}{A} = \frac{w}{A} C \frac{T}{t}$$

where

$q$  = heat flux density, Btu/ft<sup>2</sup>/sec

$w$  = weight of the painted copper disc, lb

$A$  = cross-sectional area of the disc, ft<sup>2</sup>

$C$  = heat capacity of copper, Btu/lb/°F

$\frac{T}{t}$  = slope of the temperature-time curve, °F/sec

The cavity temperature was measured by sighting vertically to the bottom of the cavity with an optical pyrometer (Leeds and Northrup Model 8622).

Temperature readings were taken before and after exposing the calorimeter. The temperatures shown in Tables 2 through 5 are the final temperatures, which were somewhat lower than the initial temperatures as a result of the thermal load imposed on the cavity by the calorimeter. On most runs, temperatures were also measured on the cavity wall just below the aperture. As previously noted, the maximum difference between the top and bottom temperatures was about 300°F, occurring when the temperatures at the bottom of the cavity measured about 4100°F.

For those runs in which the desired range fell below the optical stop, the following procedure was used. The range was marked on the vertical shaft supporting the calorimeter, the optical stop was removed, the X-Y recorder was switched on and the calorimeter lowered to the correct location. After the temperature-time curve was obtained, the calorimeter was withdrawn, the cavity temperature measured and the stop closed. This procedure was necessary in order to maintain the calorimeter at room temperature prior to the exposure. Recall that all measurements of heat flux density were taken from the initial slope of the temperature-time curves, when the calorimeter temperature was slightly above room temperature. This procedure was used consistently in order to avoid introducing errors due to reradiation from the calorimeter surface, changes in the surface emittance, and other temperature-dependent variables. After removing the optical stop, the calorimeter was lowered as rapidly as possible, this operation causing no noticeable variation in the results.

As a check on the repeatability of the measurements, several temperature-time curves were obtained using three different calorimeters at a range of 3 inches. The calorimeters used were a copper disc type, a standard NASA radiation calorimeter (Chrysler Model No. N-118, Serial No. 162), and a graphite sensor of the final configuration described in Part I of this report. The slopes of the temperature-time curves were repeatable for the first two calorimeters within about 3 percent, and for the graphite calorimeter within about 7 percent.

Based on the results using the copper disc calorimeter, the overall uncertainty of the calibrations was estimated at  $\pm 5$  percent for heat flux densities between 1 Btu/ft<sup>2</sup>/sec and 100 Btu/ft<sup>2</sup>/sec. This estimate is believed to be conservative, and allows for any systematic errors not apparent in the data. The computed error was usually less than 5 percent. For example, refer to the six runs tabulated in Table 3, Series No. 6, for calorimeters 5 and 6 at a range of 3 inches. The cavity temperature was 2700°F, allowing for an uncertainty of  $\pm 10^\circ\text{F}$  in the optical pyrometer readings. The average heat flux density and standard deviation were 1.32 Btu/ft<sup>2</sup>/sec and 0.057 Btu/ft<sup>2</sup>/sec, respectively, yielding a probable error of  $\pm 2.8$  percent.



Referring back to Figure 13, observe that the data follow the theoretically predicted curves except at the very short ranges. At ranges of 3 inches and 6 inches, the theoretical and measured values agree within 15 percent. At ranges closer than 3 inches, the deviation was larger. At ranges below 1 inch, the measured heat flux density was noticeably affected by any variation in the thickness of the insulation between the aperture and the top of the cavity.

#### ACKNOWLEDGEMENTS

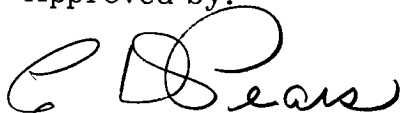
John M. Carroll performed most of the development and calibration of the graphite heat flux sensor and the blackbody source. W.T. Engelke designed and calibrated the final prototype configuration of the graphite calorimeter. H. P. Cox performed the vapor plating of tungsten on the graphite sensing elements. Hassell Hancock assisted in the calibrations. C.M. Pyron, Jr. was project leader.

Submitted by:



C.M. Pyron, Jr., Head  
Thermodynamics Section

Approved by:



C. D. Pears, Head  
Mechanical Engineering Division

7384-1481-6-XLI

(10:12) lw

July 26, 1965

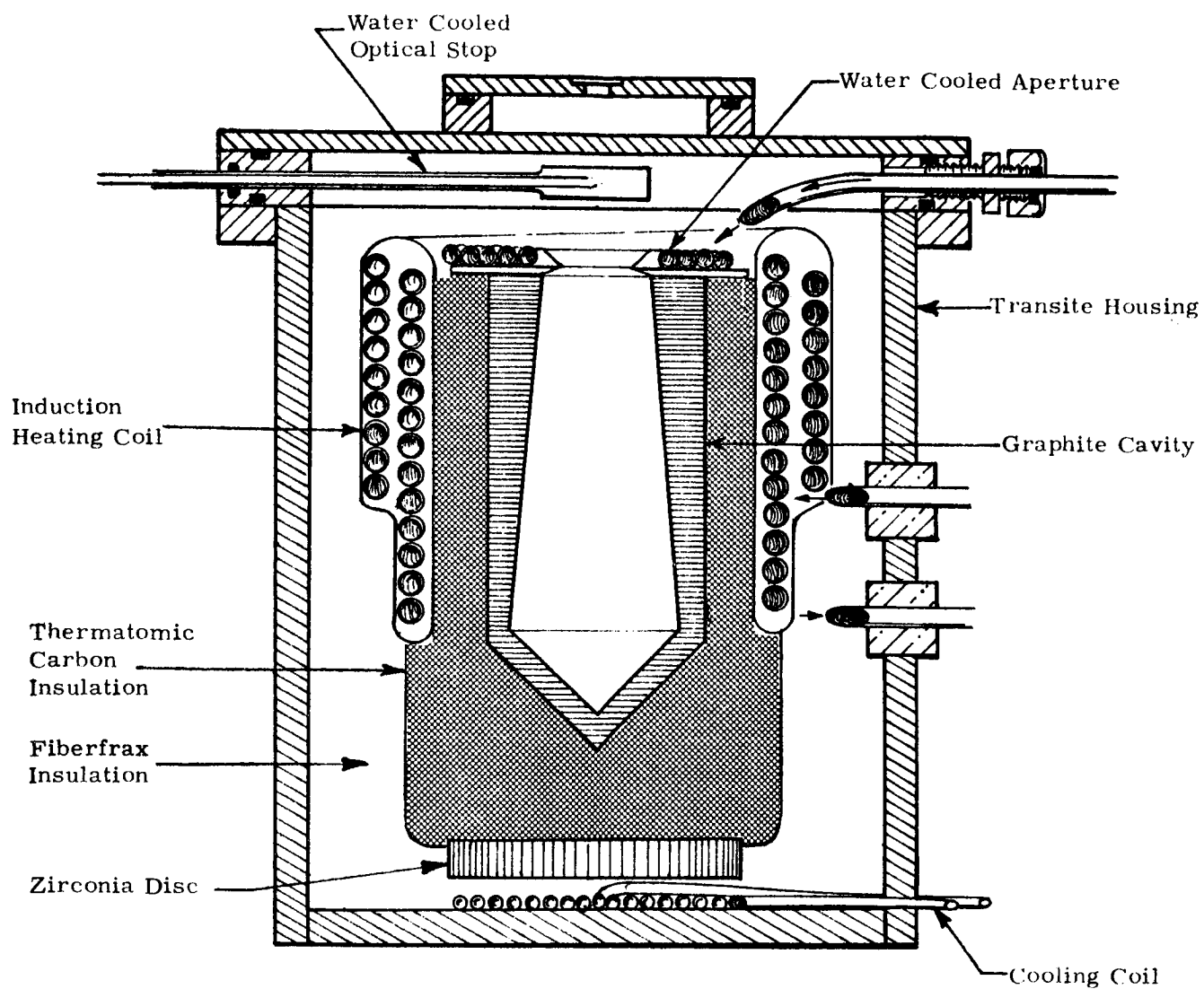


Figure 1. Cross Section of Blackbody Assembly Showing Induction Coil and Aperture Plate

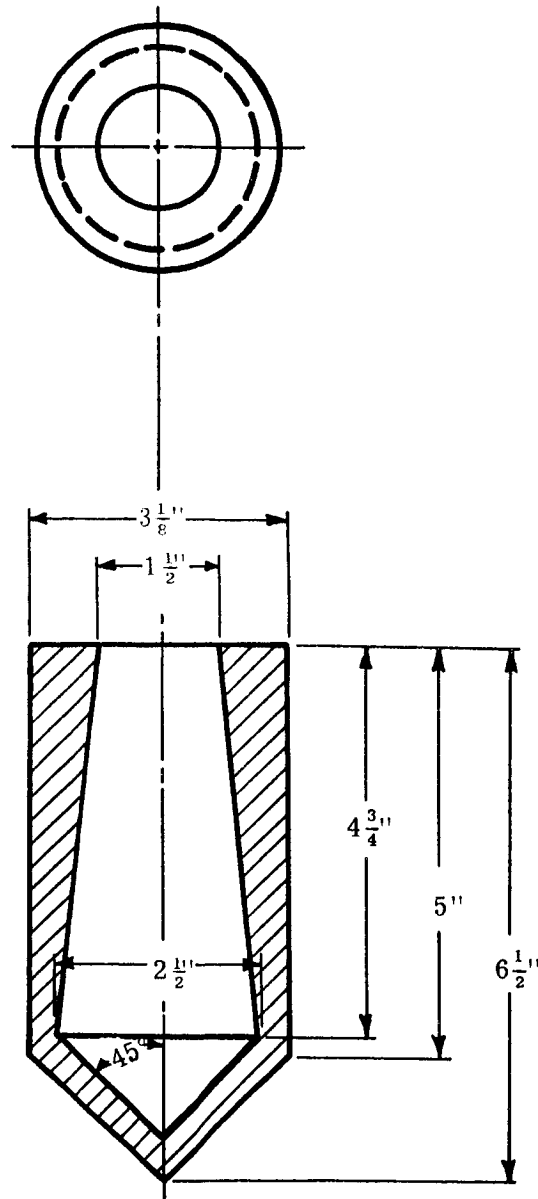


Figure 2. Final Configuration of Graphite Cavity Used in the Blackbody

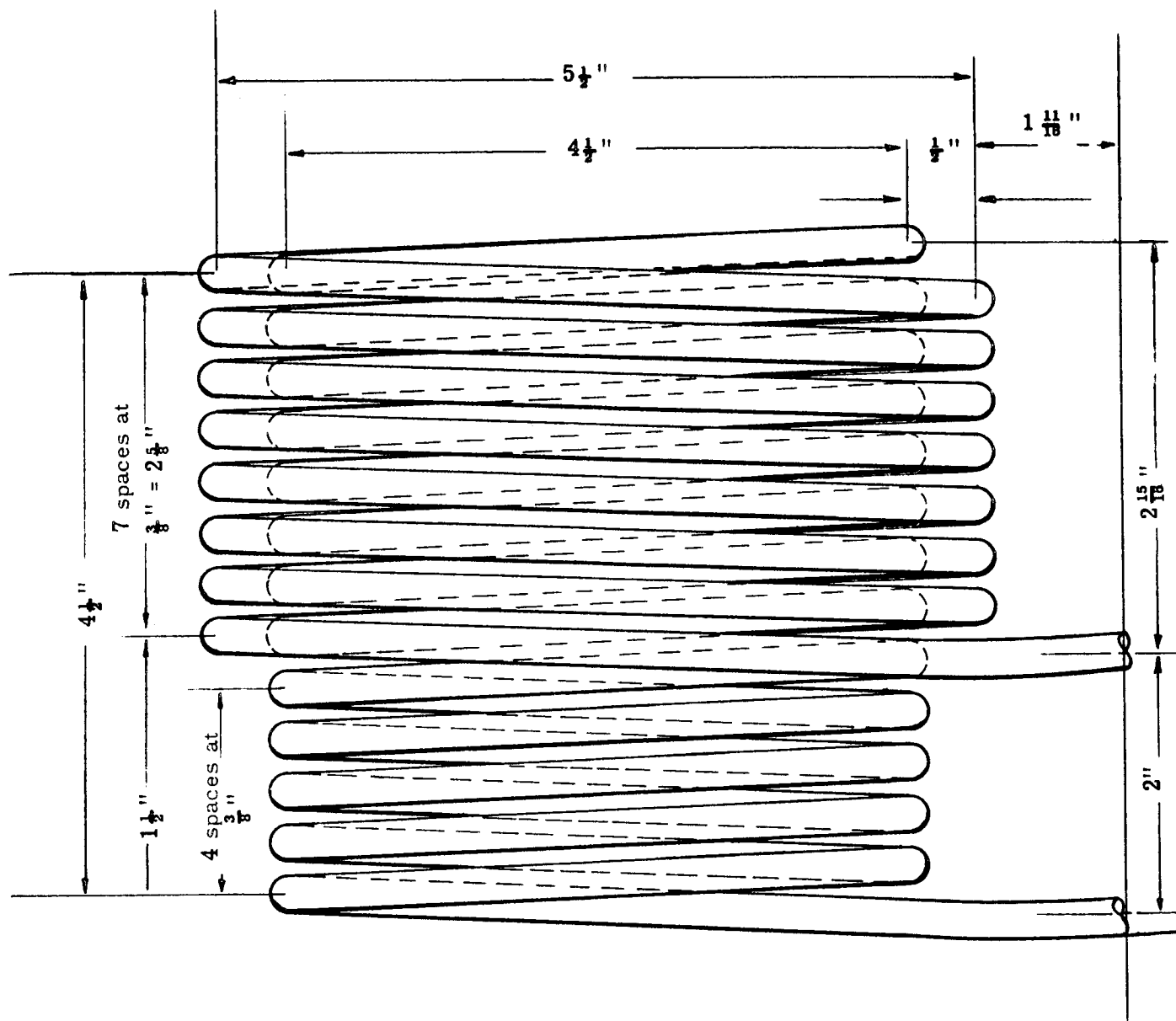


Figure 3.  $\frac{1}{4}$  inch Diameter Copper Induction Coil for Blackbody Cavity

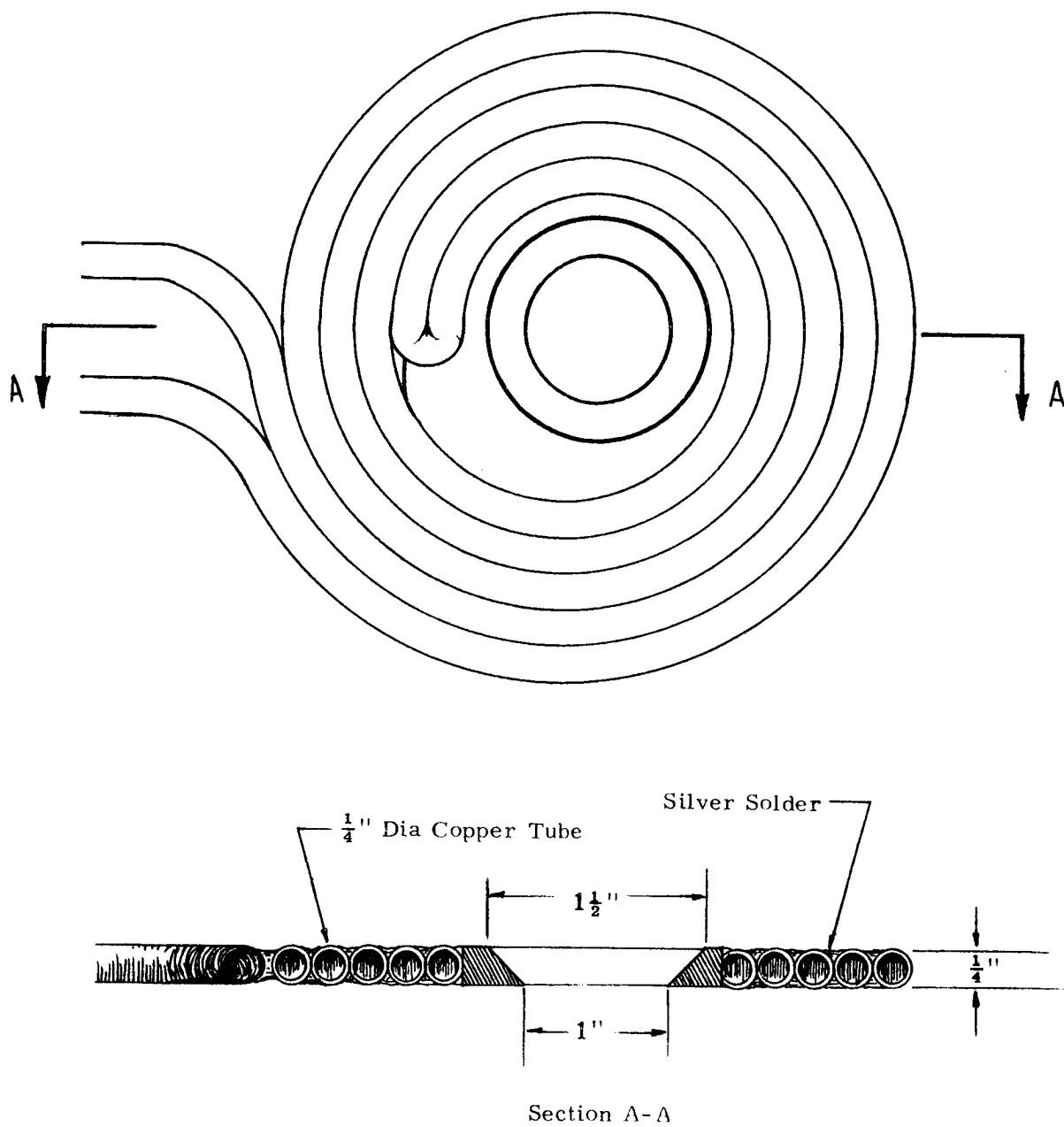
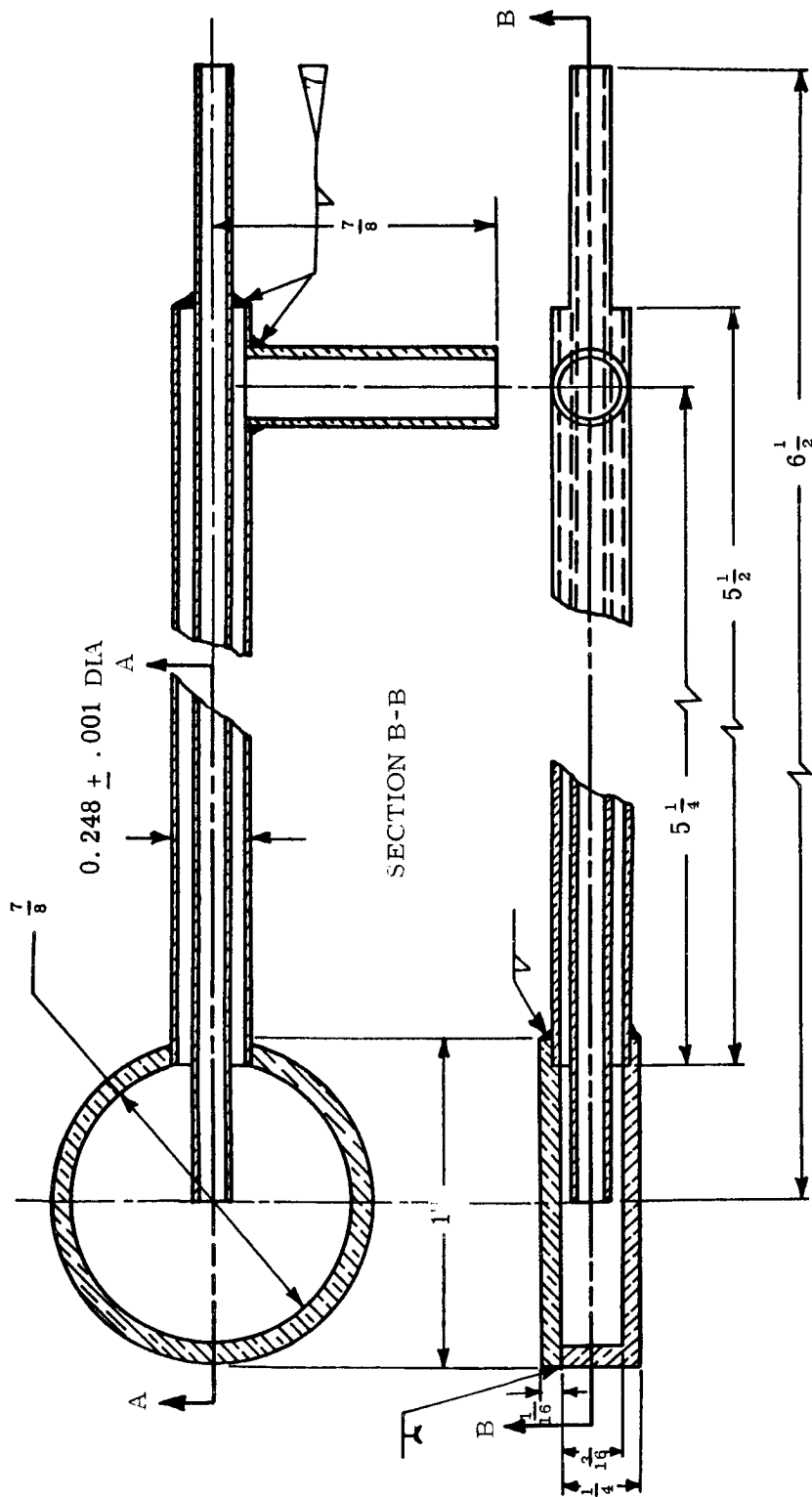


Figure 4. Water Cooled Aperture Plate



SECTION A-A  
SCALE 2" = 1"

Material: Copper

Figure 5. Water Cooled Optical Stop

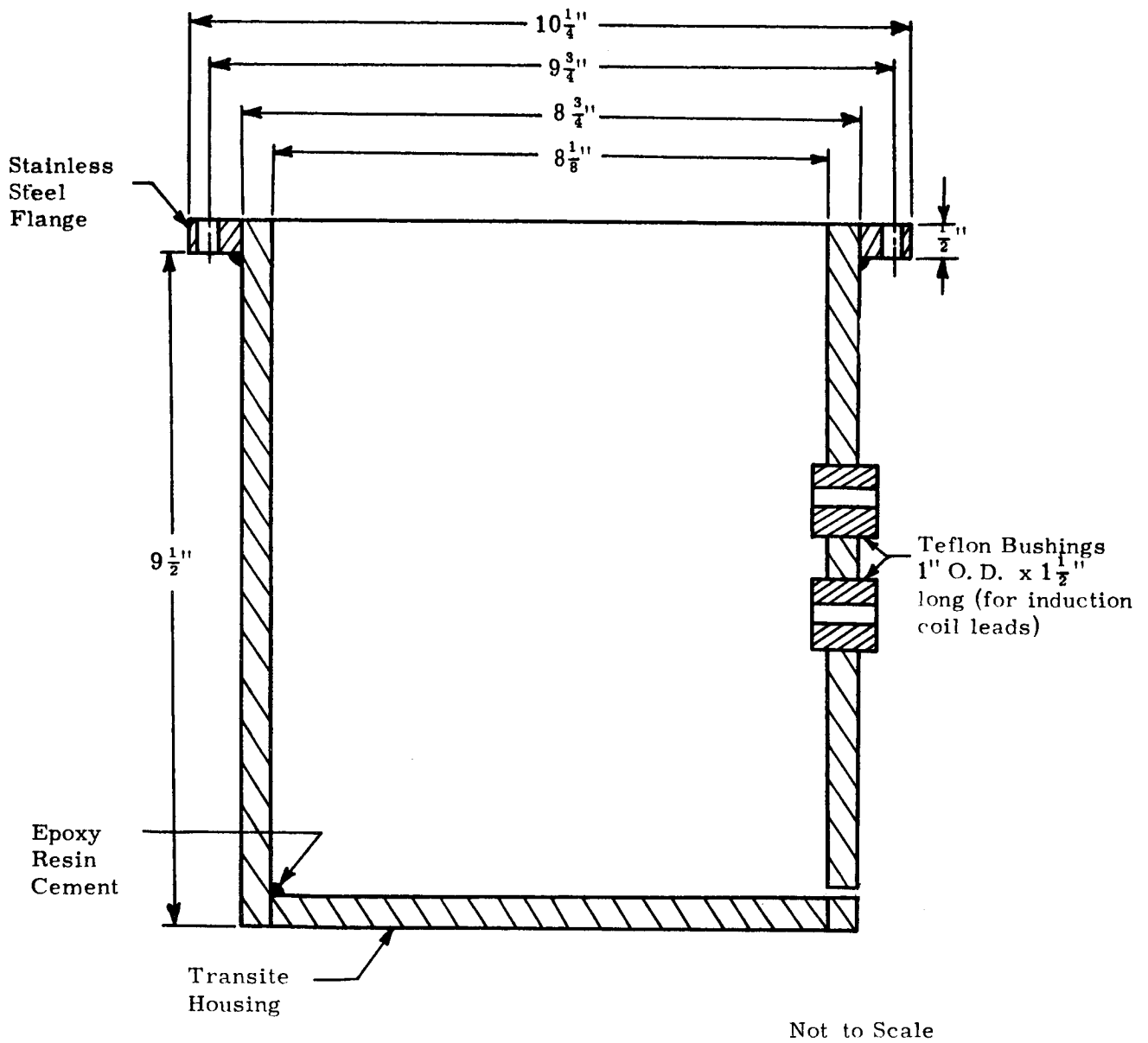


Figure 6. Housing for Blackbody Cavity

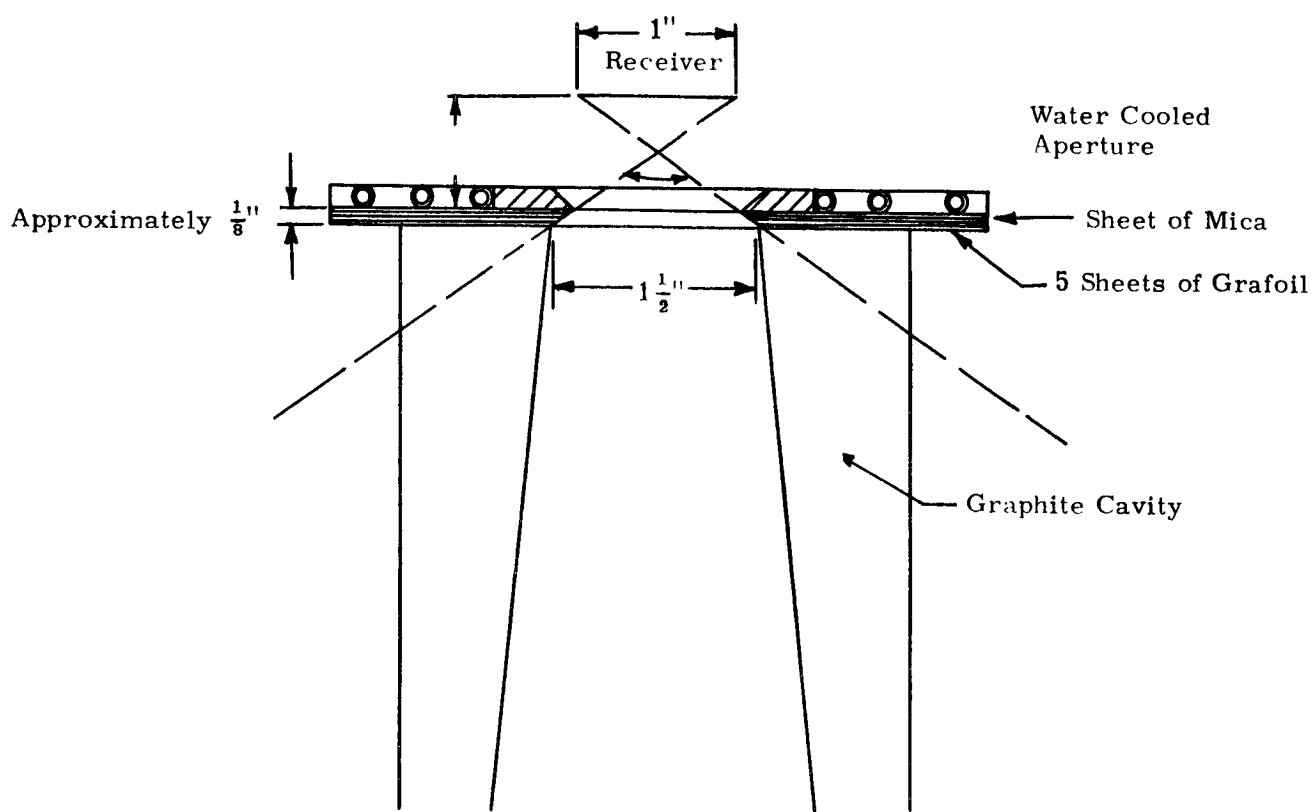
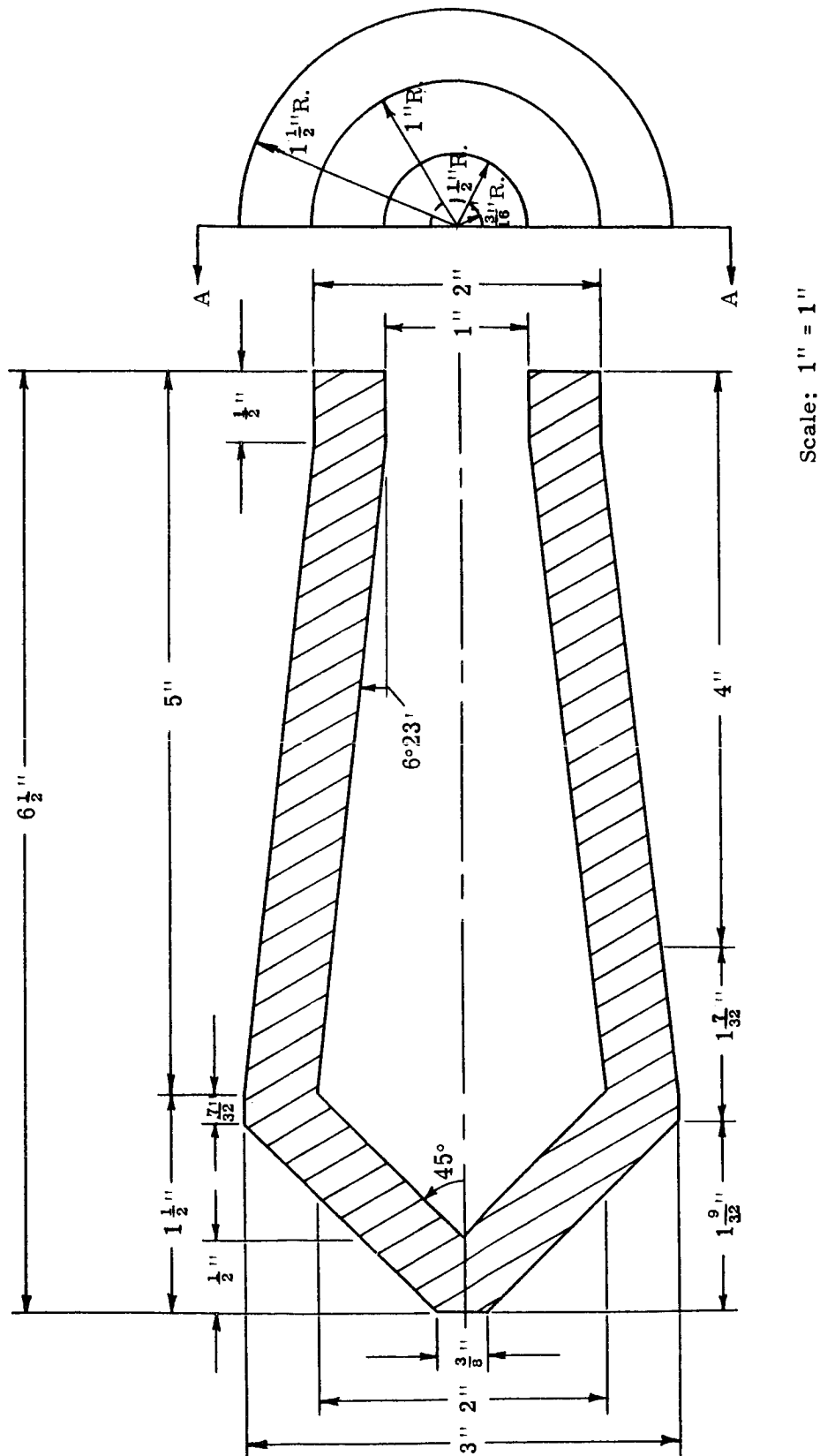


Figure 7. Sketch Showing Insulation Between Cavity and Aperture





Section A-A

Scale: 1" = 1"

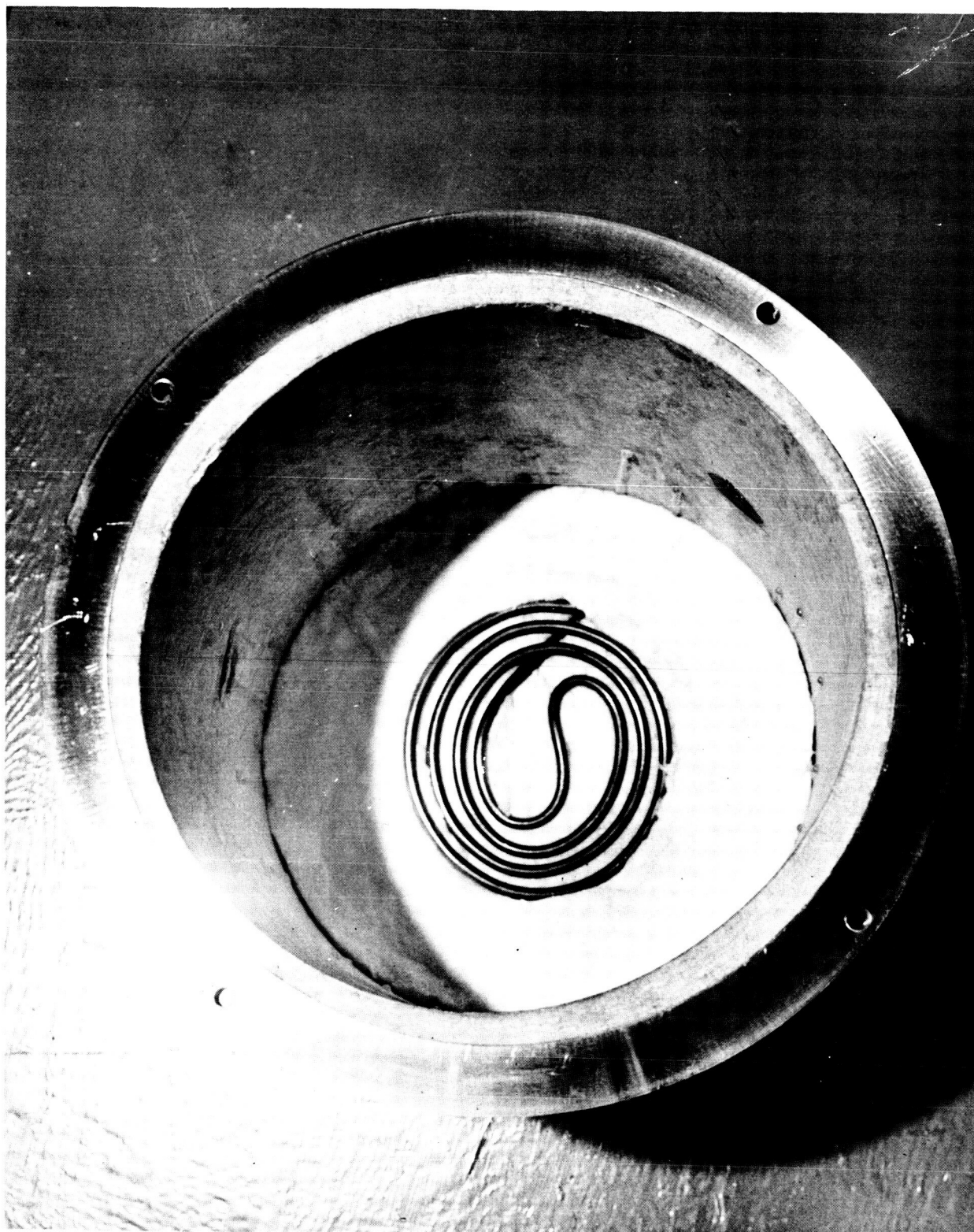
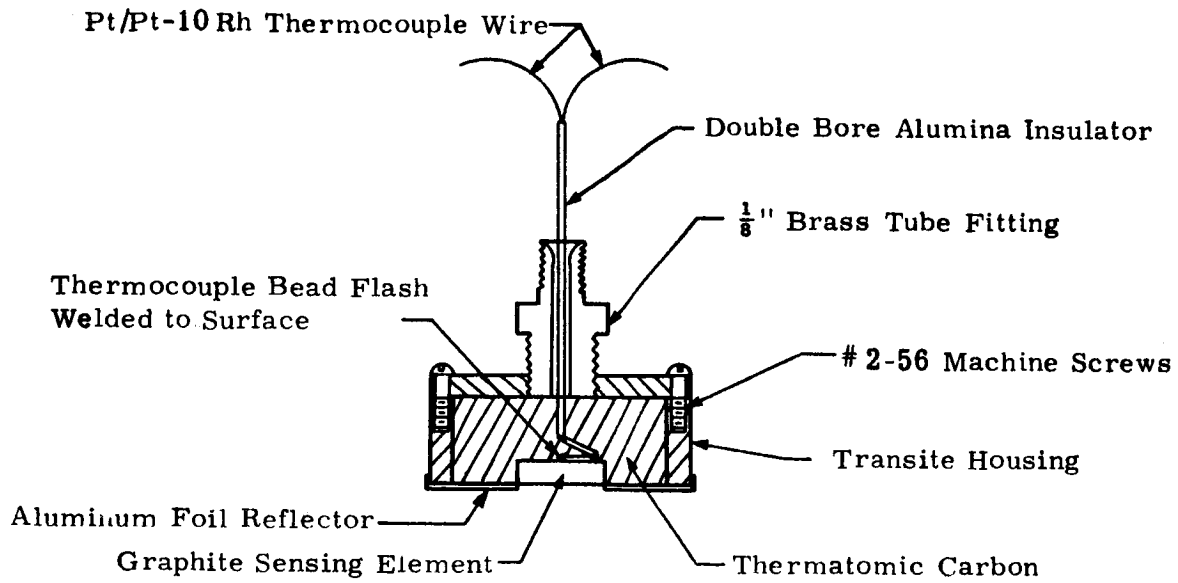
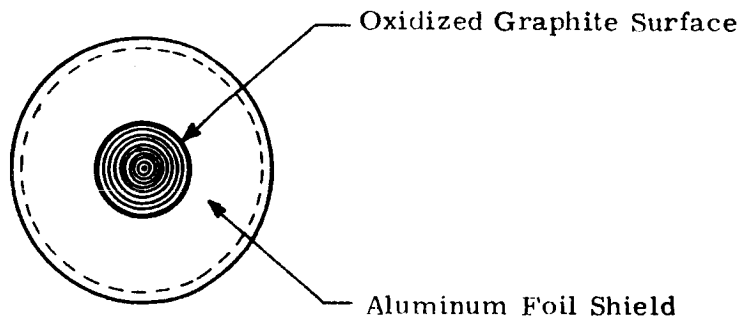


Figure 9. Photograph from the Vertical of the Blackbody Housing showing the  $\frac{1}{8}$ " Diameter Copper Cooling Coil surrounded by Fiberfrax



Cross-Sectional View



Sensing Surface

Scale: 1" = 1"

Figure 10. Cross-Sectional View and Sensing Surface of.  
the Assembled Copper Calorimeter for  
Calibrating the Blackbody Cavity

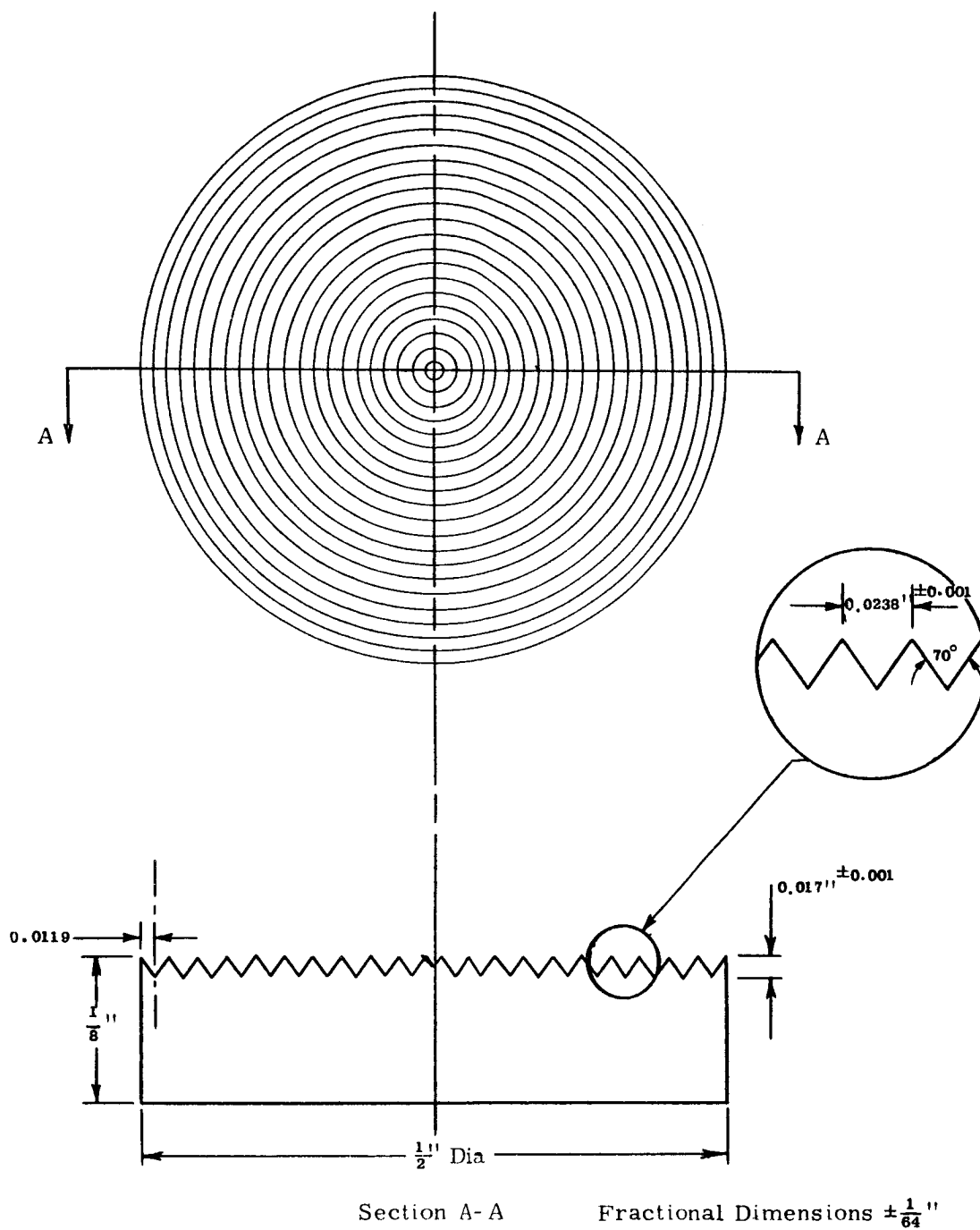


Figure 11. Grooved Copper Slug for Radiation Calorimeter Assembly  
Used in Calibrating the Blackbody Cavity

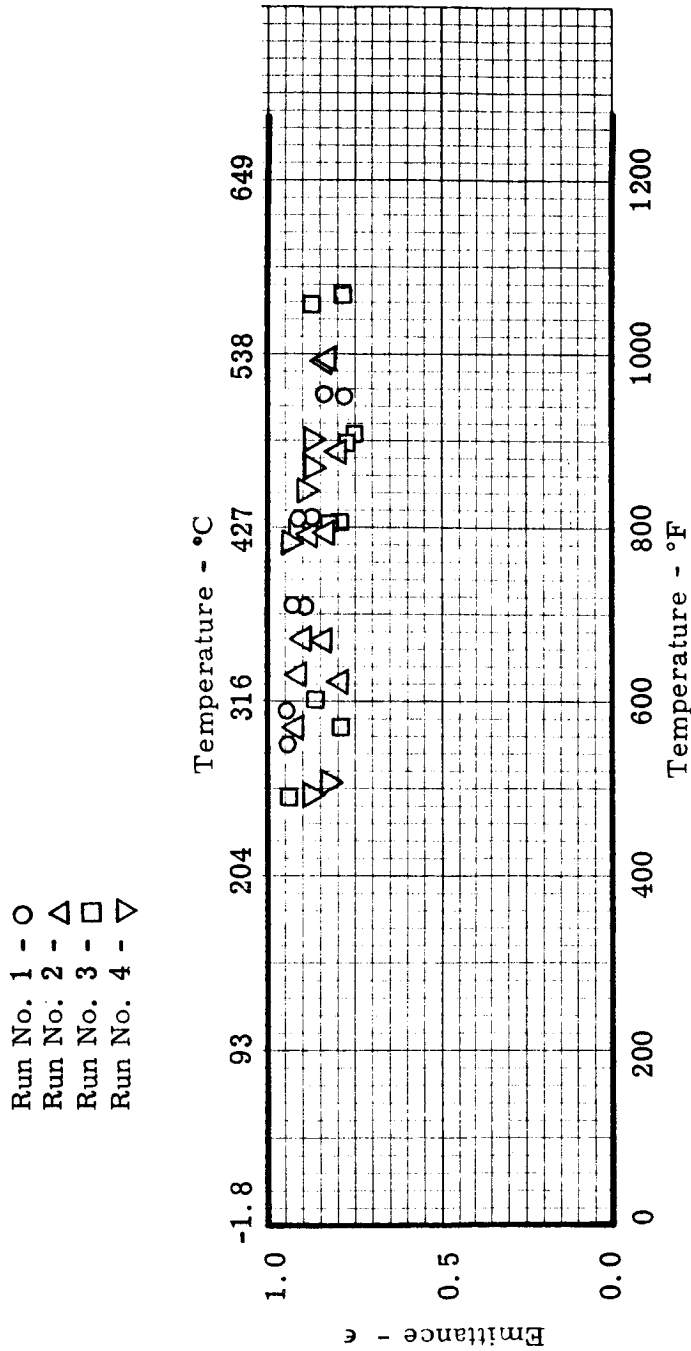


Figure 12. The Emittance During Repeated Cycles in Argon of a Grooved Copper Disc Painted with "Japalac" Flat Black Paint. Calorimeter No. 1 Used in Calibrating the Blackbody Cavity

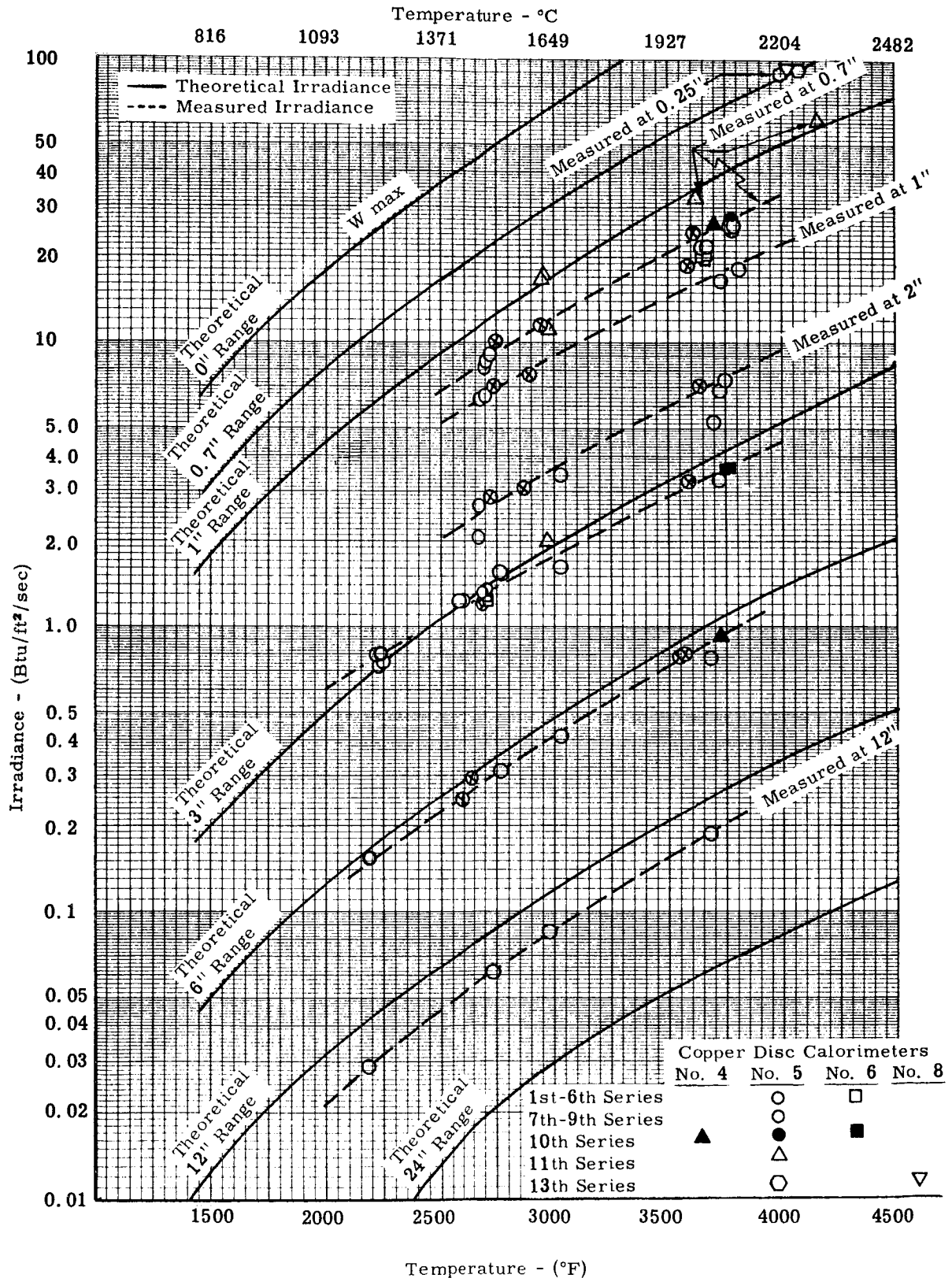


Figure 13. Theoretical and Measured Irradiances During Calibration Runs on the High Temperature Blackbody Radiation Source Using Four Copper Disc Calorimeters

Table 1

The Emittance of Grooved Copper Disc Painted with  
"Japalac" Flat Black Paint During Repeated Runs in Argon  
(Calorimeter No. 1)

Time	Thermocouple Output Millivolts	Radiometer Output Millivolts	Disc Temperature °F	Emittance	Remarks
Run No. 1					Chromel-alumel thermocouple wires flash welded to back surface. Slug size = $\frac{1}{8}$ " dia. x $\frac{1}{8}$ " thick
On 9:00					
9:10	11.75	0.013	552	0.95	
9:13	12.37	0.015	579	0.95	
9:21	15.43	0.024	711	0.90	
9:25	15.45	0.025	712	0.94	
9:34	17.61	0.034	804	0.91	
9:36	17.70	0.033	808	0.87	
9:44	21.24	0.051	957	0.84	
9:46	21.25	0.050	958	0.82	
Off 9:47					
Run No. 2					
On 9:53					
10:08	12.05	0.014	565	0.93	
10:17	13.50	0.018	628	0.92	
10:18	13.27	0.015	618	0.80	
10:27	14.55	0.022	673	0.96	
10:29	14.57	0.021	674	0.91	
10:37	17.21	0.032	787	0.90	
10:39	17.49	0.031	799	0.85	
10:45	19.75	0.040	894	0.80	
10:46	19.60	0.040	888	0.80	
10:54	21.85	0.056	983	0.85	
10:56	22.00	0.056	989	0.84	
Off 10:59					
Run No. 3					
On 12:19					
12:29	10.36	0.010	491	0.96	
12:34	12.15	0.012	569	0.80	
12:44	12.90	0.015	602	0.87	
1:00	16.23	0.029	745	0.97	
1:05	17.61	0.031	804	0.83	
1:07	17.62	0.030	804	0.80	
1:12	19.77	0.039	895	0.79	
1:14	20.05	0.040	907	0.76	
1:20	23.60	0.070	1057	0.88	
1:23	23.75	0.065	1063	0.80	
Off 1:24					
Run No. 4					
On 1:28					
1:39	10.31	0.009	489	0.87	
1:42	10.49	0.009	497	0.83	
1:58	17.08	0.033	781	0.96	
2:00	17.40	0.034	795	0.93	
2:09	19.00	0.040	863	0.88	
2:11	18.50	0.038	842	0.90	
2:17	19.90	0.045	901	0.88	
Off 2:24					

Table 2

Results of Calibration Runs on  
The High Temperature Blackbody Radiation Source

Calorimeter No. and Run No.	Range (in.)	Slope (mv/sec)	Heat Flux (Btu/ft <sup>2</sup> /sec)	Temperature on Bottom of Cavity (°F)	Remarks	
Series No. 1						
Calorimeter No. 5						
Run 1	12	0.00122	0.0289	2178	C=0.0925 Btu/lb/°F W/A=5.820 lb/ft <sup>2</sup> , X-Y calibration, Y=0.49 mv/in. X=10 sec/ in.	
2	6	0.00653	0.154	2191		
3	3	0.0335	0.791	2210		
4	12	0.00261	0.0616	2732		
5	6	0.0136	0.320	2760		
6	3	0.0657	1.55	2759		
Series No. 2						
Calorimeter No. 5						
Run 1	12	0.00360	0.0850	2929	X-Y cali- bration, Y= 0.48 mv/in. on 0.5 scale and 1.0 mv/ in. on 1.0 scale X = 10 sec/in.	
2	6	0.0174	0.410	2972		
3	3	0.0680	1.61	2971		
4	2	0.146	3.44	2971		
5	12	0.00795	0.188	3679		
6	6	0.0328	0.775	3688		
7	3	0.140	3.30	3720		
8	2	0.222	5.24	3700		
Series No. 3						
Calorimeter No. 5						
Run 1	3	0.0342	0.806	2224	X-Y calibration, Y=0.50 mv/ in., X=10 sec/in.	
Calorimeter NASA						
Run 2	3	0.0189	-	2229		
3	3	0.0186	-	2231		
4	3	0.0192	-	2224		
Calorimeter-Graphite						
Run 5	3	0.0093	-	2242		
6	3	0.0100	-	2240		
Calorimeter NASA						
Run 7	3	0.0193	-	2246		
8	3	0.0188	-	2240		
9	3	0.0184	-	2252		
Calorimeter No. 5						
Run 10	3	0.0318	0.752	2240		
11	3	0.0304	0.717	2226		
Calorimeter-Graphite						
Run 12	3	0.0101	-	2220		
13	3	0.0094	-	2214		



Table 3

Results of Calibration Runs on the High Temperature Blackbody Radiation Source

Calorimeter No. and Run No.	Range (in)	Slope (mv/sec)	Heat Flux (Btu/ft <sup>2</sup> /sec)	Temperature on Bottom of Cavity (°F)	Remarks
Series No. 4 Calorimeter No. 5					Chromel - Alumel Constant = 0.0228 mv/°F C = 0.0925 Btu/lb/°F W/A = 5.820 lb/ft <sup>2</sup>
Run 1	3	0.0518	1.22	2570	
2	3	0.0522	1.23	2582	
3	2	0.0877	2.07	2658	
4	2	0.113	2.68	2669	
5	1	0.270	6.38	2672	
6	1	0.276	6.53	2698	
7	0.7	0.365	8.62	2695	
8	0.7	0.346	8.18	2690	
9	0.7	0.385	9.09	2719	
Series No. 5 Calorimeter No. 5					Chromel - Alumel Constant = 0.0228 mv/°F C = 0.0925 Btu/lb/°F W/A = 5.820 lb/ft <sup>2</sup>
Run 1	0.7	1.10	25.87	3782	
2	0.7	1.06	24.96	3783	
3	0.7	1.09	25.81	3774	
4	11	0.763	18.02	3810	
5	1	0.707	16.69	3742	
6	2	0.313	7.40	3750	
7	2	0.287	6.75	3722	
8	3	0.147	3.48	3760	
9	3	0.148	3.50	3735	
Series No. 6					Chromel - Alumel Constant = 0.0228 mv/°F C = 0.0925 Btu/lb/°F for calorimeter No. 5 W/A = 5.820 lb/ft <sup>2</sup> for calorimeter No. 6 W/A = 5.841 lb/ft <sup>2</sup>
Calorimeter No. 5 Run 1	3	0.0570	1.32	2692	
Calorimeter No. 6 Run 2	3	0.0552	1.31	2700	
3	3	0.0532	1.26	2700	Thermocouple on back Thermocouple on front
Calorimeter No. 5 Run 4	3	0.0575	1.37	2706	
Calorimeter No. 6 Run 5	3	0.0525	1.26	2691	
6	3	0.0590	1.40	2698	Thermocouple on back Thermocouple on front
Calorimeter No. 5 Run 7	0.7	0.928	21.90	3638	
Calorimeter No. 6 Run 8	0.7	0.890	21.09	3656	
9	0.7	0.900	21.33	3655	Thermocouple on back Thermocouple on front
Calorimeter No. 5 Run 10	0.7	0.925	21.84	3669	
Calorimeter No. 6 Run 11	0.7	0.882	20.91	3657	
12	0.7	0.888	21.03	3635	Thermocouple on back Thermocouple on front

Table 4

Results of Calibration Runs on the High Temperature Blackbody Radiation  
Source with Copper Sensing Discs and Exposing Three Prototype  
Graphite Calorimeters to the Radiation Source

Calorimeter and Run No.	Range (in.)	Slope (mv/sec)	Heat Flux Density (Btu/ft <sup>2</sup> /sec)	Temperature at Bottom of Cavity (°F)	Remarks
Series No. 7					
Cal. No., Run					
5 - 1	3	0.0656	1.55	2758	Copper disc calorimeter No. 5; W/A = 5.280 lb/ft <sup>2</sup> , C = 0.0295 Btu/lb/°F. Chromel-Alumel Thermocouple = 0.0228 mv/°F Graphite Disc Calorimeter with Pt/Pt-10 Rh Thermocouple (Calorimeter No. 38)
38 - 2	3	0.0245	-	2823	
5 - 3	2	0.131	3.10	2861	
38 - 4	2	0.0448	-	2889	
5 - 5	1	0.328	7.75	2890	
38 - 6	1	0.101	-	2929	
5 - 7	0.7	0.492	11.62	2940	
38 - 8	0.7	0.165	-	2949	
38 - 9	0.7	0.177	-	2970	
38 -10	0.7	0.182	-	2975	
Series No. 8					
Cal. No., Run					
5 - 1	6	0.0105	0.248	2589	Calorimeter No. 98 is Graphite Disc Calorimeter with Pt/Pt-10 Rh Thermocouple
5 - 2	6	0.0125	0.295	2629	
5 - 3	3	0.0520	1.23	2690	
5 - 4	2	0.122	2.87	2717	
5 - 5	1	0.300	7.08	2730	
5 - 6	0.7	0.430	10.15	2747	
38 - 7	6	0.0055	-	2847	
98 - 8	6	0.0039	-	2861	
38 - 9	3	0.0245	-	2878	
98 -10	3	0.0240	-	2880	
38 -11	2	0.051	-	2890	
38 -12	2	0.045	-	2899	
98 -13	2	0.040	-	2906	
38 -14	1	0.129	-	2889	
98 -15	1	0.092	-	2899	
38 -16	0.7	0.181	-	2895	
93 -17	0.7	0.134	-	2890	
Series No. 9					
Cal. No., Run					
5 - 1	6	0.033	0.779	3546	Calorimeter No. 106 is Graphite Disc Calorimeter with Pt/Pt-10 Rh Thermocouple
5 - 2	6	0.034	0.803	3561	
38 - 3	3	0.050	-	3572	
98 - 4	3	0.040	-	3590	
5 - 5	3	0.139	3.28	3588	
38 - 6	2	0.095	-	3655	
98 - 7	2	0.076	-	3655	
5 - 8	2	0.300	7.08	3638	
38 - 9	1	0.309	-	3603	
98 -10	1	0.214	-	3599	
106 -11	3	0.036	-	3611	
5 -12	1	0.800	18.89	3580	
38 -13	0.7	0.381	-	3590	
98 -14	0.7	0.288	-	3590	
5 -15	0.7	1.04	24.56	3604	
106 -16	2	0.070	-	3615	
Series No. 10					
Cal. No., Run					
5 - 1	0.7	1.15	27.15	3770	Copper Disc Calorimeter No. 6; W/A = 5.841 lb/ft <sup>2</sup> , C = 0.0925 Btu/lb/°F, Chromel-Alumel Thermocouple = 0.0228 mv/°F
38 - 2	2	0.128	-	3757	
6 - 3	3	0.153	3.63	3759	
106 - 4	2	0.080	-	3717	
6 - 5	3	0.155	3.67	3750	
106 - 6	1	0.216	-	3711	
38 - 7	2	0.111	-	3730	
106 - 8	1	0.189	-	3710	
38 - 9	2	0.144	-	3717	
106 -10	0.7	0.288	-	3712	
106 -11	0.7	0.340	-	3710	Copper Disc Calorimeter No. 4; W/A = 5.862 lb/ft <sup>2</sup> , C = 0.0925 Btu/lb/°F, Chromel-Alumel Thermocouple = 0.0228 mv/°F
4 -12	6	0.039	0.925	3718	
4 -13	0.7	1.10	26.16	3700	
106 -14	0.7	0.355	-	3712	
106 -15	0.7	0.342	-	3700	

Table 5  
Results of Calibration Runs on the High Temperature Blackbody  
Radiation Source Using Copper Disc Calorimeters

Calorimeter and Run No.	Range (in.)	Slope (mv/sec)	Heat Flux Density (Btu/ft <sup>2</sup> /sec)	Temperature on Bottom of Cavity (°F)	Remarks
Series 11					
Cal. No. Run					
5 - 1	3	0.0842	1.99	2970	Copper Disc Calorimeter No. 5: W/A = 5.820 lb/ft <sup>2</sup> , C = 0.0925 Btu/lb/°F, Chromel-Alumel Thermocouple = 0.0228 mv/°F. Grafoil insulation $\frac{1}{8}$ in. thick between aperture and cavity.
5 - 2	1	0.469	11.1	2965	
5 - 3	0.7	0.709	16.8	2940	
5 - 4	0.7	0.725	17.2	2965	
5 - 5	0.7	1.37	32.4	3620	
5 - 6	0.7	2.54	59.8	4160	
Series 12					Abnormal Amount of Noise in X-Y Time Recorder
Series 13					
5 - 1	$\frac{1}{4}$	3.84	90.7	4003	Copper Disc Calorimeter No. 5
8 - 2	$\frac{1}{4}$	4.00	92.7	4022	Copper Disc Calorimeter No. 8: W/A = 5.709 lb/ft <sup>2</sup> , C = 0.0925 Btu/lb/°F, Chromel-Alumel Thermocouple = 0.0228 mv/°F. Aperture Plate reduced to $\frac{1}{4}$ in. thick. Pyrolytic graphite disc $\frac{1}{4}$ in. thick used for insulation between cavity and aperture plate.
5 - 3	$\frac{1}{4}$	3.93	92.8	4070	

APPENDIX FOR PARTS I AND II

TOTAL NORMAL EMITTANCE TO 5000°F

APPARATUS AND PROCEDURES FOR THE VAPOR DEPOSITION OF  
MOLYBDENUM AND TUNGSTEN ON GRAPHITE

## TOTAL NORMAL EMITTANCE TO 5000° F

### General

Emittance is measured by comparing the energy received by a radiometer from the sample to that received from a blackbody cavity maintained at the same temperature.

The equipment may be divided into three main parts: the induction heating furnace, the radiometer, and the temperature measurement equipment. Figure 1 shows a picture of the complete equipment.

### Description of Apparatus

A cross section of the apparatus is shown in Figure 2. The specimen (1) is supported in the center of the flat concentrator induction coil (2) by a zirconia cylinder filled with fine zirconia grog and tungsten wires (3). The zirconia cylinder rests on a crucible filled with coarse zirconia grog (4). The radiometer (5) views the specimen from directly above through a water-cooled tube (6). A water-cooled optical valve (7) is used to blank off the specimen from the radiometer. Optical-temperature readings are taken through the main port (8), which may be pushed in to view the specimen through a mirror (9) from directly above. When radiometer readings are being taken, the main port is pulled out and away from the line of sight of the radiometer. Auxiliary port (10) is used to view the specimen directly as a check for the main port. Both viewing ports contain sapphire windows. The portion of the furnace above the specimen (11) is water-cooled to eliminate any possibility of energy being reflected back onto the specimen surface. The emittance furnace is built of steel and sealed with "O" rings so that a vacuum may be attained.

The radiometer, see Figure 3, was constructed according to Snyder<sup>1</sup> and Gier<sup>2</sup> with some modifications. The receiver element consists of approximately 160 turns of No. 40 AWG bare-constantan wire (104 turns

---

<sup>1</sup> Snyder, N. W., Gier, J. T., and Dunkle, R. V., "Total Normal Emissivity Measurements on Aircraft Materials Between 100 and 1000° F," Trans. of the A. S. M. E., Vol. 77, 1944, p. 1011.

<sup>2</sup> Gier, J. T., and Boelter, L. M. K., "The Silver-Constantan Plated Thermopile," Temperature - Its Measurement and Control in Science and Industry, American Institute of Physics, 1941, p. 1284.

per inch) wound around a plastic insulator strip about 2" long by  $1\frac{5}{8}$ " wide by  $\frac{5}{16}$ " thick. Silver was electroplated in several stages onto the constantan coil so that two  $\frac{1}{8}$ " wide lines of silver-constantan junctions,  $\frac{1}{2}$ " apart, were formed on the same side of the coil and across all of the wire turns. The remainder of the entire coil was silver plated. Each of the two lines of junctions was covered with a thin, narrow strip of black paper. One of these junction lines is designated as the active or "hot" junction and is placed to receive energy from the sample. The other is shielded and termed the passive or "cold" junction.

In order to shield the element from extraneous radiation, a cylindrical housing is placed immediately around the thermopile. The front of the housing contains a rectangular opening  $\frac{1}{4}$ " by  $1\frac{1}{2}$ " to allow the element to "see" the specimen. The actual limiting of the receiver field is accomplished by this rectangular slit and the  $\frac{1}{4}$ " round stop (12) just above the specimen. Additional stops in the water-cooled tube were installed as an added insurance to further minimize spurious reflections. The radiometer views the specimen directly. This eliminates the possibility of dirty lenses affecting the reading and, also, eliminates the spectral selectivity of the different types of materials used as windows.

The voltage generated by the receiver is measured with a Type K-3 Leeds and Northrup potentiometer in conjunction with an L and N Type 2430 DC galvanometer of 0.43 microvolts per millimeter deflection sensitivity. Temperatures are measured with a Leeds and Northrup portable potentiometer.

The receiver element was calibrated against a carbon-filament lamp of known radiation<sup>3</sup> and demonstrated a sensitivity of 8.66 Btu/hr/sq ft/millivolt.

The radiometer was checked, also, against an Eppley thermopile with 12 bismuth-silver junctions and a 1-mm quartz window and agreed within 10% scatter of data points. By factory calibration the sensitivity of the Eppley thermopile is 0.048 microvolts/microwatt/sq cm.

The optical pyrometers used are L and N catalog type 8622 calibrated in accordance with the International Critical Table of 1948 for an emittance of unity.

---

<sup>3</sup> Lamp No. C584, calibration by the National Bureau of Standards and reported in NBS Report 132737 A, July 1, 1952.

## Calibration Procedure

To calibrate the radiometer for blackbody radiation, a blackbody cavity with a 6 to 1 aspect ratio made from graphite was used. The blackbody cavity was insulated by zirconia grog and lampblack placed in the annulus between the blackbody and the load coil, see Figure 4.

The accurate determinations of the specimen and blackbody temperatures are essential to good data. For the cavity-type blackbody, the temperatures are determined relatively easily by (1) thermocouples placed in the bottom of the cavity; (2) thermocouples dropped into the cavity; and (3) optical pyrometer observations. Up to 3000° F, agreement to within 15° F has been obtained regularly between these three readings. Above 3000° F the agreement between tungsten-rhenium couples and the optical pyrometer has been generally within 50° F or the repeatability of this type of thermocouple. Actually, the optical readings have no error other than those of the instrument calibration and the human error, which appears to provide a readout scatter of about 20° F at 4000° F.

Radiometer output versus temperature for blackbody radiation is plotted in Figure 5. Notice that the output is essentially linear from 2500° F to 5000° F with a slight curvature below 2000° F. As in house standards, the emittance of 304 stainless steel, tarnished tungsten, and graphite were measured, see Figure 6. The emittance of the stainless steel ranged from 0.15 at 700° F to 0.67 at 2000° F. These values are in close agreement with the literature values. The sanded CS graphite, also, checked out closely with the literature with values from 0.95 to 0.98.

## Operating Procedures

The specimen is placed directly on the surface provided by the zirconia tube, grog, and tungsten wires. However, if the material of interest cannot be heated inductively, tungsten and tantalum heating discs are placed under the specimen with the specimen in contact with the tungsten disc.

The furnace is then evacuated to 15 mm of Hg and filled with high-purity, dry argon. This operation is carried out at least twice to assure an inert atmosphere. Throughout the run a slight pressure is maintained in the furnace by an argon purge, which is brought in through the radiometer enclosure and exhausted from the furnace housing, see Figure 2. In addition to maintaining an inert atmosphere, the purge flow tends to keep fumes away from the radiometer.

The temperature of the specimen is raised and maintained at the desired point by transferring energy to the specimen through the induction coil. About three hours are required to complete a single run with the temperature increasing stepwise but in uniform intervals. At each temperature level a radiometer reading is taken in conjunction with the temperature readings.

To obtain the radiometer reading, the following procedure is followed: As the specimen is heated, the blank-off valve is shut so that the thermopile can see no impulse. When the specimen temperature reaches steady state, a zero reading is obtained for the thermopile output. This reading is usually in the order of  $\pm 0.02$  millivolts. The blank-off valve is then opened, and the thermopile output increases several fold in a few seconds. The reading levels off as heat is transferred down the wires to the cold junction. The radiometer output is taken at the peak reading immediately after steady state. The net reading for that temperature is then obtained as the difference between the zero and steady-state reading.

If the blank-off valve were left open, the thermopile output would decrease slowly with time. After about 10 minutes, this reading might decrease by 50%; however, if the blank-off valve were shut and a new zero reading obtained, the difference between this new output and zero reading would be about the same as the original readings. The variation might be about 5 to 10%. The shift in readings is a result of the heating of the cold junctions.

The purge to the radiometer housing has no influence on the readings within the ranges at which the purge is operated. To determine this limit, the purge rate was increased to about 10 times the normal metered reading, and a small shift in readings of less than 1% was noted.

The temperature of the specimen is monitored by (1) thermocouples mounted directly on the target surface (usually held in place by a small zirconia pad) and (2) optical pyrometer readings on the target surface. Low temperature readings were made with thermocouples; however, in the intermediate temperature range from 1600° F to 2700° F a cross check was made between the thermocouple readings and the optical readings. The high-temperature measurements are made with an optical pyrometer. A main-port optical and an auxiliary-port optical-temperature reading are taken at each temperature level. The auxiliary-port temperature is normally used only as a check; however, if conditions warrant, such as a dirty main-port window or mirror, the auxiliary-port value may be used. Usually very good agreement is maintained between the main-port and auxiliary-port optical readings.



## Emittance Calculation

The optical temperature readings must first be corrected to obtain true temperatures. The main-port reading is corrected for the sapphire window and mirror while the auxiliary-port reading is corrected for the sapphire window and the angle at which the port views the specimen. The corrections are shown as curves in Figure 7.

After assuming an arbitrary-initial, emittance value, the brightness temperature is corrected for this assumed emittance, see Figure 8. The blackbody output is then read at this "true" temperature from Figure 5. The ratio of the observed specimen radiometer output to the blackbody output is calculated and is the emittance of the material at that temperature. If the assumed emittance is correct, the calculated value will agree with it; if not, the calculated value must be used as the former assumed value and the process repeated until the assumed emittance value agrees with the calculated value. This iterative process will converge on the correct emittance value assuming graybody distribution of most of the energy at the particular temperature. The above process was programed for analysis by a digital computer.

## Error Analysis

The above procedure for determining emittance is strictly correct only for those materials that radiate as graybodies, since the total emittance is assumed to be equal to the spectral emittance at the wavelength of the pyrometer. This approximation was used above to convert the brightness temperature to true temperature.

The error in emittance values for nongray materials will vary depending on the difference between the 0.665 microns spectral and the total emittance, and the distribution of radiant energy within the particular spectrum. If the deviation from graybody becomes very great at temperatures up to 2500° F, it is indicated by the thermocouple measurements. On materials of low emittance, such as tungsten, the emittance values calculated by this procedure could be in error by as much as 20% at the highest temperatures. However, it is believed that for most materials, the accuracy is within 10%. Several things indicate that the accuracy of the emittance values is good. First, the radiometer output versus temperature curves are orderly and almost linear with only normal data scatter. Second, the data obtained on two samples of the same material are in close agreement. Third, the values of emittance for the check samples agree very well with the literature, see Figure 6.

A statistical analysis of the data accuracy is of interest. Generally, the probable error in each blackbody reading is about 4%, and the probable error in each specimen reading is about 8%. If the data points are used to calculate emissivity, the maximum probable error would then be about 12%. The curve-fitting approach undoubtedly reduces this maximum to about 5%. As a general conclusion, the accuracy of the measuring system is well within the range of variation as is experienced by different finishes on the same material, the changing chemistry of the surface at the high temperatures, surface temperature measurements, and other variables.

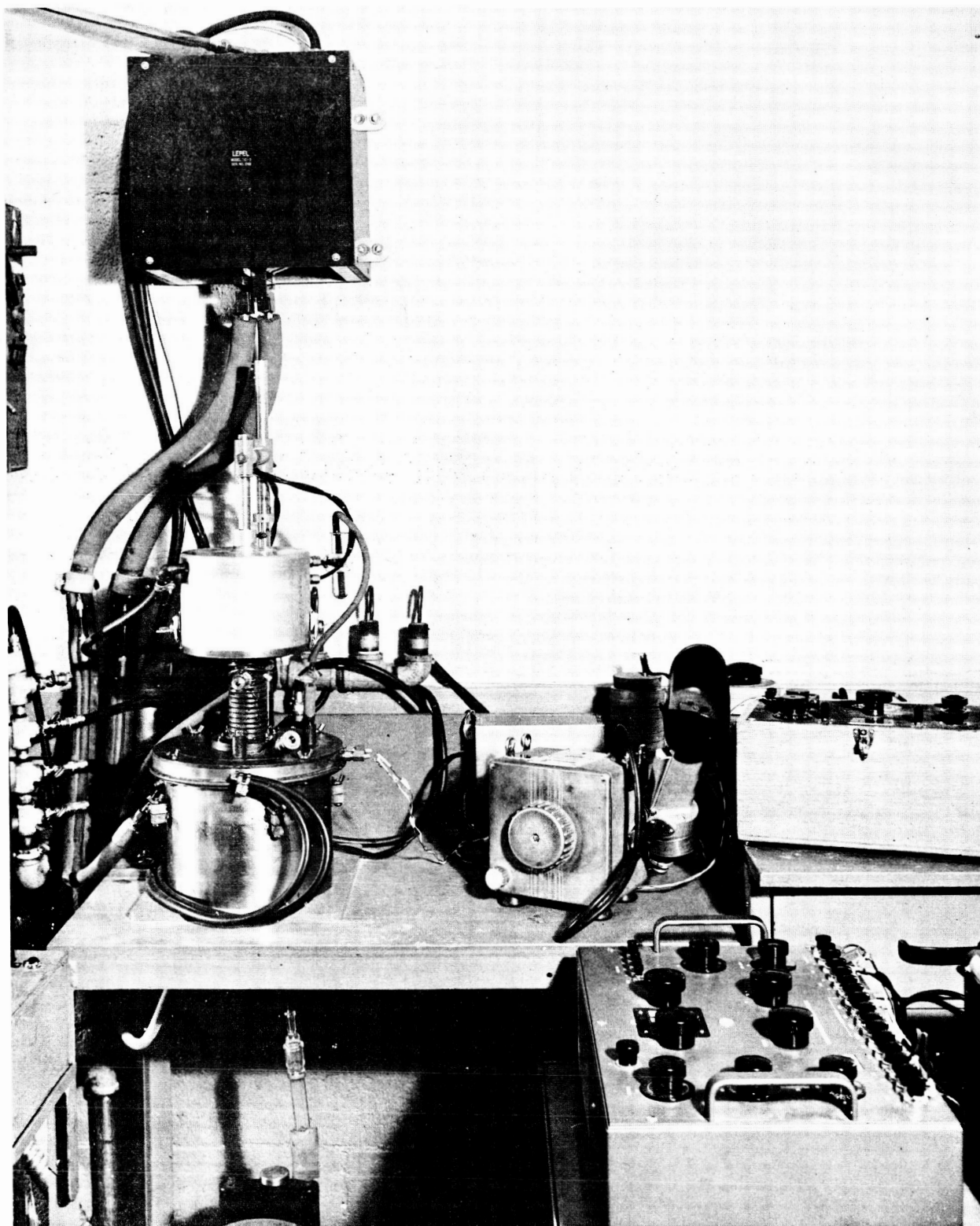


Figure 1. Picture of the Apparatus for Measuring Total Normal Emittance.

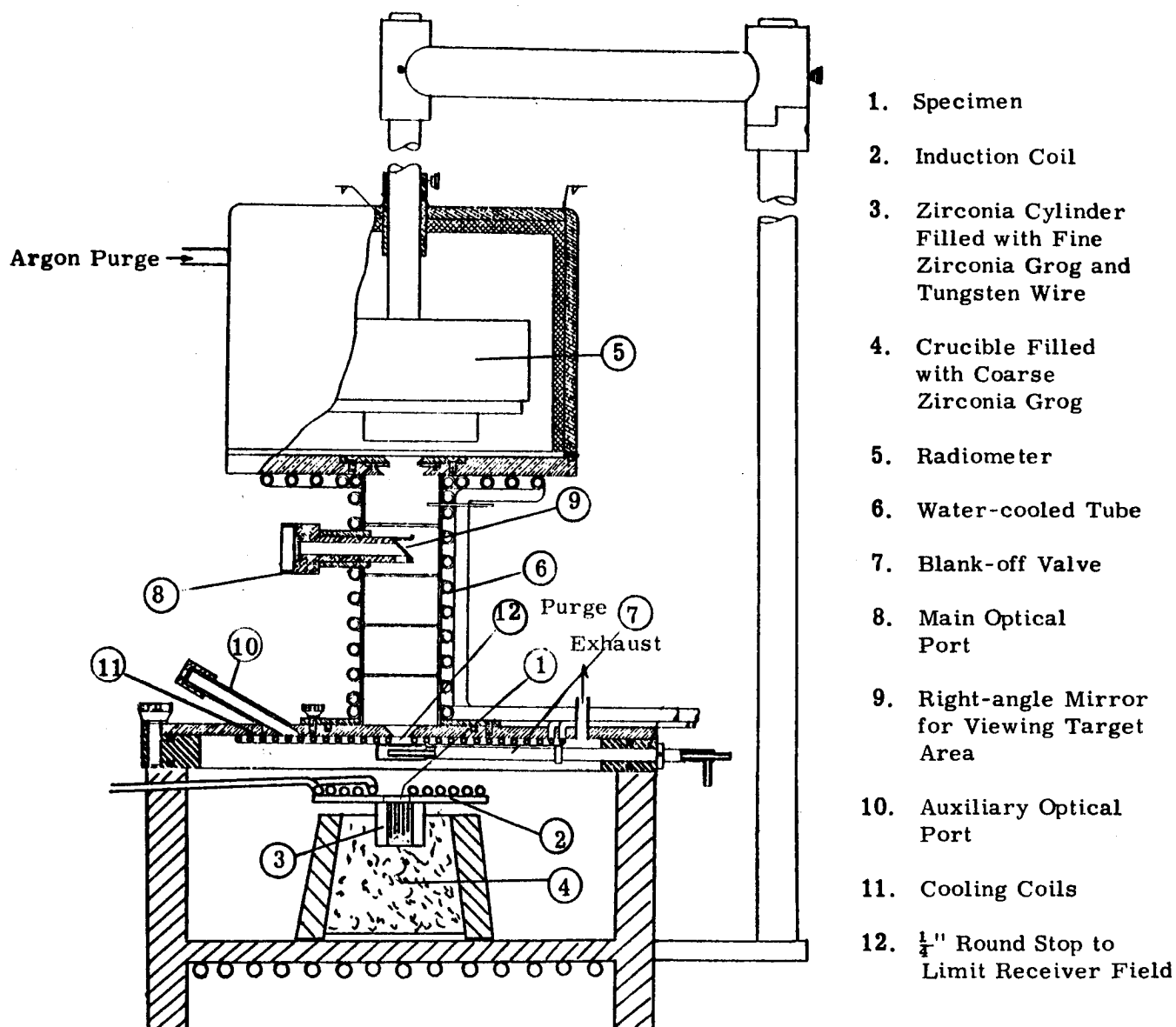


Figure 2. Cross Section of Emittance Apparatus with Flat Coil Furnace.

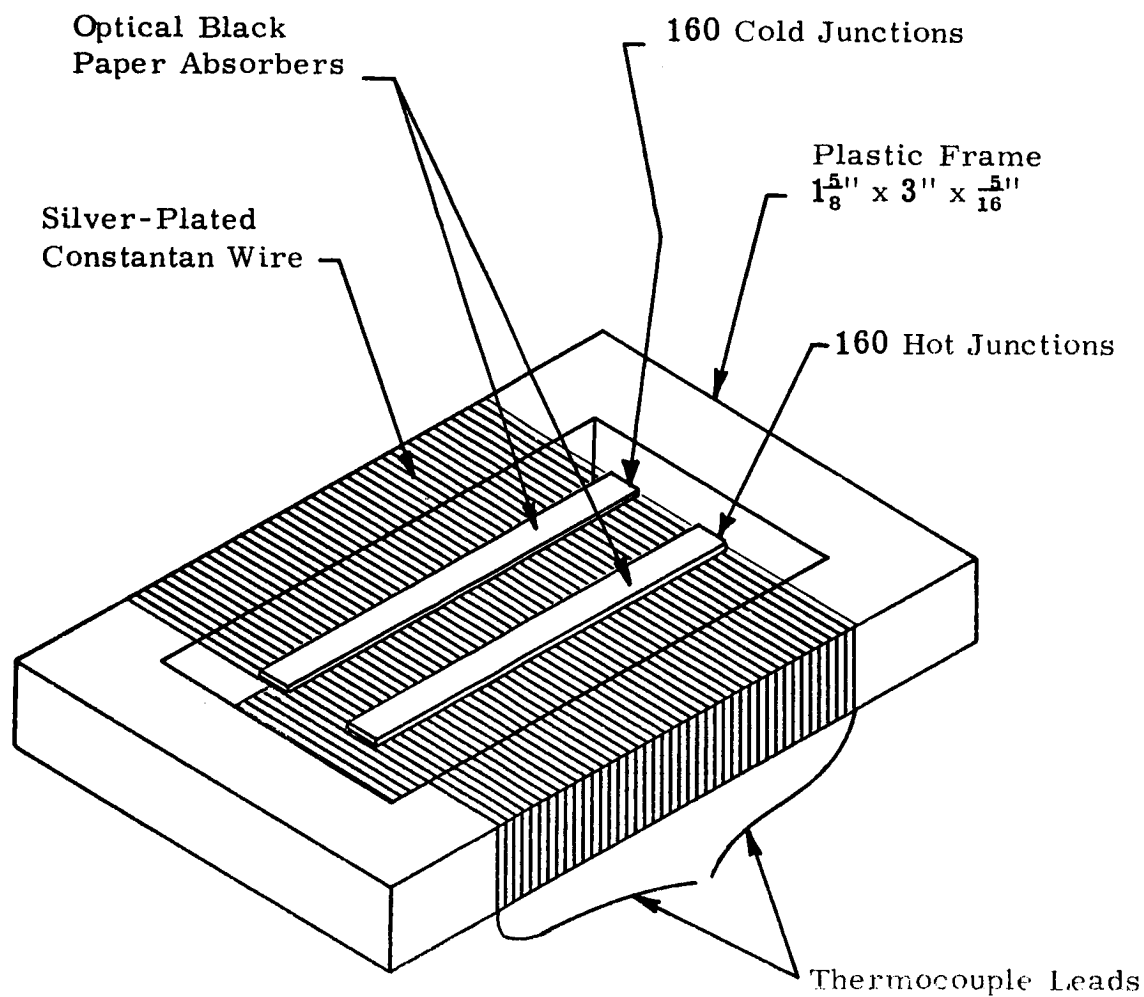


Figure 3. Schematic of 160-Junction Thermopile in Emittance Equipment.

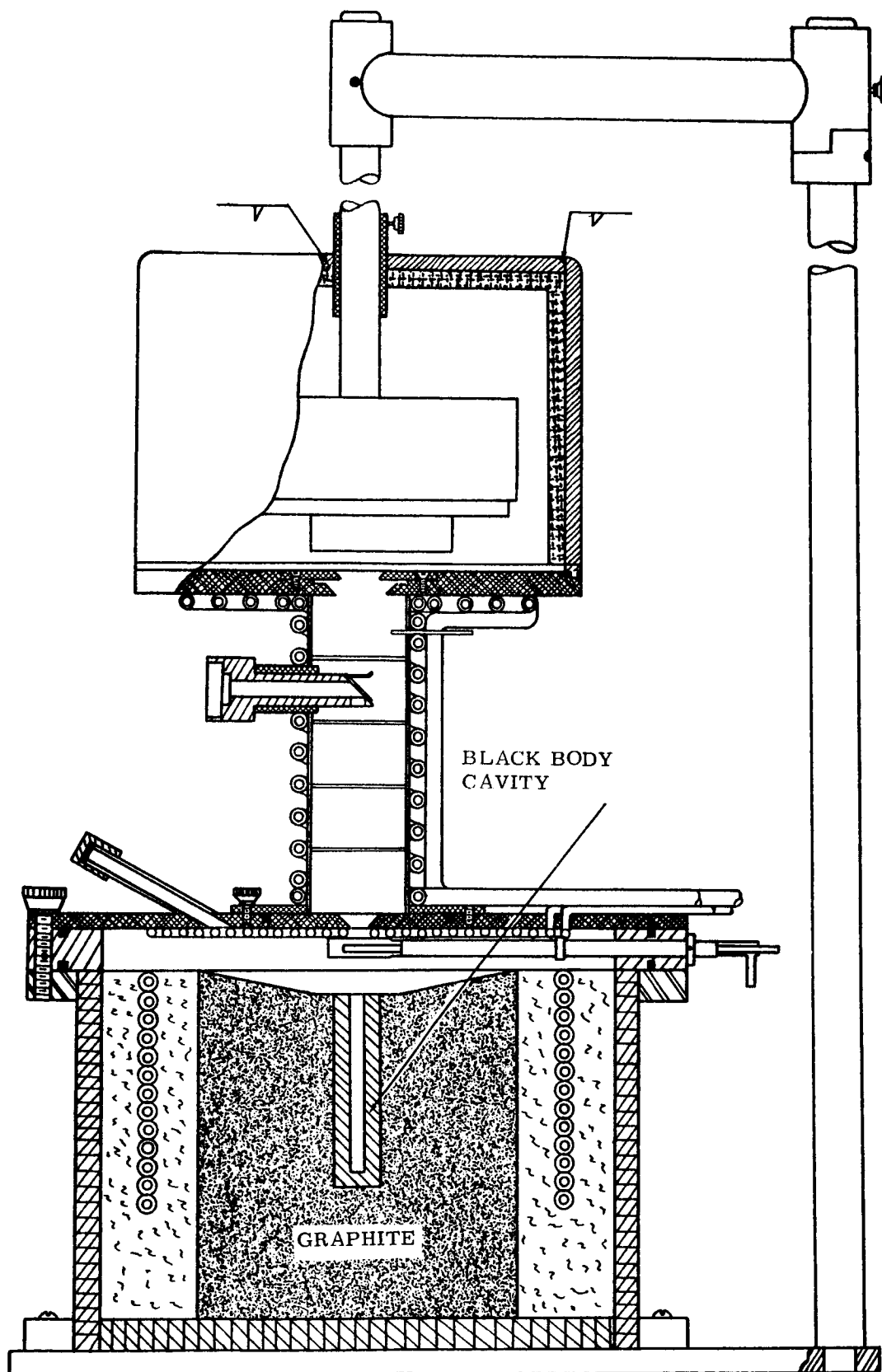


FIGURE 4. CROSS SECTION OF EMITTANCE APPARATUS  
WITH BLACK BODY FURNACE.

RADIOMETER OUTPUT - MILLIVOLTS

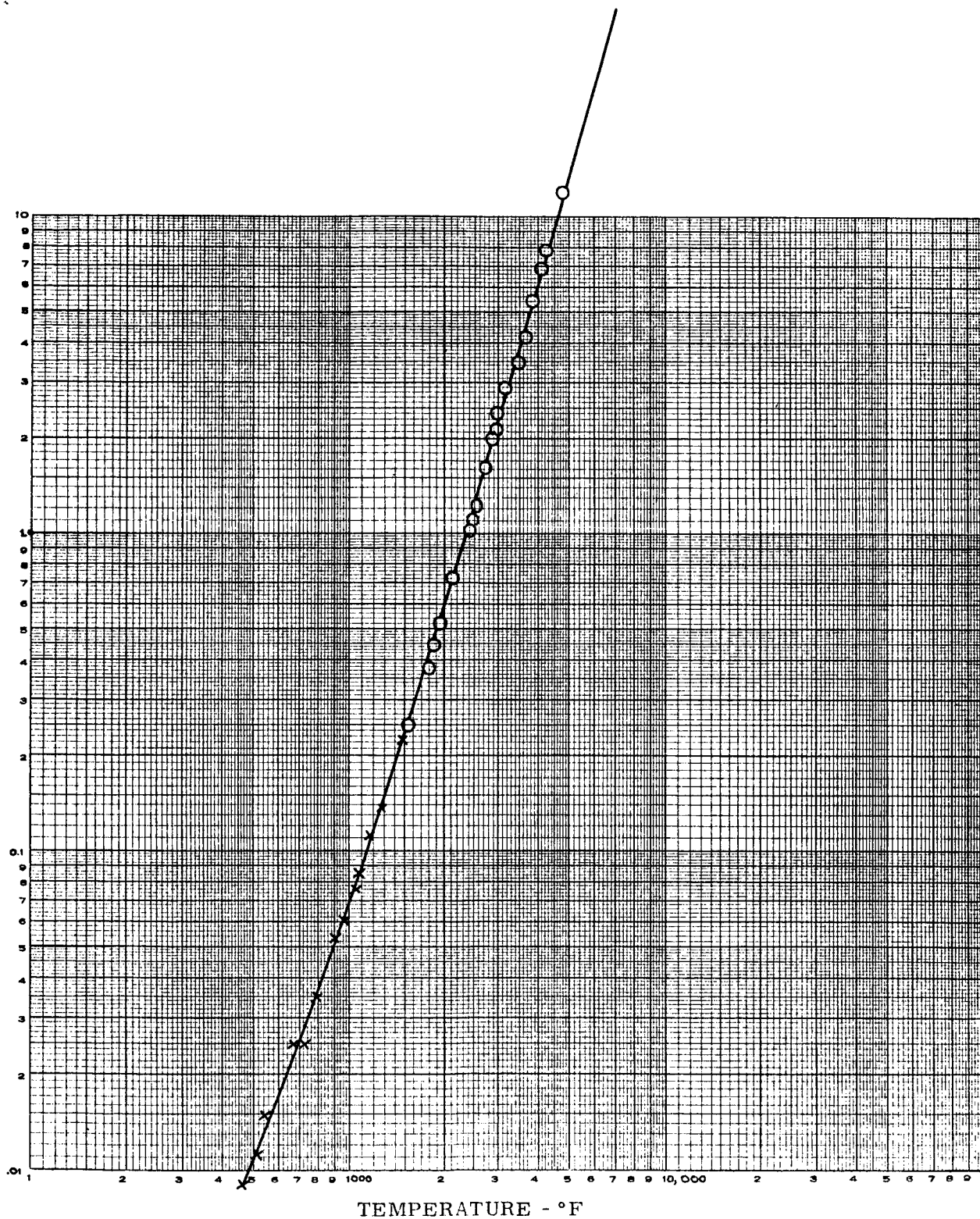


FIGURE 5 . RADIOMETER OUTPUT VERSUS TEMPERATURE FOR BLACK BODY RADIATION .

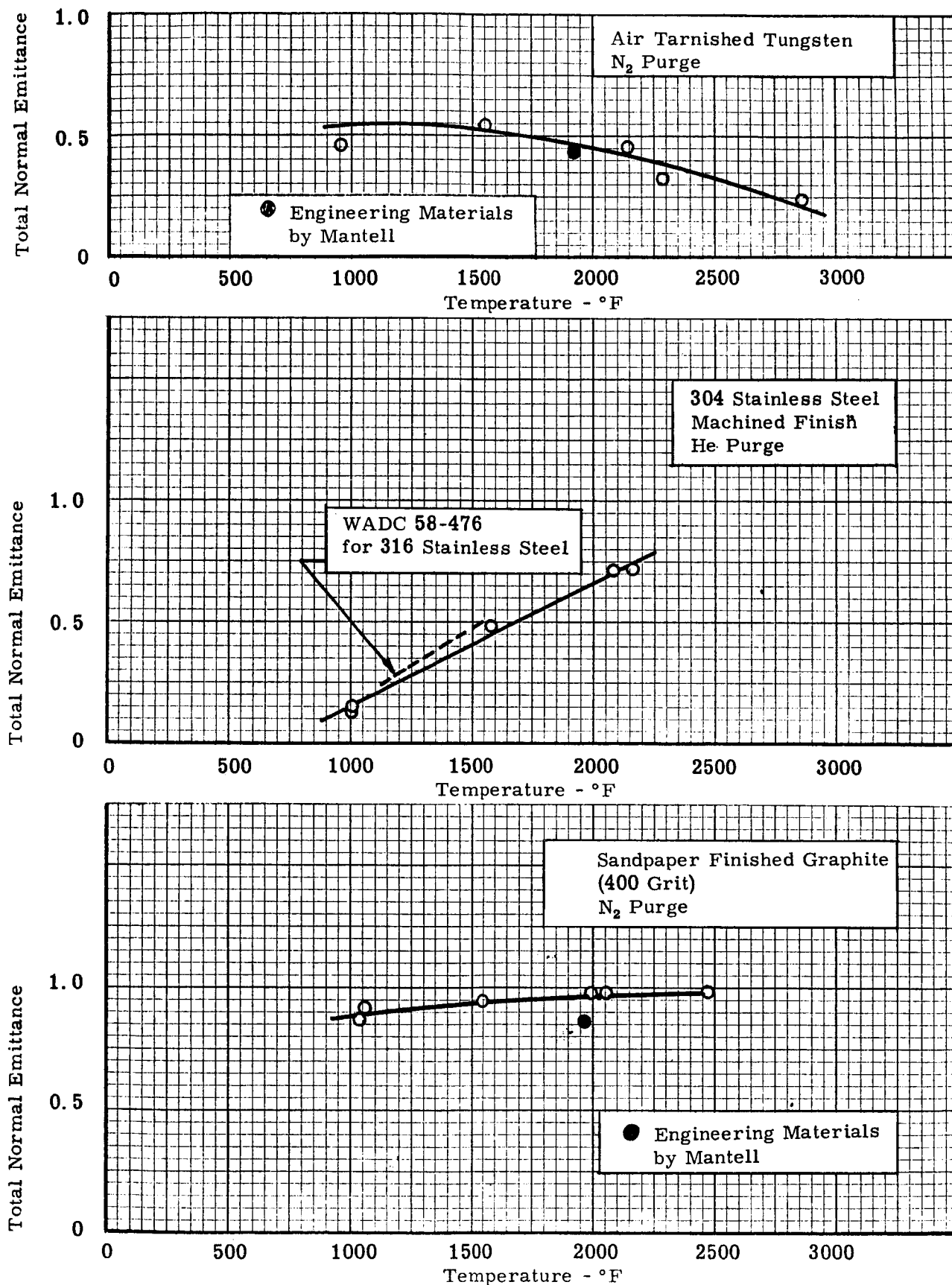


Figure 6. Calibration Standards for Total Normal Emittance.



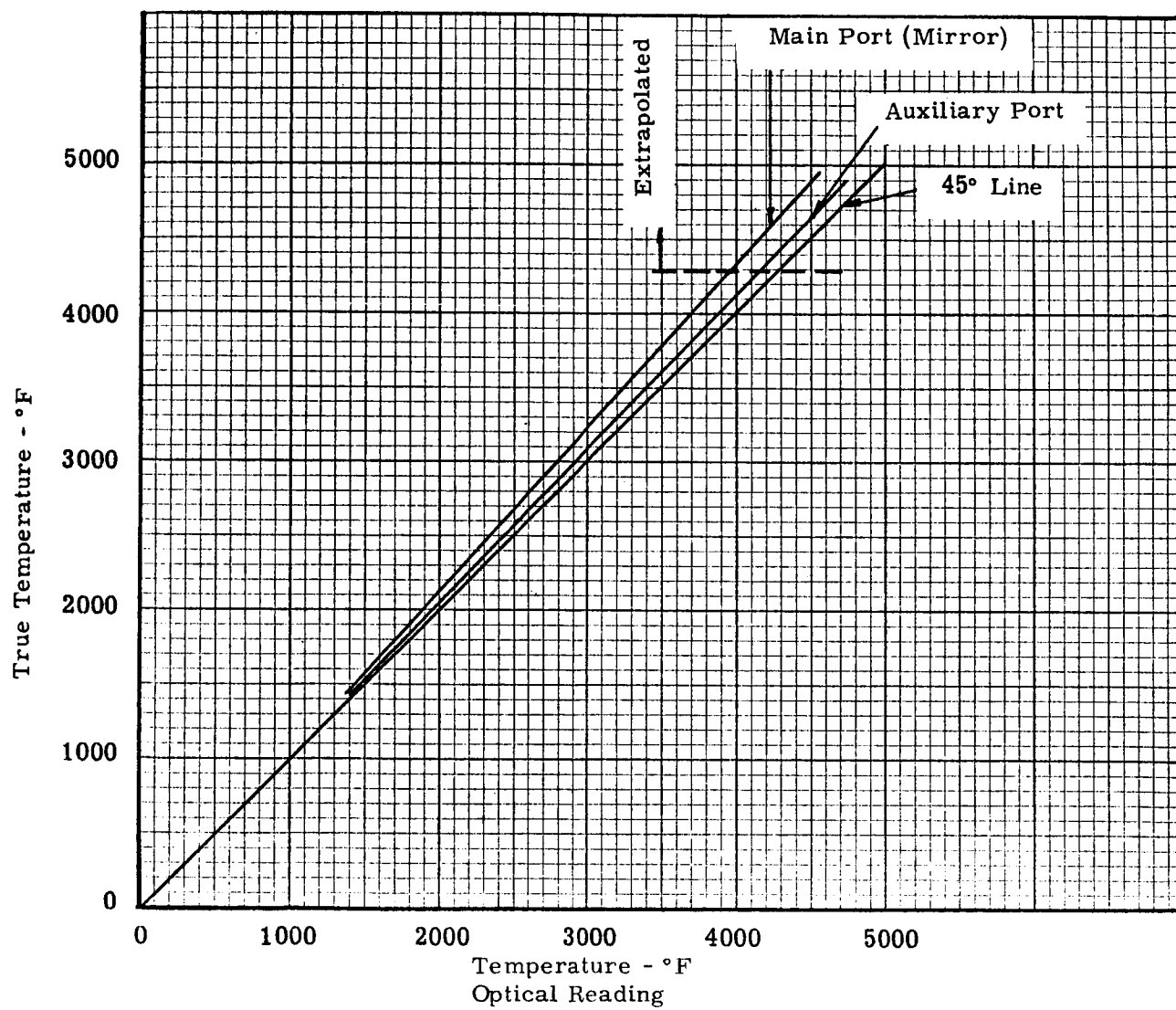


Figure 7 . Correction for Mirror and Sapphire Window in Emittance Apparatus.

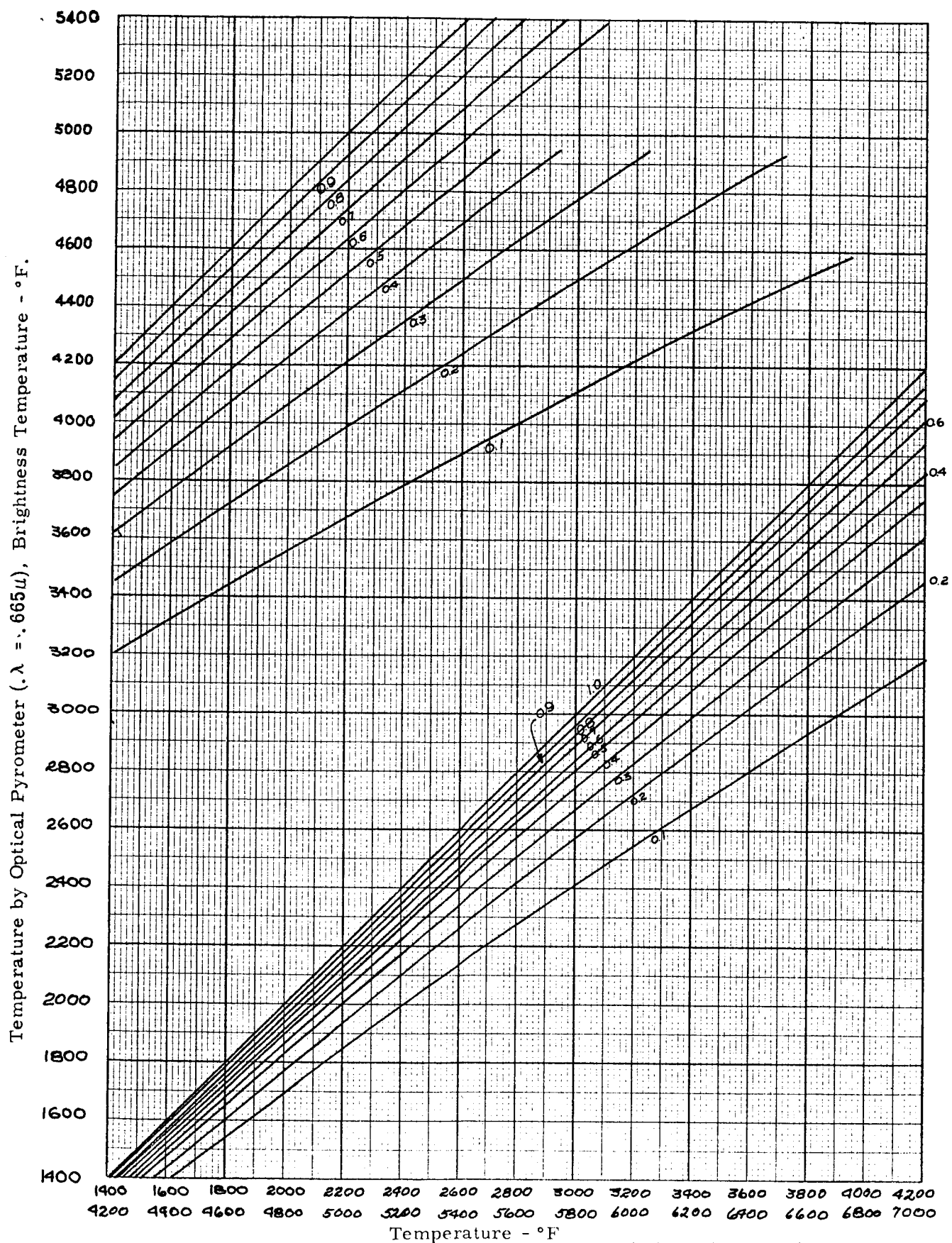


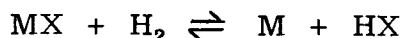
Figure 8. Correction for Brightness Temperature to True Temperature.

## APPARATUS AND PROCEDURES FOR THE VAPOR DEPOSITION OF MOLYBDENUM AND TUNGSTEN ON GRAPHITE

Two basic apparatuses and procedures are used to vapor deposit molybdenum and tungsten on graphite. One apparatus is used to deposit molybdenum and tungsten when the reactive compound is in a powdered form. The other apparatus is used only for the tungsten deposition using tungsten hexafluoride gas as the reactive compound.

### VAPOR PLATING PROCEDURE NO. 1 (Powdered Process)

Graphite discs are vapor plated with metal in the apparatus shown in Figure 1. The gross reaction for the hydrogen reduction of the metal halide vapor can be symbolized as follows:



The operating conditions that are used for plating tungsten on graphite specimens are:

Specimen temperature	$700^{\circ}\text{C} \pm 25^{\circ}\text{C}$
System pressure	$9.5 \pm 0.5 \text{ cm Hg}$
Tungsten hexachloride powder temperature	$168^{\circ}\text{C} \pm 5^{\circ}\text{C}$
Hydrogen flow rate is sufficient to prevent the appearance of metal halide fumes in the apparatus	
Deposition rate	1.6 mils per hour

The plating procedure is given below:

1. A. T. J. graphite discs are finished on one side with 400 grit emery paper and the surface is blown free of debris with air.
2. The apparatus is outgassed with a vacuum pump for a minimum of one and one-half hours with the disc and susceptor at operating temperature.
3. Tungsten hexachloride powder is introduced into the metal halide chamber against a current of argon.
4. The apparatus is again outgassed, the specimen is brought to operating temperature, and the vacuum pump is cut out of the system.
5. Hydrogen flow and argon sweep gases are adjusted, and the metal halide compartment is raised to operating temperature in 15 to 20 minutes.

6. The desired system pressure is maintained automatically with a water aspirator operating through a solenoid that is activated from a pressure sensing device.
7. After three hours at operating conditions, the metal halide chamber is allowed to cool, power to the susceptor is reduced, hydrogen flow is cut off and argon flow into the system is increased.
8. After approximately 15 minutes power to the susceptor is cut off, and the specimen allowed to cool before it is removed.

#### VAPOR PLATING PROCEDURE NO. 2 (Gas Process)

Graphite discs are plated with tungsten in the apparatus shown in Figure 2 by hydrogen reduction of tungsten hexafluoride gas. The overall reaction may be represented as follows:



A uniform layer of tungsten 2.5 mils thick can be deposited on the impinged side of the graphite disc in 15 minutes. This plating rate is uniform at least for the first hour of plating time.

The operating conditions and procedures are given below:

1. A. T. J. graphite discs are finished on one side with 400 grit emery paper, and the surface is blown free of debris with air.
2. With the disc in place and at the operating temperature of 700°C, the apparatus is outgassed initially for a minimum of one and one-half hours. A succession of discs can be coated where only 10 minutes of time is sufficient to outgas the system after the introduction of a fresh disc.
3. The system pressure is maintained at  $9.5 \pm 0.5$  cm Hg and the gas flow rates of argon, tungsten hexafluoride, and hydrogen are adjusted to give deposits of a uniform and reproducible thickness.
4. The plating operation is terminated by closing off the tungsten hexafluoride flow. After five minutes, power to the induction coils is shut off. Hydrogen and argon flows are closed after the apparatus pressure is raised to one atmosphere.

5. When sufficient time has elapsed, usually 10 minutes, for the disc to cool, it is replaced with a fresh disc. Argon gas is permitted to flow during this operation.

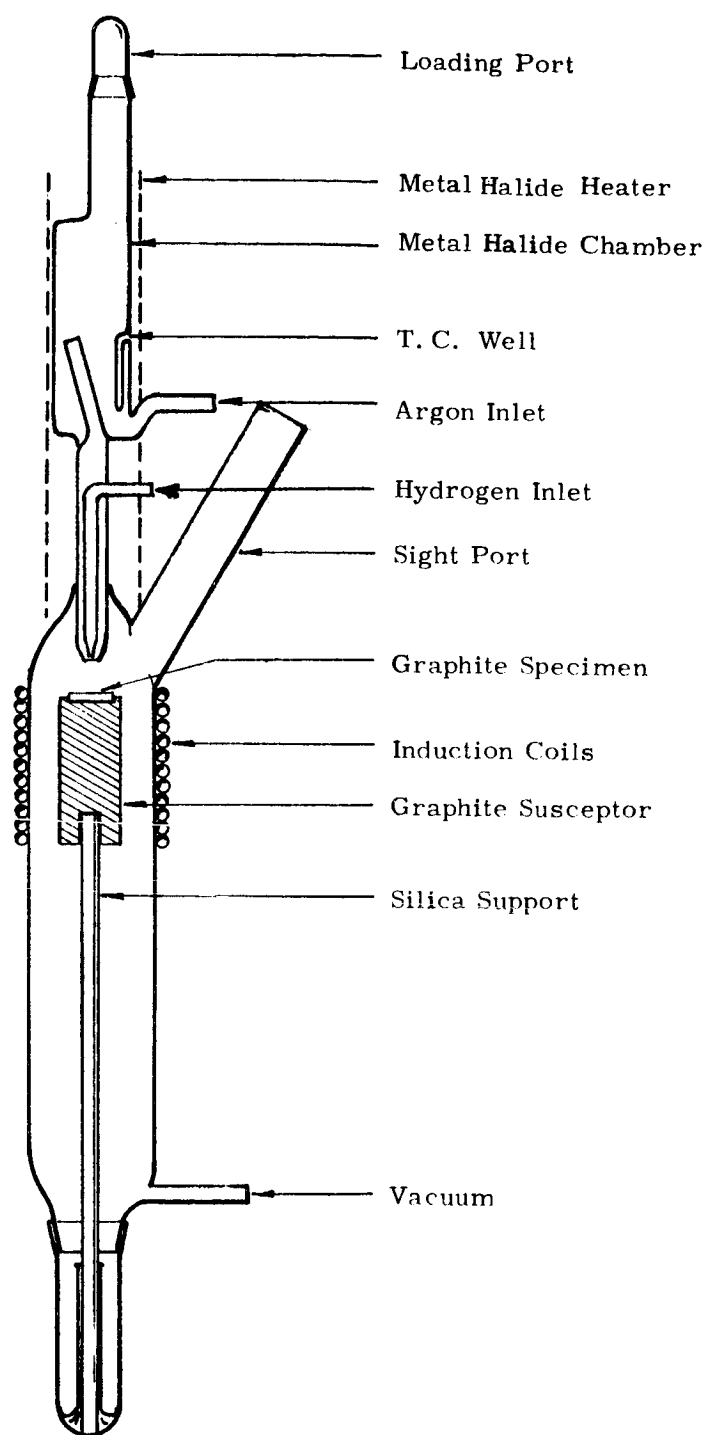


Figure 1. Vapor Deposition Apparatus for Use with Tungsten Hexachloride Powder

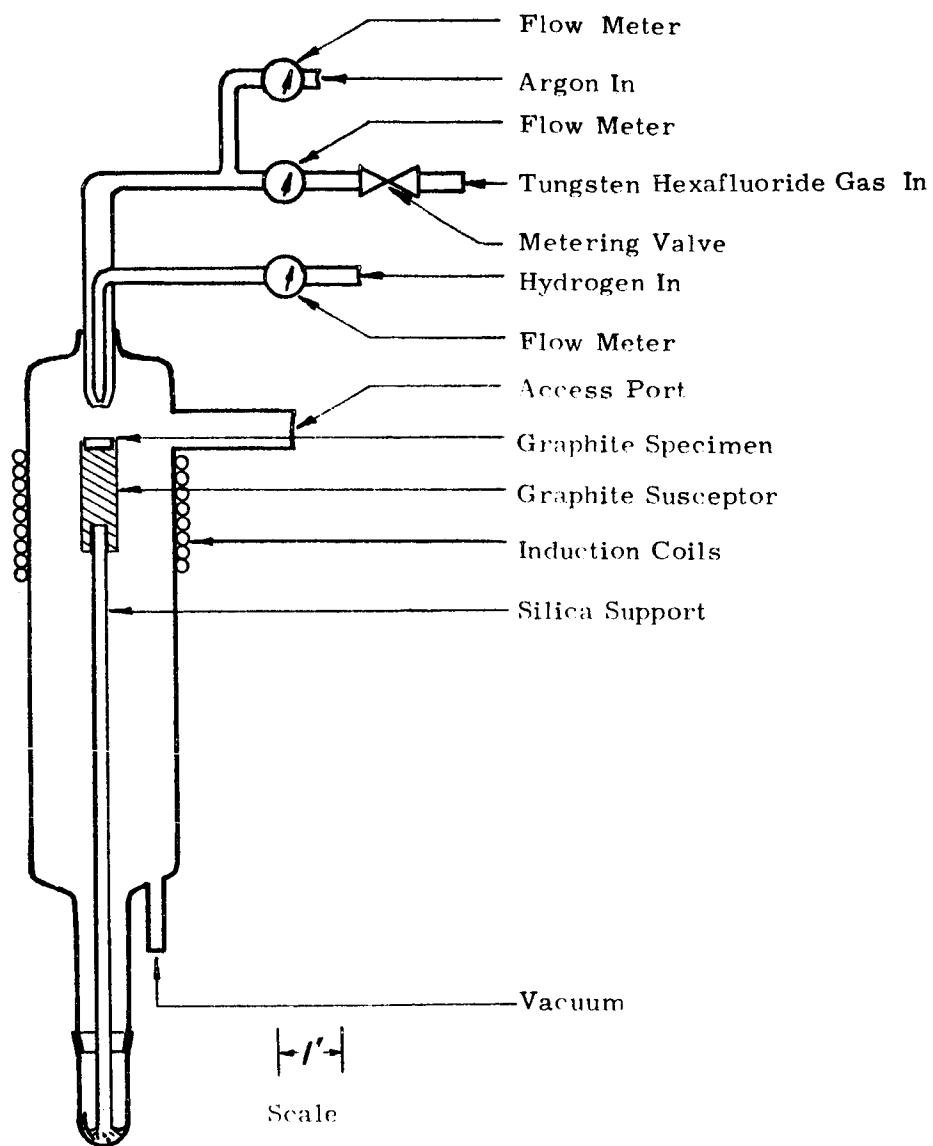


Figure 2. Vapor Deposition Apparatus for Use with Tungsten Hexafluoride Gas